Journal of Pyrotechnics

Issue 17, Summer 2003

Direct Editorial Concerns and Subscription Requests to:

Journal of Pyrotechnics, Inc.
Bonnie Kosanke, Publisher
1775 Blair Road
Whitewater, CO 81527, USA
(970) 245-0692 (Voice and FAX)
email: bonnie@jpyro.com

CAUTION

The experimentation with, and the use of, pyrotechnic materials can be dangerous; it is felt to be important for the reader to be duly cautioned. Without the required training and experience no one should ever experiment with or use pyrotechnic materials. Also, the amount of information presented in this Journal is not a substitute for necessary training and experience.
A major effort has been undertaken to review all articles for correctness. However, it is possible that errors remain. It is the responsibility of the reader to verify any information herein before applying that information in situations where death, injury, or property damage could result.

Table of Contents

Issue 17 Summer 2003

Color Purity Measurements of Traditional Pyrotechnic Star Formulas
Brian V. Ingram 1

A Study of the Combustion Behaviour of Pyrotechnic Whistle Devices
(Acoustic and Chemical Factors) M. Podlesak and M. A. Wilson 19

Reasons for Fuse Failure and Drift Distance of Spherical Fireworks Shells
Marc Speer 35

Some Properties of Explosion Generated Toroids
Fred Ryan and Joe Daugherty 53

Feasibility Study on the Use of Nanoscale Thermites for Lead-Free Electric Matches
Darren L. Naud, M. A. Hiskey, S. F. Son, J. R. Busse, and K. L. Kosanke 65

Communications:

A Curious Observation during the Burning of Bulk Whistle Composition
L. Weinman 79

Review by S. Miller of: *Proximate Special Effects Familiarization and Safety* by J. L. Mattingly, D. A. Opperman and F. Pinkerton 80

Author Instructions 34

Editorial Policy 81

Events Calendar 76

Sponsors for Current Issue 82

If you want to receive titles and/or abstracts for future issues by email, send a note to bonnie@jpyro.com. You will then receive this information about two weeks before the next issue is ready to mail.

Publication Frequency

The *Journal of Pyrotechnics* appears approximately twice annually, typically in mid-summer and mid-winter.

Subscriptions

Anyone purchasing a copy of the Journal will be given the opportunity to receive future issues on an approval basis. Any issue not desired may be returned in good condition and nothing will be owed. So long as issues are paid for, future issues will automatically be sent. In the event that no future issues are desired, this arrangement can be terminated at any time by informing the publisher. Additional discounts are available for payment in advance for issues of the *Journal of Pyrotechnics*. Contact the publisher for more information.

Back issues of the Journal will be kept in print permanently as reference material.

Color Purity Measurements of Traditional Pyrotechnic Star Formulas

Brian V. Ingram
Sandia National Laboratories, PO Box 5800 – MS 1452, Albuquerque, NM 87185-1452, USA
email: bvingra@sandia.gov

ABSTRACT

Pyrotechnic formulas designed to produce colored flames are well known, but the trends in color quality due to individual formula components are less well understood. This paper presents spectrometer work done to record spectra and processes them into chromaticity coordinates. Major formulas of the basic additive colors of red, green, and blue were tested and compared. Impact sensitivities were gathered for those major formulas. Then single suitable formulas were chosen for the basic colors, which were then systematically altered and measured for color quality performance. The formulas were altered to investigate the role of oxidizer to fuel ratio, chlorine donor content, colorant content, and colorant source.

Keywords: color purity, chromaticity diagram, chromaticity coordinate, star formula, flame emission

Introduction

Pyrotechnics are used to create light, heat, sound, smoke, ash, metal, or gas. Within the visible light effects, the creation of colored flames is one of the most commonly recognized. The pyrotechnic compositions of this class are used in fireworks and civilian and military pyrotechnics.[1] In any usage, the efficient formation of a desired color is paramount. Depth of color, or saturation, is usually a prerequisite of correct device function. In addition to the pleasing aesthetic effect of a deep, saturated color star in a firework application, high quality colors permit observer discrimination between similar signal flares at extreme distances. Because of the importance placed on function of these compositions, studies have been conducted to understand factors affecting their performance.[2–5]

In the formation of a colored flame, some species are desirable to have in the flame, and some species are not desirable. The desirable species are those that emit light at or near the hue intended for that formula. Other atomic or molecular emitters in the flame, which emit at wavelengths that detract from the intended hue, will hinder performance. Also undesirable are certain solid and/or liquid combustion products that can glow in an incandescent fashion. When these materials emit radiation, it is not radiation of a specific electronic transition, but rather a broadband radiation across a very large wavelength range. This is called blackbody, graybody, or continuous radiation. When the temperature of the glowing matter is high enough, it can emit light across the entire visible spectrum.

The desired emitters for most colored flames are well known.[2,7] For forming a red flame, the molecular emitter strontium monochloride (SrCl) is responsible for the deepest red color, with emissions at 635, 660, and 673 nm.[7–9] Strontium monohydroxide (SrOH) emits at 606 nm, which contributes an undesirable orange-red light.[7] For forming a green flame, the molecular emitter barium monochloride (BaCl) is responsible for emissions at 514 and 525 nm.[7–9] A contributing barium emitter is the triatomic barium monohydroxide (BaOH), which emits desirable light at 487, 515, and 527 nm.[3] For forming blue flames, the molecular emitter copper(I) chloride (CuCl) is responsible for emissions at 430, 436, 484, 489, and 527 nm.[7–9] As an aside, copper(II) oxide (CuO) has a weak molecular emission at 609 nm,[8] widely recognized as orange-red tips on otherwise blue flames. While there are smaller peaks in the spectra, the overwhelming contribution to the flame hue is from the emitters mentioned. Other detrimental emitters are present as well. As examples, there are the ubiquitous sodium atomic emission at 589 nm[10] and the sometimes-present

calcium monochloride (CaCl) at 594, 619, and 621 nm.[7] Both are caused by contamination of chemicals used in the formula. The sodium contamination arises because many oxidizer salts are produced by a double displacement reaction with sodium salt. The calcium contamination is typically found in ammonium perchlorate where tricalcium phosphate is used as an anti-caking additive.[11] In some orange flame formulas, the CaCl emitter is desired; however this work will not address orange, yellow or other non-primary flames.

Objective of Present Work

Study of the conditions that give rise to the desirable species is important, because understanding those conditions will allow tuning of a composition at the formulation stage. Past studies that were conducted have used elegant and ingenious techniques to show intensity and wavelength information[4,12,13] and to correlate that data to chemical species.[3] In fact, work to demonstrate the spectra due to emitters is ongoing.[14] Chromaticity coordinates have also been generated for colored flame formulas[3] in an effort to show the change in color purity as a function of formula. This study attempts to add to this field, by acquiring spectra with a spectrometer suited for visible range flame emission, and processing the spectra into CIE color coordinates. The 1931 CIE Chromaticity Diagram is shown in Figure 1.[7,15] Further, systematic experiments are performed, which follow the flame color quality as a function of formula, to identify trends in performance. These experiments are also designed to give insight into the relative importance and roles of the components of typical color formulas.

Experimental

Experiments were performed using a PC2000 spectrometer from Ocean Optics, Inc., which was outfitted with a grating optimized for the visible range, and which was especially suited to color measurements. Its blaze wavelength, which is the wavelength of greatest efficiency, was located at 500 nm. The spectrometer could read from 340 to 860 nm, with relative efficiencies of at least 40% from 380 to 700 nm. A high temperature quartz collimating lens was employed to gather light from the sample, directed into a 400 μ diameter, 8 m long fiber optic cable, which transmitted the sample light to the spectrometer. The system was calibrated using an Ocean Optics, Inc. 3100 K color temperature tungsten lamp. The Ocean Optics 16-bit OOI-Base V1.5 proprietary software, which was packaged with the spectrometer, was used to control the spectrometer and collect spectra. An Excel spreadsheet program was used to calculate CIE coordinates from wavelength-intensity data exported from the spectrometer.

For all experiments, chemicals were used as supplied straight from the source bottle, without pretreatment. Chemicals were obtained from Skylighter Pyrotechnic Supply, except for the strontium peroxide, barium peroxide, and copper(I) chloride. The strontium and barium peroxides were obtained from Firefox Enterprises, and the copper(I) chloride was obtained from Acros Organics. The compositions were prepared by first passing the components through a 100-mesh sieve, to break up any clumps.[16,17] Components that were too coarse to pass a 100-mesh sieve, were reduced with an alumina mortar and pestle, and then passed through the sieve. To achieve homogeneous mixtures, components were shaken in a 500 mL Velostat™ antistatic container, and then passed through the sieve. This procedure was repeated 3 times. Blended components were stored in airtight high-density polyethylene bottles. The formulas chosen for testing will be described in the Results section.

The samples were compacted into pellets for the data collection procedure. Cylindrical pellets were formed having a diameter of 3/8 inch (9.5 mm), and sufficient composition was used to form cylinders 3/8 inch (9.5 mm) in length. The samples were hydraulically pressed at 1000 psi (145 kPa), with 110 pounds (50 kg) of force applied to the ram. To facilitate consolidation, the compositions were dampened with 2% by weight distilled water. After ejection from the die, the pellets were allowed to dry for at least 48 hours before being used.

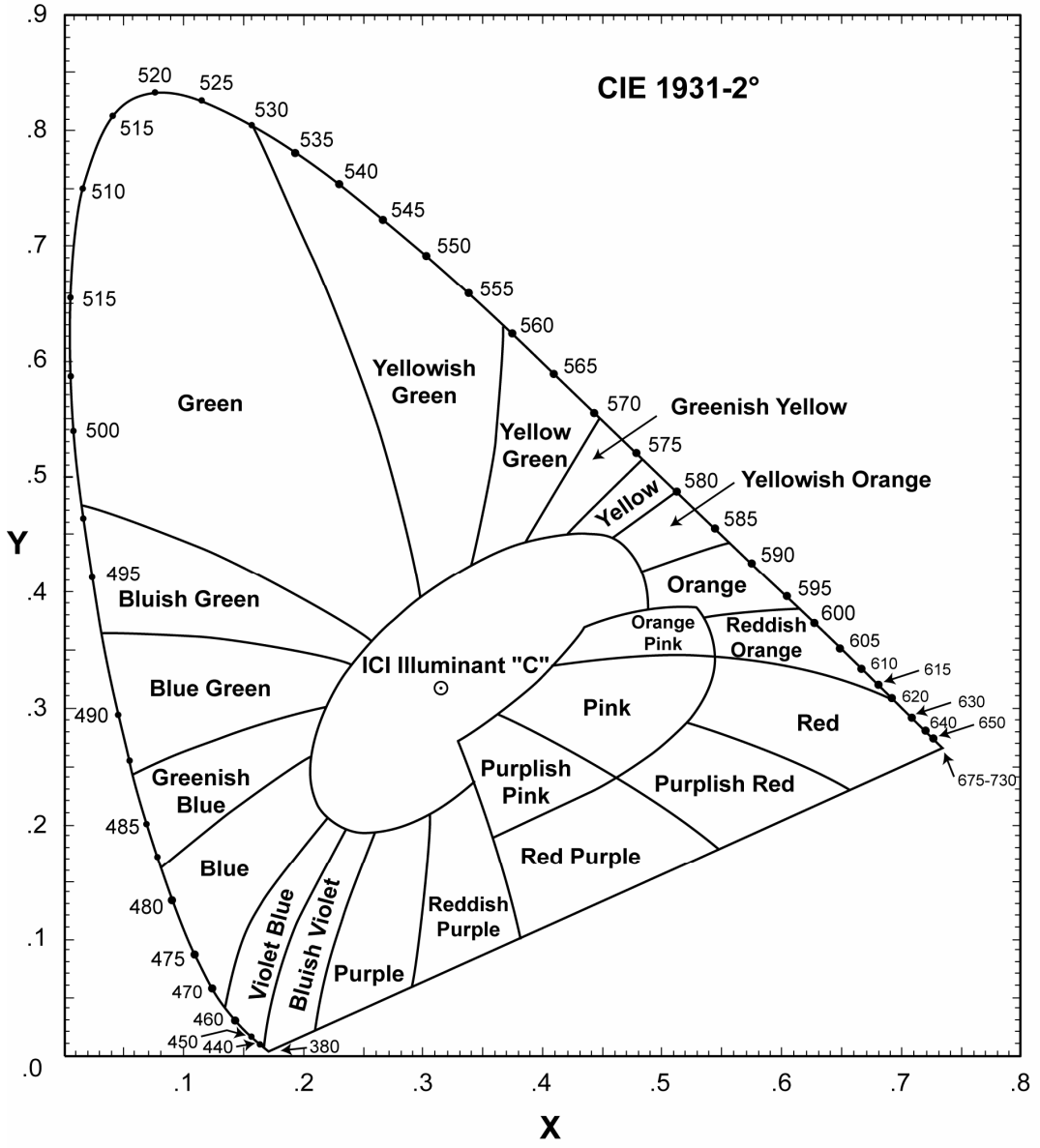

Figure 1. 1931 CIE Chromaticity Diagram. The sail-shaped area encompasses all colors visible to the human eye. The outside edge of the area defines perfect purity and complete saturation at a given wavelength. The straight line between the 700 nm right corner and the 380 nm left corner is the "nonspectral line" where purples, magentas, and other artificial red-blue blends are located. The "equal energy" (ICI Illuminant "C") point is located at x = 0.33, y = 0.33 and defines perfectly balanced white light.

The pellets tested were held above rather than set on a surface so that ash could fall away. They were ignited with a nichrome hotwire, so that remote ignition and collection were possible. Once a stable burn was achieved, the sample spectra were frozen and recorded. The chamber they were burned in was painted flat black to avoid reflections, as was the tunnel between the sampling lens and the chamber. Also, a cross-flow ducting system was constructed that carried the smoke away to avoid attenuation by the particulate matter. It was also hoped that the moving air would further simulate an operational condition. The airflow velocity was not measured, though a rough estimate would be 3 to 5 feet (1–2 m) per second.

Sensitivity Testing

Drop hammer impact sensitivity tests were performed on the 17 standard color formulas. The samples for impact sensitivity testing were taken from the larger samples blended for spectral acquisition. Samples were not desiccated prior to testing, which would certainly have caused them to be more sensitive. Also, to consolidate the sample and then granulate the material before testing would give an interesting comparison with the values reported here. The impact tester employed complied with the Modified Type 12 Impact Tool description.[18] The drop height results are reported as an H_{50}, which gives the height at which a 2.5 kg mass dropped on the sample has a 50% chance of initiating the sample. The Bruceton Up-Down calculation method was used to obtain the H_{50} values.[18]

Results and Discussion

Standard Formulas Tested

Compositions tested were in two series: a series of known traditional formulas, and a series of experimental color formulas. For the known traditional formulas, some of the literature central in the field[1,6,7,16,19–23] was surveyed to identify classes of formulas for the primary additive colors of red, green, and blue. For example, there are numerous formulas for red fire both accepted and proposed, but a majority of those formulas belong to 6 major types or classes. Six classes of green and five classes of blue were identified. There are indeed some color formulas that do not fit perfectly in any of these classes, but they are a minority and are reserved for future treatment.

The major red classes identified are:

1) $SrCO_3$ and $KClO_4$, with no metal fuel
2) $SrCO_3$ and $KClO_4$, with metal fuel
3) $SrCO_3$ and $KClO_3$, with no metal fuel
4) $SrCO_3$ and $KClO_3$, with metal fuel
5) $Sr(NO_3)_2$, with metal fuel
6) $SrCO_3$ and NH_4ClO_4

Note: a table of chemical formulas and chemical names is included at the end of this article.

	Red Flame Formulas					
Symbol →	●	○	▼	▽	■	□
Chemical↴	1	2	3	4	5	6
$KClO_4$	66	54				
$KClO_3$			70	58.5		
NH_4ClO_4						41
$K_2Cr_2O_7$						1.9
$Sr(NO_3)_2$					55	
$SrCO_3$	12	10	15	9.8		9.5
Al				19.5		
Mg					28	
Mg/Al		14				
Mg(coated)						33.3
PVC	2				17	
Parlon™		13				
Red Gum	13	4	10			9.5
Lampblack	2					
Airfloat C				2.4		
Dextrin	5	5	4	4.9		4.8
Shellac				4.9		
Reference	6	16	16	19	16	6

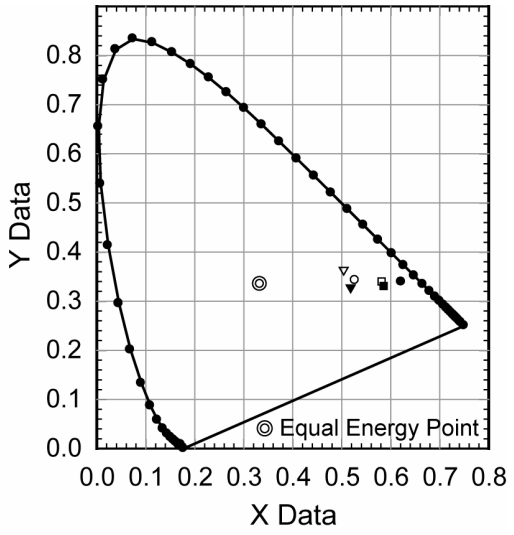

Figure 2. Red flame formula performances.

Table 1a. Chromaticity Coordinates of Standard Red Compositions.

Formula	Symbol	x-Coordinate	y-Coordinate
1	●	0.622	0.339
2	○	0.528	0.342
3	▼	0.518	0.328
4	▽	0.504	0.364
5	■	0.585	0.331
6	□	0.581	0.340

The red flame formulas were processed and tested, and their performance plotted on a chromaticity diagram shown in Figure 2. Their chromaticity coordinates are given in Table 1a. The equal energy point at (x,y) = (0.33,0.33) shows the location of perfect white on the diagram. The outside boundary of the diagram defines perfect saturation at that color. Thus, it can be seen that the best performing composition in terms of color purity is red formula 1, denoted by the solid circle, while the worst is red formula 4, which is denoted by the open triangle.

The major green classes identified are:

7) $Ba(NO_3)_2$, with metal fuel

8) $Ba(NO_3)_2$ and $KClO_4$, with no metal fuel

9) $Ba(NO_3)_2$ and $KClO_4$, with metal fuel

10) $Ba(ClO_3)_2$ and $BaCO_3$, with no metal fuel

11) $BaCO_3$ and NH_4ClO_4

12) $Ba(ClO_3)_2$, with no metal fuel

	Green Flame Formulas					
Symbol→	●	○	▼	▽	■	□
Chemical↴	7	8	9	10	11	12
$KClO_4$		47.2	10			
$Ba(ClO_3)_2$				72		87.8
NH_4ClO_4					41	
$K_2Cr_2O_7$					1.9	
$Ba(NO_3)_2$	55	28.3	50			
$BaCO_3$				4	9.5	
Mg	16					
Mg/Al			13			
Mg(coated)					33.3	
PVC	29					
Parlon™		4.7	15			
Red Gum		14.2	7	12	9.5	
Airfloat C				8		
Dextrin		5.6	5	4	4.8	2.45
Shellac						9.75
Reference	16	6	16	16	6	20

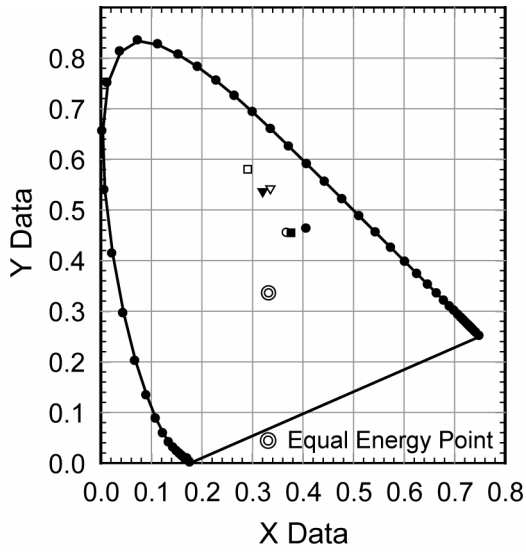

Figure 3. Green flame formula performances.

Table 1b. Chromaticity Coordinates of Standard Green Compositions.

Formula	Symbol	x-Coordinate	y-Coordinate
7	●	0.408	0.462
8	○	0.369	0.454
9	▼	0.320	0.537
10	▽	0.336	0.542
11	■	0.376	0.455
12	□	0.291	0.580

The green flame formulas were tested, and their chromaticity coordinates are shown in Figure 3 and listed in Table 1b. Formula 12 displayed the best color purity followed closely by green formula 10. Formulas 10 and 12 were both of the same type; that is, a barium chlorate formula having no metal fuel. The poorest performing green flame composition was green formula 7.

The major blue classes identified are:

13) $KClO_4$ based, with no metal fuel

14) $KClO_4$ based, with metal fuel

15) $KClO_3$ based, with no metal fuel

16) $KClO_3$ based, with metal fuel

17) NH_4ClO_4 based

The performances of the blue flame formulas are shown in Figure 4, and their chromaticity coordinates are given in Table 1c. The two best formulas tested were 14 and 17. Formula 14 is the blue primary from the Veline color system, while 17 is a formula including ammonium perchlorate. The lowest performance for a blue formula was recorded for blue formula 15.

Impact Sensitivities

The results of the standard formula impact sensitivity testing are shown in Table 2. For points of reference, on impact machines with the same tooling and falling mass, trinitrotoluene (TNT) has an H_{50} of 100 cm, and pentaerythritol tetranitrate (PETN) has an H_{50} of 17 cm.[24] TNT is widely regarded as a relatively safe secondary explosive in terms of handling, while PETN is deemed the most sensitive secondary explosive, bordering on classification as a primary explosive. From the results, it is not obvious that potassium chlorate or barium chlorate based formulas are more sensitive than formulas with other oxidizers. In fact, the most sensitive formulas appear to be those with ammonium perchlorate. The least sensitive seem to be based on metal nitrates such as barium and strontium nitrate. It is highly likely that friction sensitivity would show potassium chlorate and barium chlorate formulas are the most sensitive, but that will be left for future work.

Experimental Formulas Tested

To show the change in color quality as a function of composition, suitable formulas were chosen for further study. Formula 2 was chosen for experiments with the color red, formula 8 for the color green, and formula 13 for the color blue. With these formulas, the fuel to oxidizer ratio, chlorine donor percentage, colorant percentage and colorant source were varied and spectral and chromatic performance data were collected.

	Blue Flame Formulas				
Symbol→	●	O	▼	▽	■
Chemical↴	13	14	15	16	17
$KClO_4$	66.5	55			39
$KClO_3$			54.2	68	
NH_4ClO_4					29
CuO	13.4	15			
Shellac			1.7		
$CuCO_3$					14
Mg/Al		6			
Al			13.6		
Paris Green			27.1	22	
Colophony Resin				6	
Parlon™	5.4	15			
Red Gum	9.9	9			14
Dextrin	4.8	4	3.4	4	4
Reference	6	22	19	16	16

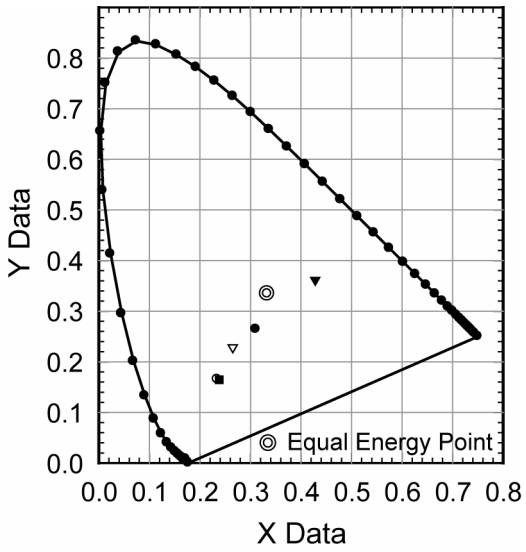

Figure 4. Blue flame formula performances.

Table 1c. Chromaticity Coordinates of Standard Blue Compositions.

Formula	Symbol	x-Coordinate	y-Coordinate
13	●	0.311	0.264
14	O	0.235	0.165
15	▼	0.428	0.362
16	▽	0.265	0.229
17	■	0.238	0.165

Table 2. Impact Sensitivity of Compositions.

Formula	Color Effect	Oxidizer, Fuel	H_{50} (cm)
1	Red	$KClO_4$, Red Gum	49
2	Red	$KClO_4$, Mg/Al	30
3	Red	$KClO_3$, Red Gum	83
4	Red	$KClO_3$, flake Al	58
5	Red	$Sr(NO_3)_2$, Mg	229
6	Red	NH_4ClO_4, Mg	23
7	Green	$Ba(NO_3)_2$, Mg	> 300
8	Green	$KClO_4$, $Ba(NO_3)_2$, Red Gum	86
9	Green	$KClO_4$, $Ba(NO_3)_2$, Mg/Al	42
10	Green	$Ba(ClO_3)_2$, Red Gum	37
11	Green	NH_4ClO_4, Mg	26
12	Green	$Ba(ClO_3)_2$, Shellac	34
13	Blue	$KClO_4$, Red Gum	32
14	Blue	$KClO_4$, Mg/Al	34
15	Blue	$KClO_3$, flake Al	180
16	Blue	$KClO_3$, Colophony Resin	57
17	Blue	NH_4ClO_4, Red Gum	34

Red Formula Experiments

The experimental formula variations begin with the fuel to oxidizer ratio experiments, starting with red formula 2. The fuel to oxidizer ratio experiments were undertaken to assess the effect of excess oxygen in a formula, as well as excess fuel. The chromaticity coordinates of the experimental mixtures are shown in Figure 5. One would expect the coordinates to lie on a straight line connecting the equal energy point and the point on the saturated border corresponding to the overall hue. This would be because color quality mainly depends on the balance between desirable emitters and undesirable broadband radiators. While there is some semblance of a linear positioning, the formula with the lowest oxidizer content moved towards the yellow region. This is likely because organics released from the fuel-rich pellet were burning in the air with a typical yellow hydrocarbon flame caused by incandescent soot.

Variation of Oxidizer to Fuel Ratio Based on Red Formula 2.

	Red Oxidizer to Fuel Ratio - ROFX				
Symbol→	O	▼	●	▽	■
Chemical↴	1	2	**Orig.**	3	4
$KClO_4$	37.0	46.8	54.0	59.5	63.8
Mg/Al	19.2	16.2	14.0	12.3	11.0
Parlon™	17.8	15.1	13.0	11.5	10.2
$SrCO_3$	13.7	11.5	10.0	8.8	7.9
Dextrin	6.9	5.8	5.0	4.4	3.9
Red Gum	5.5	4.6	4.0	3.5	3.1

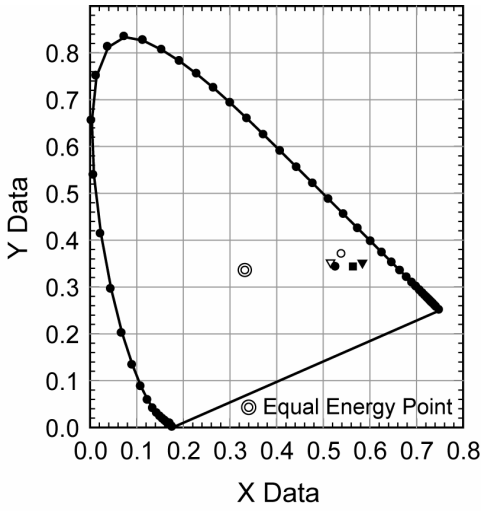

Figure 5. Red oxidizer to fuel ratio experimental composition performances.

Table 3. Chromaticity Coordinates for Oxidizer to Fuel Ratio Experimental Red Compositions. [ROFX-#]

Oxidizer (%)	Symbol	x-coordinate	y-coordinate
37.0	O	0.539	0.371
40.8	▼	0.584	0.352
54.0	●	0.528	0.342
59.5	▽	0.516	0.352
63.8	■	0.564	0.344

The next experiments performed were variations of the chlorine donor content. Those spectra are shown in Figure 6, and the chromaticity results are shown in Figure 7. Note that the peak at 606 nm is due to SrOH emissions. As the amount of chlorine in the flame increases, the SrOH is converted to SrCl. However, it seems that as long as some chlorine is present, the performance seems to be about the same.

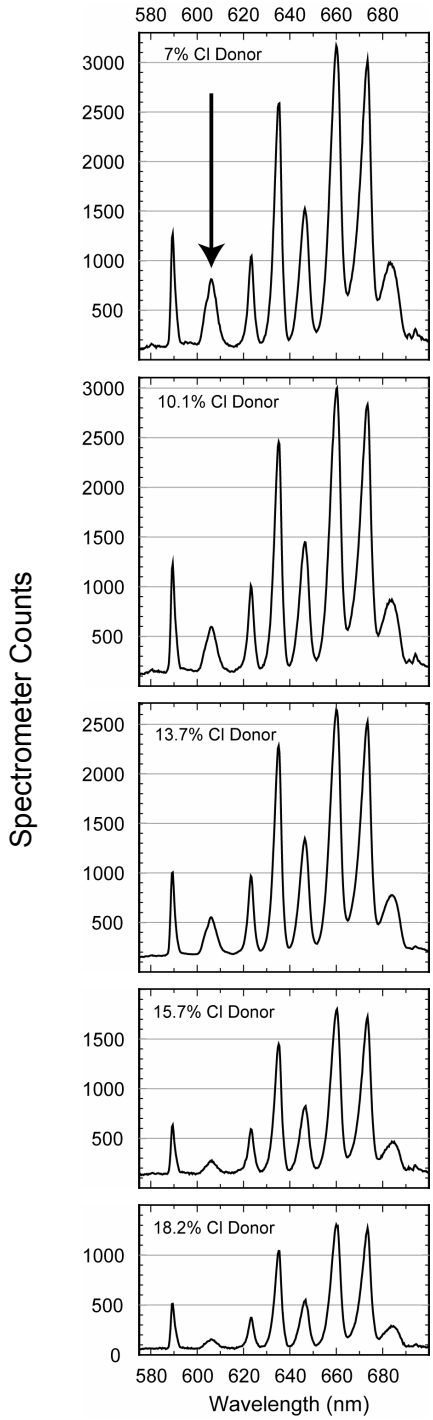

Figure 6. Spectra of red chlorine donor ratio experiments. The top spectrum, number 1, is of the mixture RCDX1, with the least chlorine donor. Spectrum 5, at the bottom, is of RCDX4, with the highest fraction of chlorine donor. Note the gradual suppression of the SrOH peak at 606 nm as more chlorine is present in the flame. The chromaticity points computed from these spectra are shown in Figure 7.

Variation of Chlorine Donor Percentage Based on Red Formula 2.

	Red Chlorine Donor % - RCDX-				
Symbol→	O	▼	●	▽	■
Chemical↴	1	2	**Orig.**	3	4
Parlon™	7.0	10.1	13.0	15.7	18.2
$KClO_4$	57.8	55.8	54.0	52.4	50.8
Mg/Al	15.0	14.5	14.0	13.6	13.2
$SrCO_3$	10.7	10.3	10.0	9.7	9.4
Dextrin	5.3	5.1	5.0	4.8	4.7
Red Gum	4.3	4.1	4.0	3.9	3.8

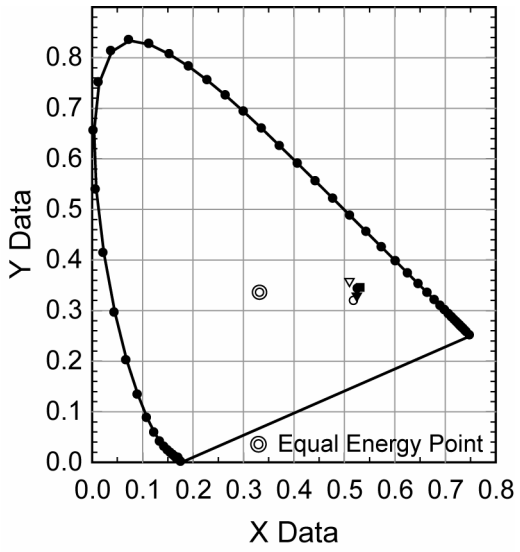

Figure 7. Red chlorine donor percentage experimental composition performances.

Table 4. Chromaticity Coordinates for Percentage Chlorine Donor for Experimental Red Compositions. [RCDX-#]

Chlorine Donor (%)	Symbol	x-coordinate	y-coordinate
7.0	O	0.520	0.520
10.1	▼	0.525	0.525
13.0	●	0.528	0.528
15.7	▽	0.510	0.510
18.2	■	0.531	0.531

The amount of colorant in the formula was then varied, and the results of those experiments are shown in Figure 8. Interpreting these results, the amount of colorant in a formula is indeed

Variation of Colorant Percentage Based on Red Formula 2.

	Red Colorant % – RCPX-				
Symbol→	O	▼	●	▽	■
Chemical↴	1	2	**Orig.**	3	4
$SrCO_3$	5.3	7.7	10.0	12.2	14.3
$KClO_4$	56.8	55.4	54.0	52.7	51.4
Mg/Al	14.8	14.4	14.0	13.7	13.4
Parlon™	13.6	13.3	13.0	12.6	12.3
Dextrin	5.3	5.2	5.0	4.9	4.8
Red Gum	4.2	4.1	4.0	3.9	3.8

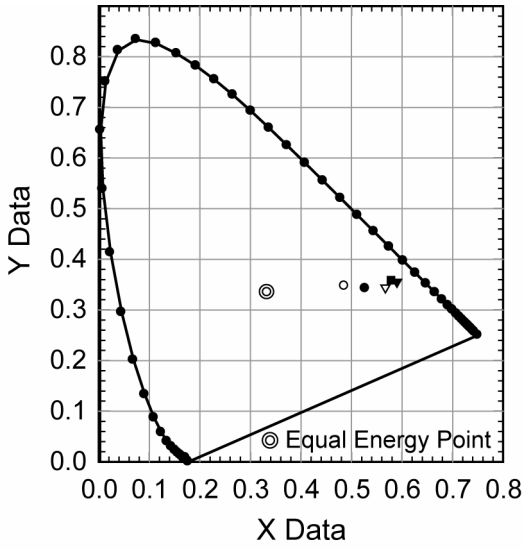

Figure 8. Red colorant percentage experimental composition performances.

Table 5. Chromaticity Coordinates for Percentage Colorant for Experimental Red Compositions. [RCPX-#]

Colorant (%)	Symbol	x-coordinate	y-coordinate
5.3	O	0.486	0.347
7.7	▼	0.590	0.355
10.0	●	0.528	0.342
12.2	▽	0.567	0.344
14.3	■	0.578	0.359

important; however, once a certain amount is attained, adding more does not improve performance. Once the amount of colorant in the formula was at or above the level in the original formula, the color performance changes were very slight. A likely reason for this is that as more colorant is added, the heat generated by the fuel and oxidizer is lost in melting and vaporizing excess colorant, cooling the flame below the optimum temperature for the emitting species excitation.

Finally, the effect of changing the source of colorant was explored, and the results of those experiments are shown in Figure 9. The mass percentage of each colorant source was determined by calculating the mass required to offer the same number of moles of colorant atoms as the number that the reference colorant supplied. Strontium chloride and strontium peroxide appear to act as very good strontium donors. Strontium carbonate and strontium nitrate both had similar performance.

Variation of Colorant Source Based on Red Formula 2.

	Red Colorant Source – RCSX-				
Symbol→	O	▼	●	▽	■
Chemical↴	1	2	**Orig.**	3	4
$KClO_4$	50.0	52.8	54.0	51.9	55.0
Mg/Al	13.0	13.7	14.0	13.5	14.3
Parlon™	12.0	12.7	13.0	12.5	13.2
Dextrin	4.7	4.9	5.0	4.8	5.1
Red Gum	3.7	3.9	4.0	3.8	4.0
$SrCl_2$	16.6				
$SrSO_4$		12.0			
$SrCO_3$			10.0		
$Sr(NO_3)_2$				13.5	
SrO_2					8.3

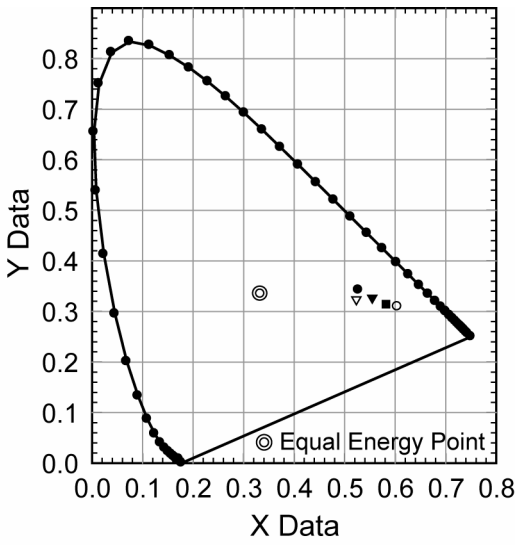

Figure 9. Red colorant source experimental composition performance.

Table 6. Chromaticity Coordinates for Colorant Source for Experimental Red Compositions. [RCSX-#]

Colorant	(%)	Symbol	x-coordinate	y-coordinate
$SrCl_2$	7.0	O	0.605	0.309
$SrSO_4$	10.1	▼	0.555	0.327
$SrCO_3$	13.0	●	0.528	0.342
$Sr(NO_3)_2$	15.7	▽	0.523	0.323
SrO_2	18.2	■	0.582	0.314

Green Formula Experiments

Green formula 8 was treated in the same way, and results of the oxidizer experiments are shown in Figure 10. As with the red experiments, the excess fuel burning in the air drove the lowest oxidizer mixture towards the yellow region. The rest of the formulas formed a line, between a point in the pale yellow, stretching towards the green region.

Variation of Oxidizer to Fuel Ratio Based on Green Formula 8.

	Green Oxidizer to Fuel Ratio - GOFX				
Symbol→	O	▼	●	▽	■
Chemical↴	1	2	**Orig.**	3	4
$KClO_4$	30.9	40.1	47.2	52.8	57.3
$Ba(NO_3)_2$	37.0	32.1	28.3	25.3	22.9
Red Gum	18.6	16.1	14.2	12.7	11.5
Dextrin	7.3	6.3	5.6	5.0	4.5
Parlon™	6.1	5.3	4.7	4.2	3.8

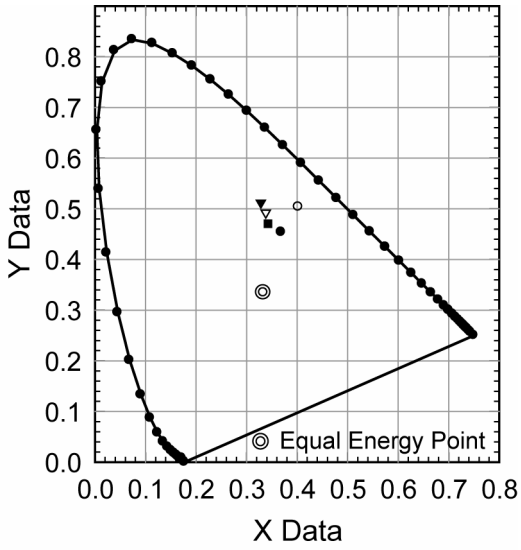

Figure 10. Green oxidizer to fuel ratio experimental composition performances.

Table 7. Chromaticity Coordinates for Oxidizer to Fuel Ratio Experimental Green Compositions. [GOFX-#]

Oxidizer (%)	Symbol	x-coordinate	y-coordinate
30.9	O	0.404	0.503
40.1	▼	0.328	0.512
47.2	●	0.369	0.454
52.8	▽	0.338	0.492
57.3	■	0.342	0.470

When the chlorine donor amount was varied, the cluster showed a very slight trend with the greatest color quality corresponding to the mixture containing the most chlorine donor. These results are shown in Figure 11.

Variation of Chlorine Donor Percentage Based on Green Formula 8.

	Green Chlorine Donor Ratio - GCDX				
Symbol→	O	▼	●	▽	■
Chemical↴	1	2	**Orig.**	3	4
Parlon™	2.4	3.6	4.7	5.8	6.9
$KClO_4$	52.1	47.7	47.2	46.6	46.1
$Ba(NO_3)_2$	29.0	28.6	28.3	28.0	27.7
Red Gum	14.5	14.4	14.2	14.0	13.9
Dextrin	5.8	5.7	5.6	5.6	5.5

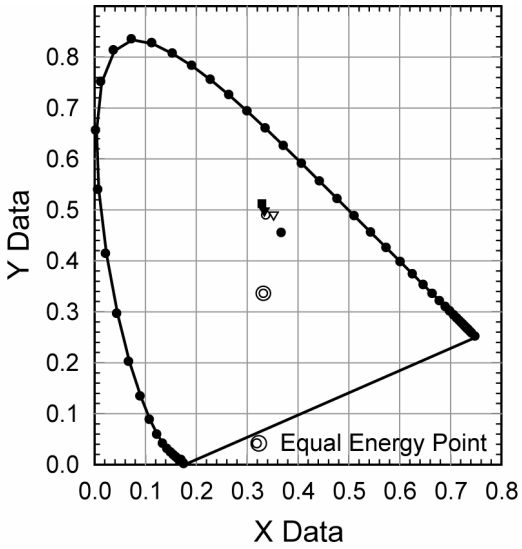

Figure 11. Green chlorine donor percentage experimental composition performances.

Table 8. Chromaticity Coordinates for Chlorine Donor Percentage Experimental Green Compositions. [GCDX-#]

Chlorine Donor (%)	Symbol	x-coordinate	y-coordinate
2.4	O	0.339	0.488
3.6	▼	0.334	0.498
4.7	●	0.369	0.454
5.8	▽	0.352	0.490
6.9	■	0.329	0.512

The amount of colorant was varied, and the results from these experiments are shown in Figure 12. As can be seen, there is not a great deal of order to the results, possibly indicating that there is not a great dependence of color performance on the amount of colorant.

Variation of Colorant Percentage Based on Green Formula 8.

	Green Colorant Ratio - GCPX				
Symbol→	O	▼	●	▽	■
Chemical↴	1	2	**Orig.**	3	4
$Ba(NO_3)_2$	16.5	22.8	28.3	33.0	37.2
$KClO_4$	54.9	50.8	47.2	44.1	41.3
Red Gum	16.5	15.3	14.2	13.3	12.4
Dextrin	6.5	6.0	5.6	5.2	4.9
Parlon™	5.5	5.1	4.7	4.4	4.1

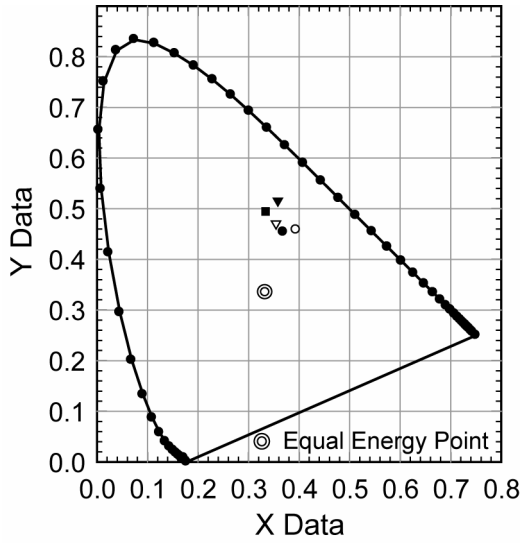

Figure 12. Green colorant percentage experimental composition performances.

Table 9. Chromaticity Coordinates for Colorant Percentage Experimental Green Compositions. [GCPX-#]

Colorant (%)	Symbol	x-coordinate	y-coordinate
16.5	O	0.394	0.458
22.8	▼	0.358	0.516
28.3	●	0.369	0.454
33.0	▽	0.354	0.471
37.2	■	0.334	0.494

The source of colorant was varied, and spectra collected and analyzed. The results of these experiments are shown in Figure 13. As in the

Variation of Colorant Source Based on Green Formula 8.

	Green Colorant Source - GCSX				
Symbol→	O	▼	●	▽	■
Chemical↴	1	2	**Orig.**	3	4
$KClO_4$	48.1	50.7	47.2	48.6	52.4
Red Gum	14.5	15.3	14.2	14.6	15.8
Dextrin	5.7	6.0	5.6	5.8	6.2
Parlon™	4.8	5.1	4.7	4.9	5.3
$BaCl_2$	26.9				
$BaCO_3$		22.9			
$Ba(NO_3)_2$			28.3		
$BaSO_4$				26.1	
BaO_2					20.4

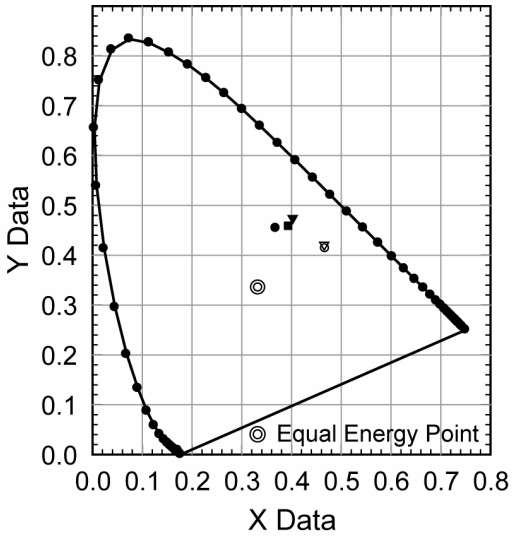

Figure 13. Green colorant source experimental composition performances.

Table 10. Chromaticity Coordinates for Colorant Source Green Compositions. [GCPX-#]

Colorant	(%)	Symbol	x-coordinate	y-coordinate
$BaCl_2$	16.5	O	0.369	0.454
$BaCO_3$	22.8	▼	0.469	0.413
$Ba(NO_3)_2$	28.3	●	0.403	0.474
$BaSO_4$	33.0	▽	0.466	0.421
BaO_2	37.2	■	0.393	0.459

experiments with the red flame formulas, there is obviously a large dependence for performance on the source of colorant used. The barium nitrate, carbonate, and peroxide performed well, while the barium sulfate and chloride were poor. This is in contrast to the experiments with red, where the strontium chloride offered good performance. The reason for this may lie in the fact that the melting and boiling points of the barium chloride are both 100 °C or more higher than the same physical state changes for the strontium salt. Barium chlorate was shown to be an excellent source of colorant, as its decomposition creates $BaCl_2$. This is a different case than introducing solid crystalline $BaCl_2$ because the decomposition product is already at high temperature and needs little additional energy to decompose into the barium monochloride emitting molecule.

Blue Formula Experiments

Starting with formula 13 for blue, the oxidizer experiments were repeated, and those results are shown in Figure 14. The results indicate a very definite trend in color quality, increasing as the amount of oxidizer is increased. This may, however, have more to do with the poor oxygen balance generating a cooler flame, than the effect of excess oxygen in the flame envelope.

Variation of Oxidizer to Fuel Ratio Based on Blue Formula 13.

	Blue Oxidizer to Fuel Ratio - BOFX				
Symbol→	O	▼	●	▽	■
Chemical↴	1	2	**Orig.**	3	4
$KClO_4$	49.9	59.8	66.5	71.3	74.9
CuO	20.0	16.1	13.4	11.5	10.0
Red Gum	14.8	11.9	9.9	8.5	7.4
Parlon	8.1	6.5	5.4	4.6	4.0
Dextrin	7.2	5.7	4.8	4.1	3.6

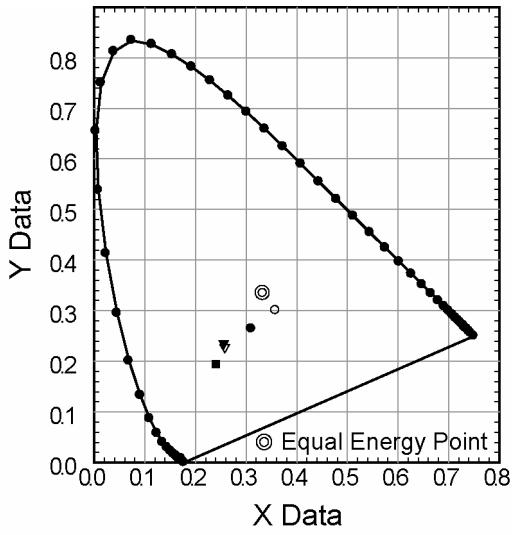

Figure 14. Blue oxidizer to fuel ratio experimental composition performances.

Table 11. Chromaticity Coordinates for Oxidizer to Fuel Ratio for Experimental Blue Compositions. [BOFX-#]

Oxidizer (%)	Symbol	x-coordinate	y-coordinate
49.9	O	0.359	0.300
59.8	▼	0.256	0.235
66.5	●	0.311	0.264
71.3	▽	0.258	0.228
74.9	■	0.240	0.194

When the chlorine donor experiments were conducted, they gave results that did not show a change in performance until the highest increment of chlorine donor, which gave a very much better flame than the other four mixtures, see Figure 15. This may be enough extra material in the mixture to cool the flame, or it may simply show the importance of chlorine availability to the formation of CuCl.

Variation of Chlorine Donor Percentage Based on Blue Formula 13.

	Blue Chlorine Donor % - BCDX				
Symbol→	○	▼	●	▽	■
Chemical↴	1	2	**Orig.**	3	4
Parlon	2.8	4.1	5.4	6.7	7.9
$KClO_4$	68.3	67.4	66.5	65.6	64.7
CuO	13.8	13.6	13.4	13.2	13.0
Red Gum	10.2	9.8	9.9	9.8	9.6
Dextrin	4.9	4.7	4.8	4.7	4.7

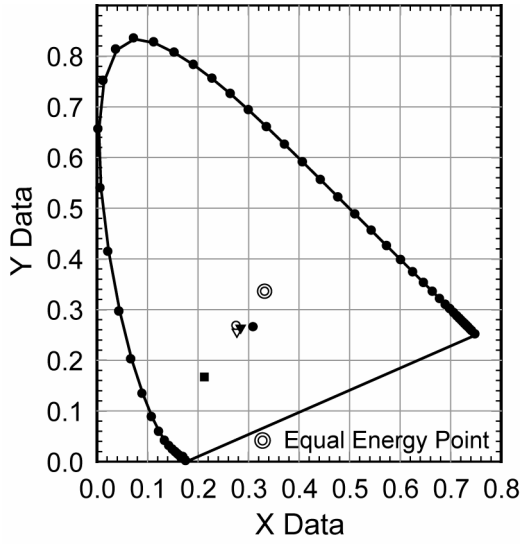

Figure 15. Blue chlorine donor ratio experimental composition performances.

Variation of Colorant Percentage Based on Blue Formula 13.

	Blue Colorant % - BOFX				
Symbol→	○	▼	●	▽	■
Chemical↴	1	2	**Orig.**	3	4
CuO	7.2	10.4	13.4	16.2	18.8
$KClO_4$	71.1	68.6	66.5	64.2	62.2
Red Gum	10.6	10.2	9.9	10.2	9.3
Parlon	5.8	5.6	5.4	5.6	5.1
Dextrin	5.1	5.0	4.8	5.0	4.5

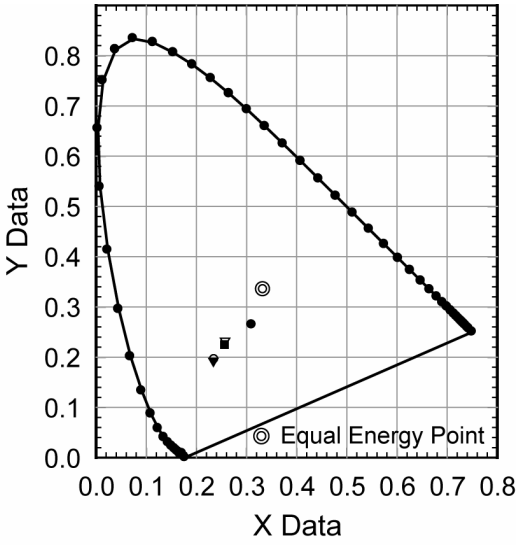

Figure 16. Blue colorant ratio experimental composition performances.

Table 12. Chromaticity Coordinates for Chlorine Donor Percentage for Experimental Blue Compositions. [BCDX#]

Chlorine Donor (%)	Symbol	x-coordinate	y-coordinate
2.8	○	0.277	0.267
4.1	▼	0.284	0.264
5.4	●	0.311	0.264
6.7	▽	0.277	0.256
7.9	■	0.213	0.167

Table 13. Chromaticity Coordinates for Colorant Percentage for Experimental Blue Compositions. [BCPX-#]

Colorant (%)	Symbol	x-coordinate	y-coordinate
7.2	○	0.237	0.195
10.4	▼	0.234	0.192
13.4	●	0.311	0.264
16.2	▽	0.257	0.232
18.8	■	0.256	0.225

When the amount of colorant was varied, as shown in Figure 16, the results were again curious. The data indicates, in general, that a smaller amount of colorant may allow slightly better performance than more colorant would allow. If cooling the flame to limit CuCl dissociation were important, it seems as though the larger amounts of colorant would also serve that purpose.

Experiments were carried out where the colorant source was changed, and those results are plotted in Figure 17. In these experiments, the copper oxychloride served as the best chlorine

donor, followed by the copper sulfate. Interestingly, copper oxide and copper carbonate, both commonly used donors, were not among the best performers. These results may not be observed for other formulas, however.

Variation of Colorant Source Based on Blue Formula 13.

	Blue Colorant Source - BCSX				
Symbol→	O	▼	●	▽	■
Chemical↴	1	2	**Orig.**	3	4
$KClO_4$	53.6	63.2	66.5	51.6	64.2
Red Gum	8.0	9.4	9.9	7.7	9.6
Parlon	4.3	5.1	5.4	4.2	5.2
Dextrin	3.9	3.9	4.8	3.7	4.6
Cu_2CO_3	30.1				
CuOCl		17.5			
CuO			13.4		
$CuSO_4$				32.7	
CuCl					16.2

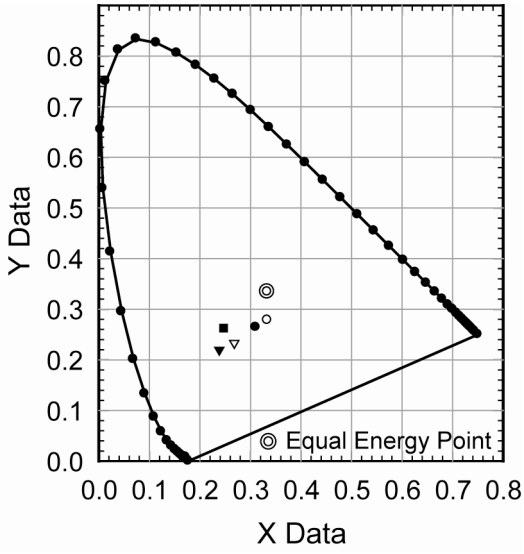

Figure 17. Blue colorant source experimental composition performances.

Colorant	(%)	Symbol	x-coordinate	y-coordinate
Cu_2CO_3	16.5	O	0.334	0.278
CuOCl	22.8	▼	0.238	0.219
CuO	28.3	●	0.311	0.264
$CuSO_4$	33.0	▽	0.268	0.233
CuCl	37.2	■	0.247	0.263

Conclusions

Experiments such as these, varying mixture components and attempting to draw conclusions based on the results, are difficult. In pyrotechnic formulas, many components serve two roles, as most chlorine donors are also fuels. Almost all binders serve as fuels, and some colorants serve as oxidizers. Some oxidizers bring with them chlorine. In these cases, to attempt to vary only the oxidizer and fuel balance, while keeping the chlorine and colorant content constant, is very difficult, and impossible in most cases.

Even more difficult, is the collection of spectra that fairly represent the mixture performance. When burned in a static fashion, pellets shed virtually none of the ash generated. The resultant effect is that the ash is heated to incandescence, diluting the color of the flame. This would not be an issue were the pellet functioning as an aerial shell star—moving at high velocity and tumbling while moving through air. In this case, the ash and smoke would be stripped away to a much larger extent than in static testing. Another difference between static testing and true performance lies in the chemistry of the flame envelope. As a burning pellet moves through the air, oxygen diffuses into the flame envelope much more effectively than in static testing. Also, the flame envelope will be at a somewhat lower temperature in true performance because of the cooling effect on the flame envelope of the high velocity air moving past the pellet and flame envelope. Even with these test conditions built into a testing rig, good data collection was difficult, as the flame envelope tended to dance and move, giving a spectrum with relative peak intensities that were constantly changing with time.

With these shortcomings recognized, there are conclusions that can be drawn from the experiments conducted:

- The most important single component contributing to good spectral performance was the selection of colorant source.
- The oxidizer content of the mixture, amount of colorant, and amount of chlorine donor are secondary in determination of color quality.

- With some exceptions, as long as the mixture will support combustion, it also seems to be able to generate colored light.
- There are chemical equations that illustrate equilibria important in color flame chemistry, for example:

$$CuCl + O \Leftrightarrow CuO + Cl$$

$$BaCl + O \Leftrightarrow BaO + Cl$$

$$SrCl + O \Leftrightarrow SrO + Cl$$

These show the effect of oxygen in the flame on the desired emitters. When excess oxygen (radical or molecular) is present, it is possible that a collision with a metal monochloride emitter will destroy the emitter and form an oxide, which may emit as an undesirable molecular emitter, or condense and emit as an even less desired broadband radiator. Analogous reactions can be represented as:

$$CuCl + Cl \Leftrightarrow CuCl_2$$

$$BaCl + Cl \Leftrightarrow BaCl_2$$

$$SrCl + Cl \Leftrightarrow SrCl_2$$

In these examples, chlorine in the flame envelope may interact destructively with the emitting species. However, for strontium, barium and copper, the boiling points of the chloride salts are many hundreds of degrees lower than the boiling points for the oxides. This would indicate that the chloride salts may stay as a vapor and decompose again to produce the monochlorides. However, once an oxide is formed, it is likely to condense into ash, which not only is *not* an effective color emitter but also *is* a destructive broadband emitter. Thus, the reasoning of the argument for maintaining a reducing flame, as well as a flame with a high level of available chlorine, seems obvious. While the experiments performed may not have clearly shown the dependence of color quality on these elements, it remains a logical goal in composition formulation.

Adjusting a mixture only to give the best quality of light has other pitfalls. Unrelated properties that a composition may possess, such as critical wind velocity, ease of ignition, ease of processing, safety, and cost are also important issues. A blue star that gives a pure blue color on the ground is useless, if it cannot be reliably ignited or does not support a robust combustion. In fact, some of the mixtures generated in this work were barely combustible. An interesting note: it was often possible to discern differences in color performance with the naked eye that were relatively close together on the chromaticity diagram. In fact, it was usually possible to determine with the eye approximately where the coordinates were going to fall. However, the ultimate usefulness of the spectrometer and the coordinates thus generated lie in the fact that they are definite and objective values, which can be recorded and archived for future reference. While the eye can typically tell one formula as being better than the next, the memory of those observations is subjective and will be suspect. Unless a candidate color formula is burned alongside a sample pellet of a previous formula, the observer's perception of the purity differences in those two formulas may be erroneous.

Outlook

Future work in this area may be done along several lines. First, constructing a test fixture to address some of the pitfalls of collecting this type of data would be a top priority. For instance, pressing core-burning pellets of color composition may provide a flame that is geometrically fixed and giving a spectrum that is easier to capture. Second, other chlorine donors could be evaluated by directly replacing the chlorine donor in a well-characterized formula. Presumably there would be an increase in flame color purity as a more efficient donor is introduced. Third, the development of a formula designed specifically for formula adjustments would be an interesting approach. As an example, chlorine donors such as PVC (polyvinylchloride), saran, and Parlon™ would not be used, but instead a chlorine donor such as ammonium chloride (NH_4Cl) could be used, which has less fuel value per chlorine atom. And finally, there are more colorant sources to sample and more types of formulas to investigate. Including the high nitrogen colors[25,26] or composite formula colors[27] would be worthwhile. It would also be interesting to obtain the chromaticity coordinates of a larger selection of well-established formulas.

Acknowledgement

Work presented here was conducted at the New Mexico Institute of Mining and Technology in Socorro, New Mexico.

References

1) H. Ellern, *Military and Civilian Pyrotechnics*, Chemical Publishing Co. Inc., New York, NY, 1968, pp 5, 97, 122–130.

2) B. E. Douda, "Theory of Colored Flame Production," RDTN No. 71 (1964), U.S. Naval Ammunition Depot, Crane, IN, USA.

3) B. E. Douda, "Emission Studies of Selected Pyrotechnic Flames," *Journal of the Optical Society of America*, Vol. 55, No. 7 (1965) pp 787–793.

4) T. Shimizu, *Selected Pyrotechnic Publications of Dr. Takeo Shimizu, Part 3, Studies on Fireworks Colored-Flame Compositions*, Journal of Pyrotechnics, 1999.

5) T. Shimizu, *Fireworks from a Physical Standpoint, by Dr. Takeo Shimizu, Part II* Pyrotechnica Publications, 1983.

6) T. Shimizu, *Fireworks, the Art, Science, and Technique*, Pyrotechnica Publications, 1981, pp 47-66, 214219.

7) A. P. Hardt, *Pyrotechnics*, Pyrotechnica Publications, 2001.

8) G. Herzberg, *Spectra of Diatomic Molecules*, 2nd ed., Van Nostrand Co., Inc., New York, NY, 1950.

9) G. Herzberg, *Electronic Spectra of Polyatomic Molecules*, Van Nostrand Co., Inc., Princeton, NJ, 1967.

10) R. C. Weast (Ed.) *Handbook of Chemistry and Physics*, 72nd ed., CRC Press, Cleveland, OH, 1991–1992.

11) W. Meyerriecks, "Comment on 'Composite Color Stars'", *Journal of Pyrotechnics*, No. 9 (1999) p. 62.

12) K. L. and B. J. Kosanke, "Development of a Video Spectrometer," *Journal of Pyrotechnics*, No. 7 (1998) pp 37–49.

13) C. Leeflang, "A Photometric Method of Analysis for Pyrotechnic Color Compositions," *Pyrotechnica No. XV* (1993) pp 46–57.

14) W. M. Meyerriecks and K. L. Kosanke, "Spectra of the Principal Emitters in Colored Flames", in preparation for publication in the *Journal of Pyrotechnics*.

15) Commission Internationale de l'Eclairage, 1931.

16) R. Lancaster, *Fireworks; Principles and Practice*, Chemical Publishing Co., Inc. New York, NY, 1992, pp 81–84, 113–135, 245–248.

17) J. H. McLain, *Pyrotechnics, from the Viewpoint of Solid State Chemistry*, Franklin Institute Press, Philadelphia, PA, 1980, pp 200–215.

18) *Transport of Dangerous Goods, Tests and Criteria*, 2nd ed., United Nations Publications, ST/SG/AC.10/11/Rev.1, New York, 1990.

19) T. L. Davis, *The Chemistry of Powder and Explosives*, Angriff Press, Las Vegas NV, 1943.

20) G. W. Weingart, *Pyrotechnics*, Chemical Publishing Co. Inc., New York, NY, 1947.

21) J. A. Conkling, *Chemistry of Pyrotechnics, Basic Principles and Theory*, Marcel Dekker, Inc., New York, NY, 1985, pp 150–165.

22) K. L. and B. J. Kosanke, and C. Jennings-White, *Lecture Notes for Pyrotechnic Chemistry*, Journal of Pyrotechnics (1997) p X-10.

23) A. A. Shidlovskiy, *Principles of Pyrotechnics*, 3rd ed., American Fireworks News, Dingmans Ferry, PA, USA, 1997, pp 162–172.

24) D. E. Chavez, M. A. Hiskey, and D. L. Naud, "High Nitrogen Fuels for Low-Smoke Pyrotechnics", *Journal of Pyrotechnics*, No. 10 (1999) pp 17–36.

25) P. W. Cooper and S. R. Kurowski, *Introduction to the Technology of Explosives*, Wiley-VCH, New York, New York, 1996, p88.

26) D. E. Chavez and M. A. Hiskey, "High Nitrogen Pyrotechnic Compositions," *Journal of Pyrotechnics*, No. 7 (1998) pp 11–14.

27) S. Anderson, "Composite Color Stars," *Journal of Pyrotechnics*, No. 8 (1998) pp 19–30.

List of Chemicals Used in Formulations in Text.

Chemical Name	Formula	Familiar Name/Formula
Abietic acid	$C_{20}H_{30}O_2$	Colophony Rosin
Aluminum	Al	
Ammonium perchlorate	NH_4ClO_4	AP
Amorphous carbon (pure)	C	Lamp Black
Barium carbonate	$BaCO_3$	
Barium chlorate	$Ba(ClO_3)_2{\cdot}H_2O$	
Barium chloride	$BaCl_2$	
Barium nitrate	$Ba(NO_3)_2$	
Barium peroxide	BaO_2	
Barium sulfate	$BaSO_4$	Barite
Carbon (with impurities)	C	Air Float Charcoal
Chlorinated isoprene rubber		Parlon™
Cupper(II) acetoarsenite	$Cu(C_2H_3O_2)_2{\cdot}3Cu(AsO_2)_2$	Paris Green
Copper(II) carbonate	$Cu_2(OH)_2CO_3$	Basic copper carbonate
Copper(I) chloride	CuCl	
Copper(II) oxide	CuO	
Copper(II) oxychloride	$Cu_2(OH)_3Cl$	Dicopper(II) chloride trihydroxide
Copper(II) sulfate	$CuSO_4$	Hydrocyanite
Cupric acetoarsenite	$Cu(C_2H_3O_2)_2{\cdot}3Cu(AsO_2)_2$	Paris Green
Dextrin	$(C_6H_{10}O_5)_n{\cdot}xH_2O$	Dextrin
Magnesium	Mg	
Magnesium with $K_2Cr_2O_7$	Mg (coated)	
Magnesium/aluminum alloy	Mg/Al	Magnalium
Polyvinyl chloride	$(C_2H_3Cl)_n$	PVC
Potassium chlorate	$KClO_3$	KC
Potassium dichromate	$K_2Cr_2O_7$	
Potassium perchlorate	$KClO_4$	KP
Shellac	$C_6H_{9.6}O_{1.6}$	Lac, Lacca
Strontium carbonate	$SrCO_3$	
Strontium chloride	$SrCl_2$	
Strontium nitrate	$Sr(NO_3)_2$	
Strontium peroxide	SrO_2	
Strontium sulfate	$SrSO_4$	
Xanthorrhea resin	$C_6H_{5.95}O_{2.63}N_{0.01}$	Red Gum, Accroides Resin

A Study of the Combustion Behaviour of Pyrotechnic Whistle Devices (Acoustic and Chemical Factors)

M. Podlesak* and M. A. Wilson**

*Weapons Systems Division, System Sciences Laboratory, DSTO, PO Box 1500, Edinburgh 5111, Australia

** Pains Wessex (Australia) Pty Ltd, PO Box 90, Lara 3212, Australia
Formerly of Weapons Systems Division, Aeronautical and Maritime Research Laboratory, DSTO, Melbourne, Australia

ABSTRACT

Pyrotechnic whistles have long been used in both civilian and military applications. It is known that, under certain conditions, these compositions burn in an oscillatory manner and have exhibited a tendency occasionally to explode with great power during combustion. Based on the results of experimental work and a study of the thermochemical properties of whistle fuels, a hypothesis is proposed that attempts to account for the observed high levels of explosive and acoustic power of pyrotechnic whistles. The formation of < 10 μm diameter hollow carbon spheres was observed in laboratory experiments involving the thermal decomposition of potassium benzoate (a whistle fuel) in a reducing atmosphere. At the moment of formation, the spheres may possibly be filled with combustible hydrocarbon gases and would be extremely reactive. If formed during the quiet cycles of an operating whistle device, their existence may explain the higher than expected acoustic power of pyrotechnic whistles. Such a hypothesis may also lead to an understanding of other hitherto unexplained explosions, where under conditions such as 'cook-off', the thermal decomposition of organic fuels used in some other pyrotechnics would result in the formation of new substances which are more reactive than the parent chemicals.

Keywords: whistle, combustion, acoustics, oscillating burning, pyrotechnics

1. Introduction

Pyrotechnic whistle compositions are usually formulations consisting of the salt of an aromatic acid such as potassium benzoate ($KC_7H_5O_2$) or sodium salicylate ($NaC_7H_5O_3$) as the fuel and a strong oxidant such as potassium perchlorate ($KClO_4$). When the powder mixture is consolidated and burnt as an open-faced pellet, it burns at a constant linear rate and emits virtually no sound. However, if the pressed composition is ignited at the bottom of a short tube, it burns in an oscillatory manner and emits a loud, high-pitch whistling sound.

Pyrotechnic whistles have been used in a number of military and civilian applications, however, it has long been known that whistles have a propensity to explode during combustion and have been responsible for serious injuries. As part of a study to reduce the hazards associated with the manufacture and use of whistles, an investigation was undertaken to determine the mechanism by which high intensity oscillatory sound is produced by the combustion of consolidated whistle formulations.

This is described in a more comprehensive report[1] where modern instrumentation techniques, including high speed video, were employed to examine the combustion characteristics of the whistle composition MRL(X) 418, which contains 30% potassium benzoate and 70% potassium perchlorate. In particular instances, comparisons were made between this composition and a US formulation, which incorporates sodium salicylate as the fuel.

In addition, it has been established through acoustic considerations that the energetic output of each cyclic pulse of a burning whistle device

is considerably greater than that expected from the thermochemical properties of the simple fuel-oxidiser system. Experimental evidence confirmed that when whistle composition was deliberately made to explode, sufficient energy was released to fragment the metal test cylinders into which it was filled. However, the projected fragments exhibited relatively large dimensions, with velocities not exceeding 100 m/s—factors indicating that detonation of the filling did not occur. When equal masses of other pyrotechnics, including flare composition and gunpowder (Black Powder) were similarly tested, no fragmentation of the cylinders was evident.[1]

These observations have led to the hypothesis that, under the specific conditions extant in the burning zone of a whistle device, highly reactive secondary fuels may be created through the thermal decomposition of the primary fuel. It is proposed that while these conditions occur during the quiescent phase of a burning whistle device, the resultant mass of reactants is limited by inherent physical control factors. However, should uncontrolled changes in the combustion surface geometry occur, the mass of these reactants can increase, leading to the explosion of the device.

2. Computer Modeling of Combustion

The NASA-Lewis CEC 76 computer code was used to predict the reaction products of a mixture of 70% $KClO_4$ and 30% $KC_7H_5O_2$ burning within a tube (i.e., in the absence of excess air). At atmospheric pressure, the predicted species consisted mainly of KCl, H_2O, CO_2 and CO; the latter two being in equal proportions. In an actual whistle device, it was questioned whether the subsequent reaction of hot CO in air at the tube mouth would generate sufficient acoustic energy to produce the oscillating sound inherent in this type of device.

To test this contention, a pyrotechnic whistle was ignited inside an open drum from which the air had been displaced with argon. When compared with an identical whistle burning in an air-filled drum, no difference in either frequency or amplitude could be discerned, inferring that the oscillatory sound is produced within the tube, and most likely, at the burning front.

3. Acoustic Model

The acoustic model presented here is approximate and quite simplistic in as far as the following assumptions were used:

- the model is based on linear acoustic theory (the model is less accurate for large amplitude waves),
- the acoustic propagation properties of the gas in the chimney of the whistle are homogenous,
- the effect of gas flow on the acoustic wave propagation is neglected,
- the free field impedance of the acoustic propagation medium inside and outside the chimney is nearly the same, and
- thermal and viscous losses are neglected in the propagation of acoustic waves.

Figure 1 provides the basic framework for understanding the proposed acoustic model of the whistle device. The acoustic behaviour of the device has been modelled on the classic quarter-wave resonator, where the reaction front of the burning pyrotechnic composition provides both a high acoustic impedance boundary and an acoustic energy source, and the open end, or mouth of the whistle chimney, provides a low impedance boundary.

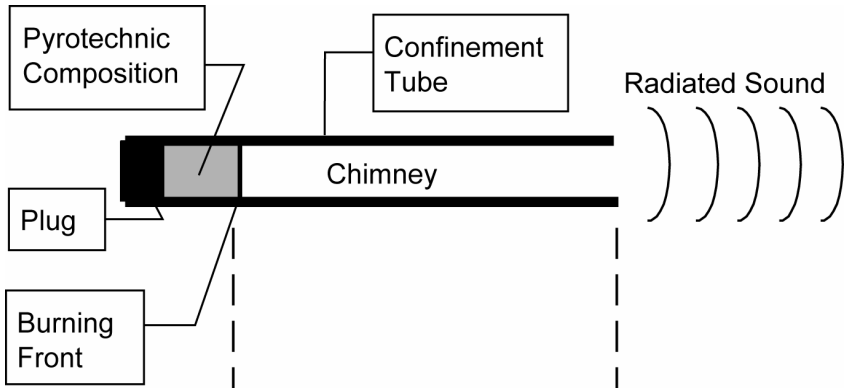

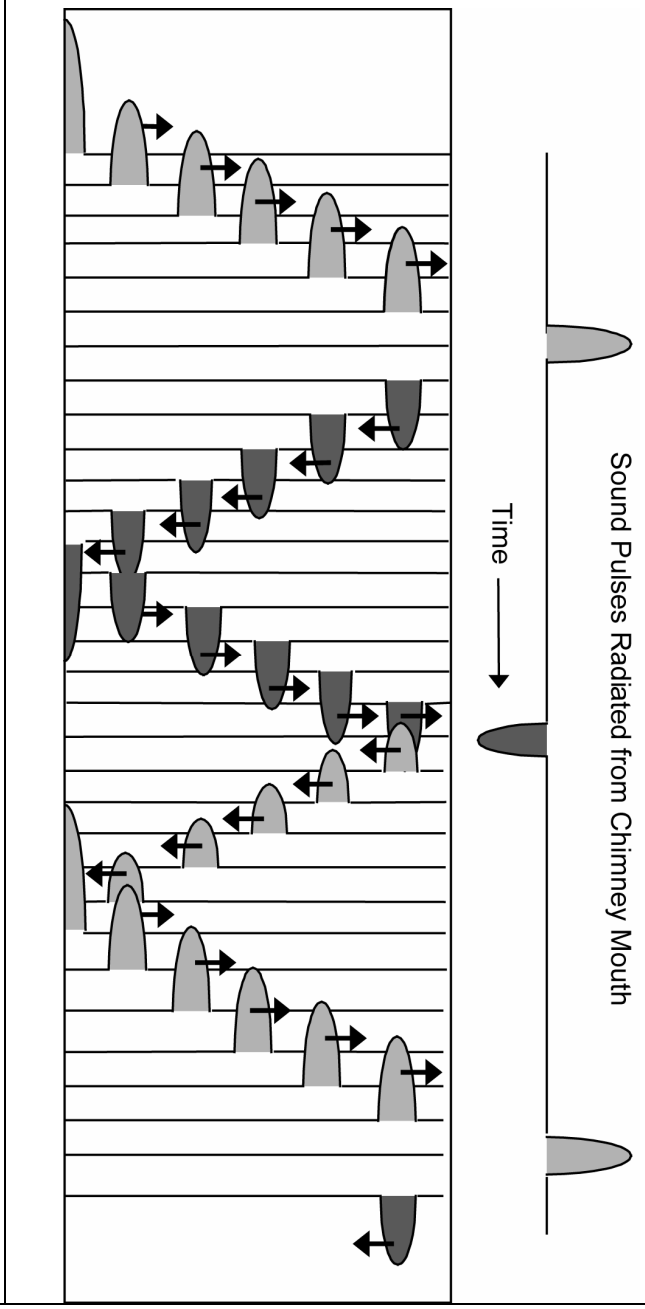

Figure 1. Schematic representation of a pyrotechnic whistle device showing an acoustic pressure pulse propagating through the chimney in a sequence of snapshots in time. Changes in pulse height occur at points of reflection. Positive pressure pulses have light shading whereas negative or rarefaction pulses have darker shading. The left-hand side of the time sequence box corresponds to the position at the burning front and the right-hand side to the position at the chimney mouth. Arrows indicate the direction of pulse propagation. A graph of radiated pressure pulses is shown on the right-hand side of the time sequence box. The radiated pressure pulses are generated each time the internal pressure pulse is reflected at the chimney mouth. A drop in the internal pulse height indicates this radiation loss.

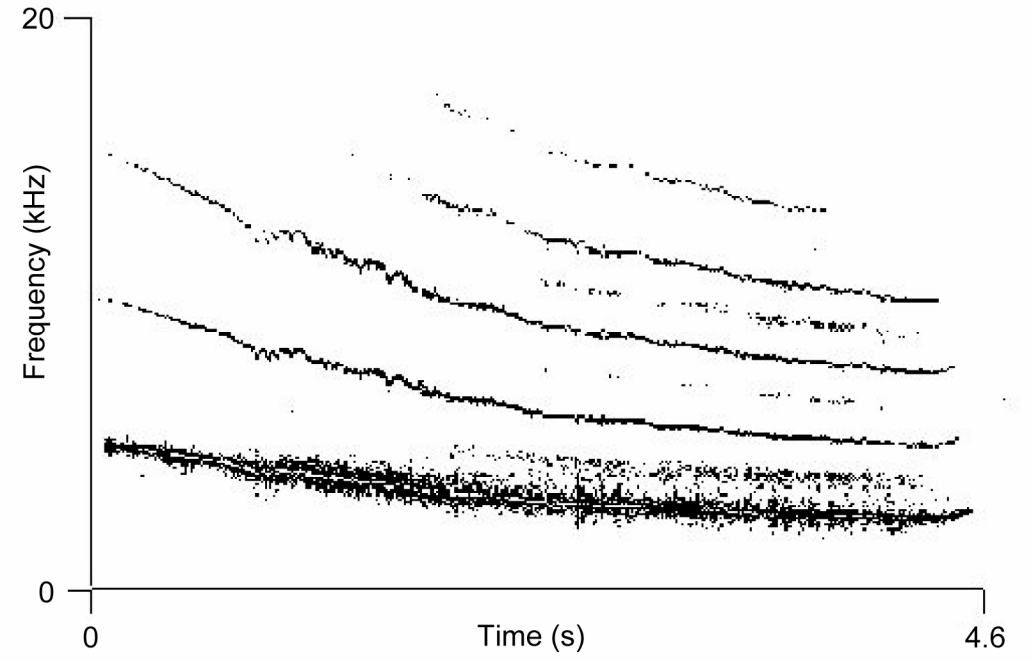

Figure 2. Spectrogram of whistle output, showing the peaks of the whistle spectrum as a function of time. The lowest line represents the first harmonic, or the fundamental, and the upper lines represent the higher harmonics.

There appears to be some confusion about such a model in the literature, where an open organ pipe model was suggested by Maxwell.[2] The open organ pipe model represents a half-wave resonator with two low impedance boundaries[3] where the ratio of the frequencies of the upper harmonics and the fundamental follows a simple 1, 2, 3, 4, ... relationship, termed here as the modal ratio. While the experimental data show such a relationship between the mode frequencies (see Figure 2), it does not fit the half-wave resonator model, which yields unrealistically low acoustic propagation velocities when calculated as the product of frequency and wavelength, with the wavelength equal to twice the effective chimney length. The modal ratio for a quarter-wave resonator, however, normally follows a 1, 3, 5, 7 … relationship, but it can be shown that non-linear distortions in the acoustic wave output are capable of producing the observed 1, 2, 3, 4 … modal ratios. So far, it has been found to be extremely difficult to account for the non-linear acoustic behaviour in the absence of suitable experimental measurement techniques capable of operating in a very hostile environment, and to simulate the process computationally would require considerable developmental effort. However, the simplified acoustic model still offers useful insights, particularly when the whistle chimney, or quarter-wave tube resonator, is considered as an acoustic wave trap. This helps to provide a better basis for understanding the possible effect of acoustic feedback on the chemical reaction rates in the whistle composition burn.

Experiments show that the whistle oscillations build up gradually after initiation.[3] It is presumed that before the periodic whistle noise is established, the initial pyrotechnic burn generates its own random noise, which is trapped by the whistle chimney and fed back towards the reaction front where it may be reinforced under favourable conditions. Therefore, the initial stage of the development of the oscillatory burn is considered to be a random process as shown in frame (b) of Figure 3, where random fluctuations precede the onset of coherent oscillations.

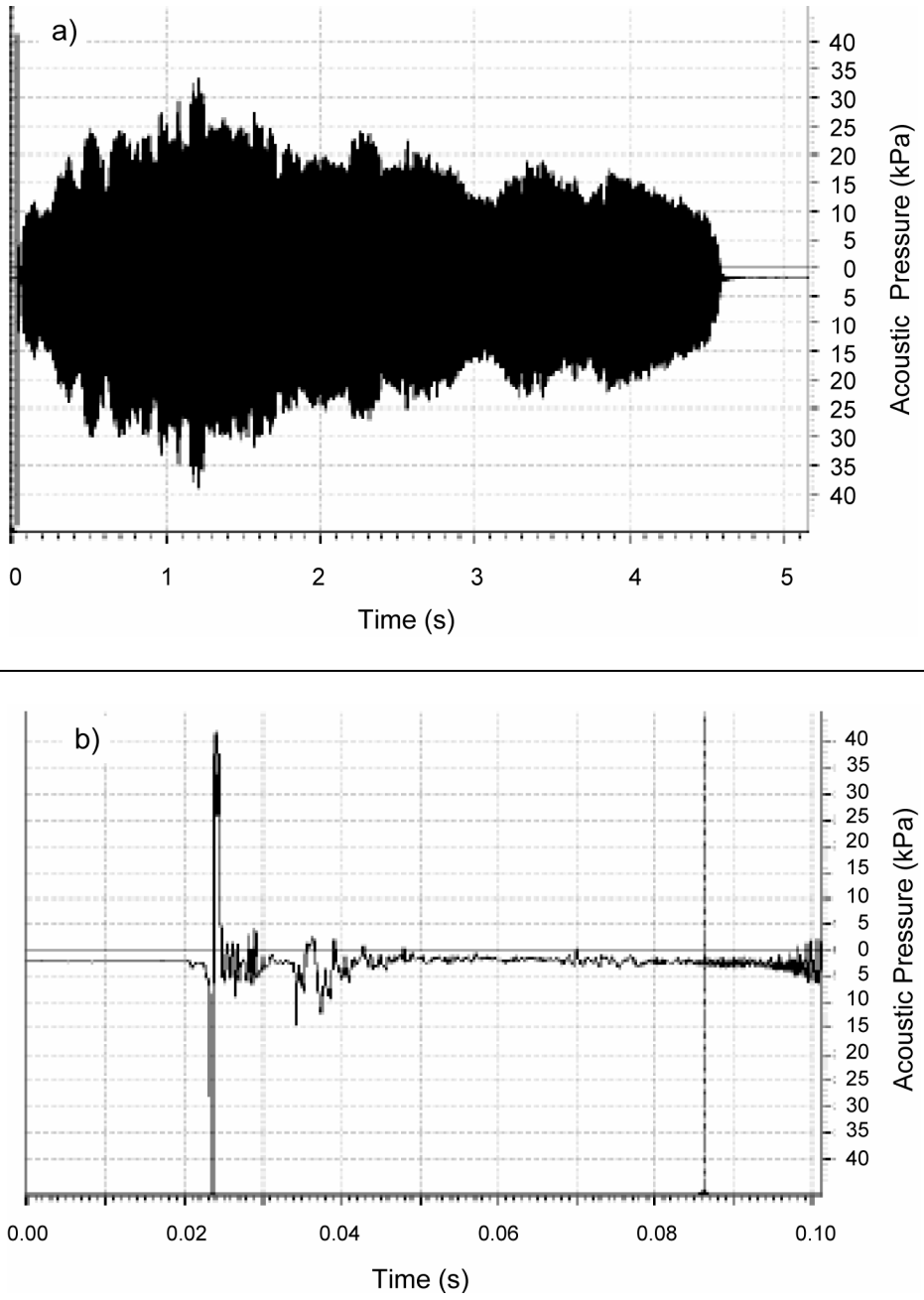

Figure 3. An example of the acoustic output of a pyrotechnic whistle device as a function of time with a vertical scale of approximately ± 40 kPa. Frame a) shows the complete record of sound output of nearly 5 seconds duration and frame b) shows the first 0.1 s comprising an initial transient due to the electric match-head initiator, random reverberant sound decay, and onset of coherent narrow-band oscillations. Unsuccessful attempts at resonant feedback are evident from the random fluctuations just to the left of the cursor at approximately 0.087 s followed by the onset of build up in coherent whistle resonance.

The effect of the acoustic pressure on the reaction rate of whistling pyrotechnic compositions is not yet properly understood, but it is clear from the literature as well as experimental evidence that the acoustic pressure wave trapped in the chimney controls the combustion process. Moreover, the energy of the combustion feeds back positively into the trapped acoustic wave.

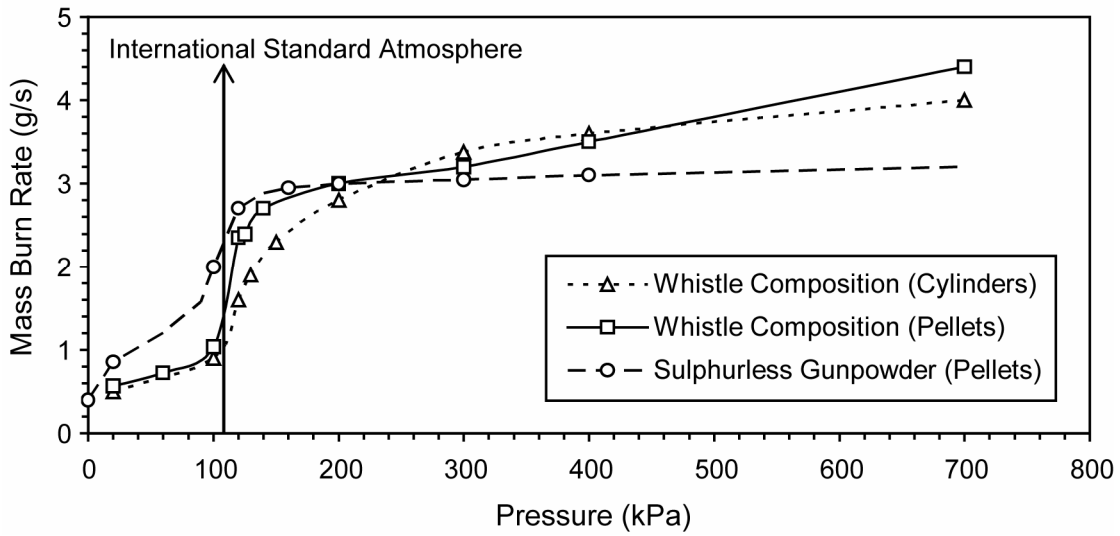

Figure 4. The relationship between static pressure (kPa) and mass burn rate (g/s) for whistle composition burning both as inhibited pellets in the open air, and at the bottom of open cylinders; in comparison to pellets of sulphurless gunpowder (Black Powder). The combustion of whistles ceased at pressures below 20 kPa, probably due to thermal losses from the burning front.

This process is sometimes called thermo acoustic feedback since the combustion is expected to impart energy to the acoustic wave through the addition of heat. The wave-trap model highlights one feature, which may be of considerable significance in the acoustic control mechanism of the combustion, namely acoustic pressure doubling at the reaction front. In the model, as portrayed in Figure 1, a compressional pulse is generated at the reaction front and propagates towards the chimney mouth where it is reflected, but proceeds as a rarefaction pulse of somewhat diminished magnitude back towards the reaction front. At the chimney mouth, the pulse magnitude becomes nearly zero due to the low acoustic impedance boundary condition, and all of the potential energy of the pulse is momentarily converted into kinetic energy. During this reflection process, some of the pulse energy is dissipated through acoustic radiation into open space. At the reaction front, the rarefaction pulse is reflected and its pressure magnitude is momentarily doubled because of the high acoustic impedance at the reaction front boundary. The doubling is due to conversion of all of the kinetic energy of the pulse into potential energy while in the rebound phase. The pulse then reverts to its previous magnitude (assuming zero losses) and proceeds back towards the chimney mouth. There it undergoes a reflection as described previously, but now it returns as a compressional pulse to the reaction front and completes the cycle, doubling temporarily in magnitude during the rebound phase.

3.1. Thermo Acoustic Feedback Mechanism

To build up oscillations in the pyrotechnic whistle device, a mechanism must exist that periodically adds energy to the trapped acoustic wave. Rayleigh[4] stated that vibrations in a resonant column might be generated through periodic addition of heat in phase with pressure wave condensation (compression). In an attempt to understand how this energy is imparted by the combustion process, the relationship between pressure and reaction rate was considered. Maxwell[2] asserted that the rate of burning of whistle compositions is not abnormally sensitive to pressure and that the acoustic pressure fluctuations do not appear to change the reaction rates sufficiently to account for the observed acoustic power of whistling compositions. These assertions are supported by the data (reference 1) set out in Figure 4, which demonstrate that pressure fluctuations about the atmospheric mean of 100 kPa of absolute pressure produce little more than a six-fold difference in average mass burning rate. Note that gun powder (Black Powder),

which produces a similar volume of permanent gas as whistle composition (~300 L/g), exhibits a similar increase in the mass burn rate with pressure, but does not exhibit oscillatory burning.[1]

Based on experimental observation and the above acoustic wave-trap model, it is believed that the acoustic pressure doubling at the reaction front controls the reaction process through thermochemical switching. It is suggested that acoustic pressure wave doubling at the reaction front is able to influence the temperature and pressure in the reaction zone and lead to differential fuel and oxidant decomposition rates. Thermochemical analysis of whistle fuels and oxidants by Wilson[1] showed that lowering of reaction temperature in a whistle composition is expected to lead to decreased decomposition rate of the oxidant while the fuel decomposition rate may continue relatively unabated. According to Wilson the layer of aromatic fuel thermally decomposes, producing solids and combustible gases including hydrocarbons and a highly reactive form of carbon. Thus, a doubled rarefaction pulse at the reaction front may lower the temperature and pressure at the reaction front and hence increase the net production of secondary fuels while decreasing the oxidant decomposition rate. A one half-cycle later, the doubled compression pulse will increase the temperature and pressure at the reaction front with a concomitant increase in the decomposition rate of the oxidant. The resultant combustion will be more energetic than in the preceding half-cycle and is therefore capable of adding energy to the acoustic wave, meeting the Rayleigh criterion. A build-up in the acoustic pulse height is possible via this mechanism with increasing contrast between the decomposition rates of the fuel and oxidant as the pulse height increases. In a fully developed oscillatory burn, the occurrence of distinct alternating half cycles of active and quiescent phases would be expected. Such behaviour was observed in experiments involving the recording (at 12,000 pictures per second) on a Kodak SP 2000C high-speed video system of combusting whistle devices pressed into transparent test blocks (see Figure 5).[1]

Maxwell demonstrated that the acoustic frequency of a pyrotechnic whistle decreases as the length of chimney above the burning front increases.[2] A series of experiments with 0.45 m long chimney extensions was designed to reduce the oscillation frequency to enable the combustion process to be more effectively recorded on high-speed video. The records of these devices exhibited a very clear distinction between the active (light) and quiescent (dark) phases of the combustion cycle as seen in Figure 6. Maxwell also made similar observations using streak camera photography.

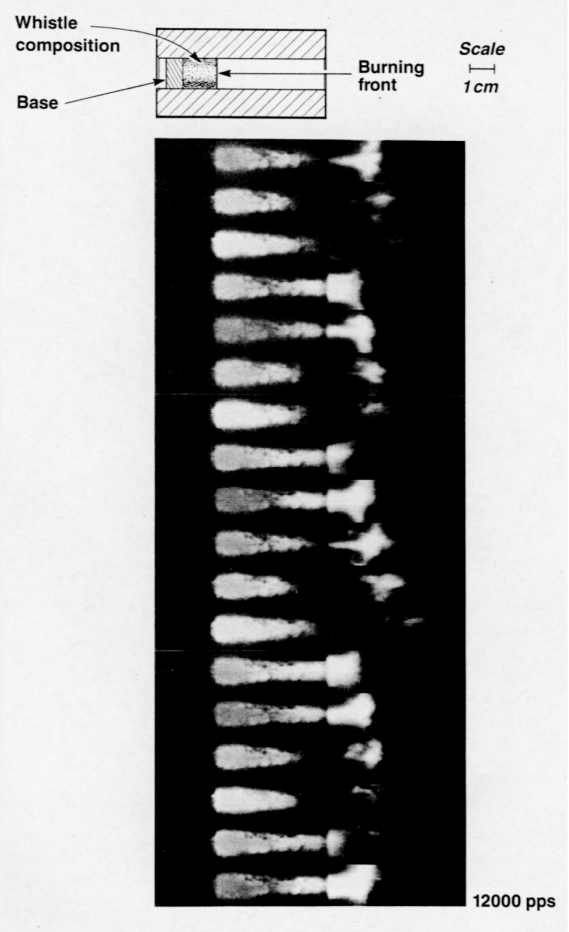

Figure 5. High-speed video record of a burning (3 kHz) whistle device showing combustion cycle 'switching' at the burning front.

It should be noted that during the dark period, the reaction is not extinguished, but is sustained, possibly as a smouldering process of hot carbon particles in an oxygen deficient, low-pressure environment. If the environmental temperature were to fall below that at which the fuel decomposes, the combustion reaction would likely be extinguished. This probably explains

why the whistles would not burn reliably at pressures much below atmospheric values, as indicated in Figure 4.

3.2 Quantitative Analysis of Acoustic Data

Useful information can be obtained from quantitative analysis of the acoustical data, such as acoustic pressure levels generated at the reaction front of a whistle device and specific impulse output, when compared with other energetic materials. The acoustic output of experimental whistle devices was measured (reference 1) with a Bruel and Kjaer Impulse Precision sound level meter located at a safe distance from the chimney mouth, and the sound pressure levels at the chimney mouth were calculated according to spherical spreading law. The acoustic pressure levels at the reaction front may be estimated from the acoustic properties of the chimney, considered here as a closed-open cylindrical waveguide. A more detailed derivation has already been performed in reference 1 so this study only considers some of the pertinent data and results.

In most of the experiments, the sound pressure level (SPL) was measured at a distance of one metre from the mouth of the whistle, with the SPL meter positioned at right angles to the whistle body. The initial chimney length, L, was 19.5 mm and the bore diameter, d was 12.5 mm. To calculate the effective wavelength, λ, of the wave trapped in the chimney, an end correction was applied to L so that

$$\lambda = 4L + 1.2\,d \cong 93 \text{ mm}$$

For the MRL(X) 418 whistle composition, the starting frequency was a little over 5 kHz and the recorded acoustic pressure waveform was nearly sinusoidal. Using the standard definition of SPL, the recorded waveform was converted to sound pressure and the spherical spreading law was applied to deduce the pressure amplitude just outside the chimney mouth. To calculate the pressure amplitude within the chimney, it is necessary to apply a transfer factor based on the reflection coefficient at the chimney mouth. This is called the resonant amplification factor (RAF), which determines the required build-up of internal wave amplitude until the acoustic energy imparted by the combustion is equivalent to the acoustic energy radiated from

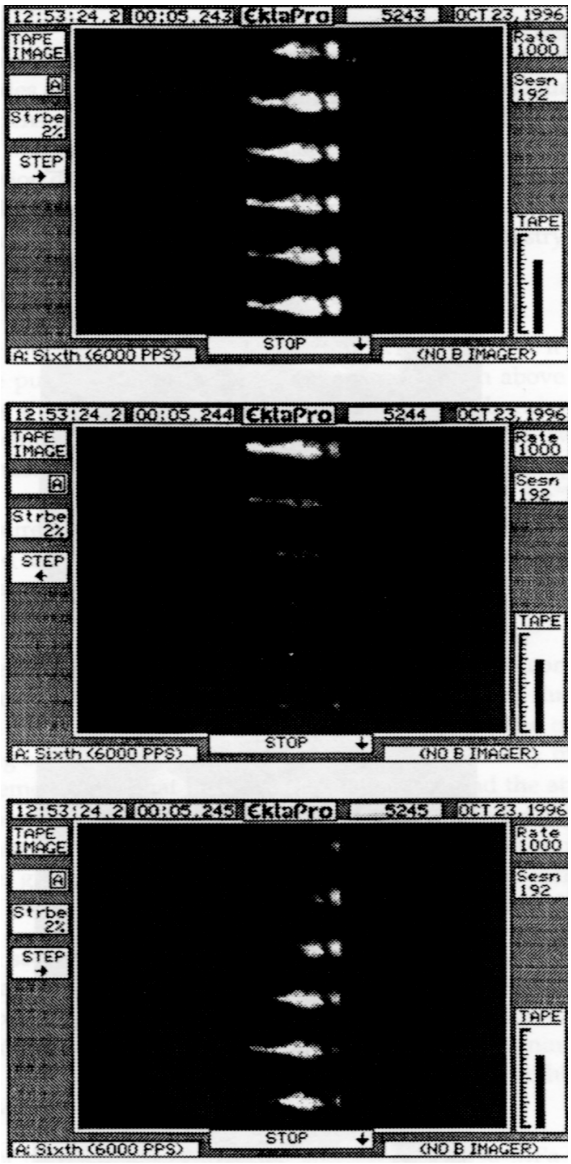

Figure 6. High-speed video record of a low frequency pyrotechnic whistle, showing the active (bright) and quiescent (dark) combustion cycles. To slow the whistle frequency to enable a full cycle to be recorded, an extended chimney tube was fitted to the device. When, in another experiment, a 'normal' 3 kHz whistle was located and ignited at a distance of 15 mm from the end of the low frequency whistle, pointing directly at the mouth of the extended tube, the combustion frequency of the first whistle was observed to increase.[1] This experiment demonstrated that the whistling frequency is controlled by the incoming pressure pulses (normally as a result of reflection from the tube mouth).

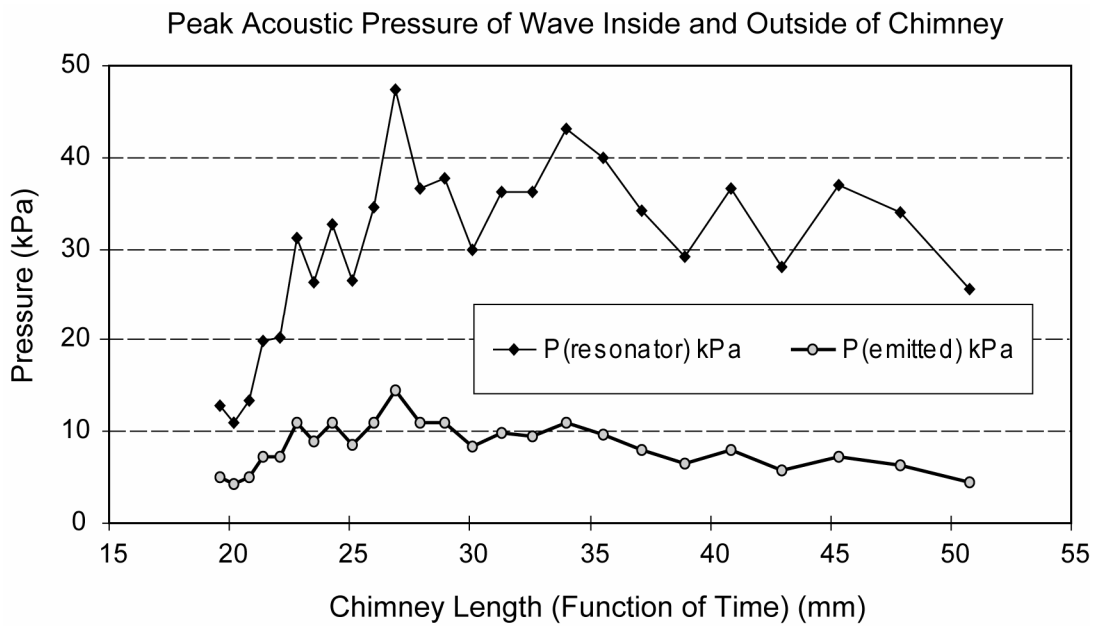

Figure 7. Translation of peak acoustic pressure for waves radiated from the chimney ($P_{emitted}$) to peak pressure for waves trapped inside the chimney ($P_{resonator}$). The translation is a function of chimney length, which varies with time as the whistle composition is consumed, and is governed by RAF (the resonant amplification factor).

the chimney mouth. The RAF may be derived from first principles using acoustic theory for waves radiated from open cylinders, assuming no acoustic losses except by radiation from the chimney mouth. Adopting the approach and formulation of Fletcher and Rossing,[3] it is found that the RAF varies linearly with chimney length, starting at a value of 2.5 at the beginning of the burn, and closing at a value of about 6 at the end of the burn.

Figure 7 shows an approximate RAF translation between internal and external peak pressure for the same sound-pressure record as depicted in Figure 3. This illustration raises two important issues:

1) The internal wave amplitude is vacuum limited (i.e., it cannot exceed 50% of ambient pressure). Otherwise, pressure doubling at the reaction boundary during the rarefaction phase would demand negative pressures, which cannot be physically achieved. Hence, at atmospheric pressure, the amplitude is limited to about 50 kPa.

2) As the chimney length increases, the RAF increases, and therefore, the maximum possible output of the whistle decreases because of the vacuum limit. For the experiments with 0.45 m extensions, the RAF ≅ 50 and the expected maximum amplitude radiated from the chimney would be of the order of 1 kPa only. This corresponds to a 20-fold reduction in amplitude, or a drop of about 25 dB in sound output.

4. Energetics

4.1 Acoustic Impulse

Normally, pyrotechnic compositions are designed to burn at a relatively slow rate to produce the required physical effect (e.g., light, smoke, heat, gas or a delay interval). This is usually achieved by a combination of ingredient selection and formulation, and by either pressing or casting the composition into a container so that propagation proceeds by inherently slow layer-to-layer thermal processes. In certain cases, however, the burning rate must be greatly increased to produce the required effects.

In the case of photoflash compositions, where a pulse of light, sound and smoke must be produced in a very short time (e.g., in a spotting

charge for an artillery shell), the composition is filled as a loose powder into a container; greatly increasing the surface area available for combustion. The container provides a level of confinement, which serves to increase the internal pressure rapidly. The high thermal output of photoflash compositions (over 8 kJ/g, compared with gun powder (Black Powder), approximately 3 kJ/g) is a result of the use of metallic fuels and this, in conjunction with the other factors, produces a fast reaction rate (often several hundreds of metres per second) and high pressures. The reaction proceeds throughout the void spaces present in the filling and the entire mass of composition combusts, virtually simultaneously. The container ruptures and a single, high amplitude acoustic impulse is produced. Hitherto, the deflagration of loose, metal-fueled photoflash compositions has been regarded as probably the most energetic of the more common pyrotechnic sound-producing reactions when considered on a mass for mass basis.

To compare the acoustic output of loose-filled photoflash composition with loose-filled whistle composition, cardboard-cased test charges were prepared, each containing 50 mg of:

- the magnesium fueled photoflash composition MRL(X) 206, which contains 40% magnesium, 59% potassium perchlorate, and 1% acaroid resin and
- the whistle composition MRL(X) 418.

The electrically-initiated charges were tested for acoustic output; the specific impulse produced by the charges was 1.1 and 0.76 Pa s/g, respectively. Because the positive phase duration of the events were similar, the value produced by the whistle composition can be considered as a surprisingly high result, given the non-metallic nature of its fuel. It is important to note that the specific impulse produced by a single active cycle at the reaction front of *consolidated* whistle composition is estimated to be about 3,500 Pa s/g (using an 11 kPa half-sinusoidal pulse, a frequency of 3,000 Hz and an average burn rate of 1 g/s).[1]

High amplitude, non-cyclic impulse sound can also be produced using primary explosives, but neither the container nor the need to use a loose filling is a critical requirement. This is because the propagation mechanism of primary explosives is often detonation resulting from the formation of a supersonic shock wave. However, Wilson[1] demonstrated that whistle composition, when initiated with a detonator, did not produce an indentation in the witness plate—a test designed to indicate the formation of a detonation wave.

Clearly, a pyrotechnic whistle device is a very efficient converter of chemical to acoustic energy, but the mechanism of sound production from the consolidated burning front within an open tube is evidently different (producing a greater acoustic impulse) from that when the composition deflagrates in the normal sound-producing mode (i.e., when filled as a loose powder and ignited under confinement).

4.2 The Consumption of Mass

The mass of the reactants involved in the production of each acoustic impulse in an operating whistle device would normally be expected to be determined by the area of the burning surface and the degree of thermal energy intrusion into the pressed compact ahead of the reaction front (which is in turn determined by its gas permeability). However, under examination, pressed whistle compositions exhibited very low void spaces,[1] a characteristic likely to limit the mass of composition available to contribute to each acoustic impulse. The mass burning rate figures quoted in this work for whistling MRL(X) 418 are average values; that is the sum of the mass required to produce the acoustic impulses and the mass consumed during the quiescent periods per second. It has been demonstrated (Figure 4) that the mass burning rate of a 12.5 mm calibre, 3000 Hz whistle functioning at ambient pressure is about 1 g/s and that the lowest mass burn rate at which linear combustion is reliably sustained is about 0.5 g/s. But, even if it is assumed that during the quiescent interval, the mass consumption rate is zero (e.g., a 'smouldering' reaction of hot carbon particles) and that virtually all the available mass of whistle composition is required to produce the observed acoustic pulse, each single acoustic impulse consumes a maximum of only $1/3000 = 3.3 \times 10^{-4}$ g of composition. This mass, burning as a reaction between discrete fuel and oxidiser particles, appears much too low to account for the observed acoustic power.

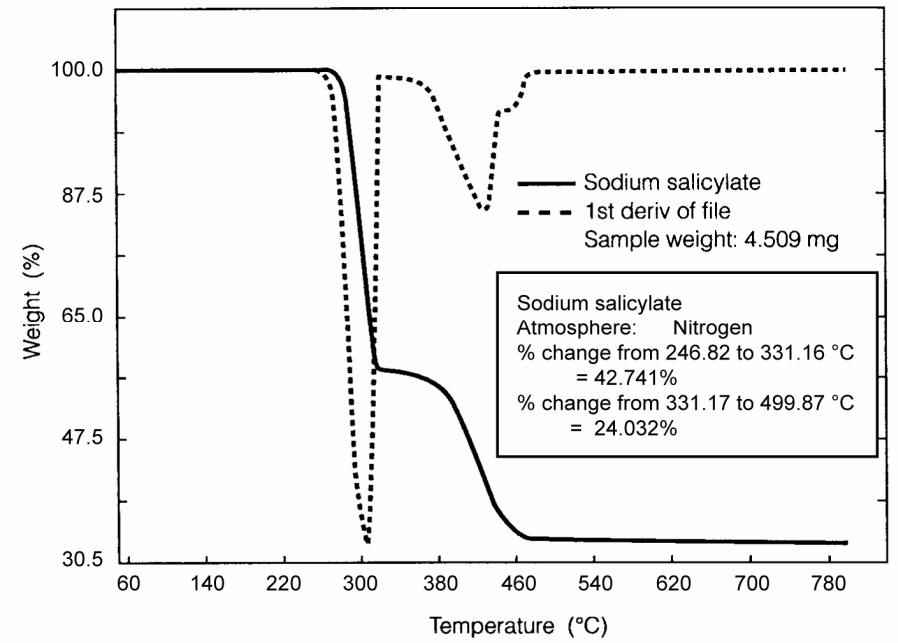

Figure 8. TGA of sodium salicylate. The analysis reveals a two-stage decomposition process commencing at approximately 250 °C.

From the foregoing, pyrotechnic whistles are unusual as acoustic impulse generators in that:

- whistle compositions contain an organic fuel (which would be expected to produce a low combustion temperature and resultant pressure),
- a higher acoustic impulse is produced from the reaction front of a functioning whistle compact than from a greater mass of the same composition ignited as a loose filling under confinement,
- whistle compositions are unlikely to propagate by a cyclic detonation mechanism (inferring a relatively slow reaction rate), and
- the very small mass of reactants consumed to produce each acoustic impulse would likely preclude a simple combustion process involving solids.

4.3 Fuel and Oxidiser Decomposition Temperatures

Thermo gravimetric analyses (TGA) of a typical whistle fuel ($NaC_7H_5O_3$ – Figure 8) and oxidiser ($KClO_4$ – Figure 9) were conducted to determine the relative onset decomposition temperature of the ingredients.

At the relatively slow heating rate of the thermal analysis instrument (40 °C/min), the results indicate approximately a 350 °C disparity between the onset decomposition temperatures of the whistle fuel and oxidiser. While the values of the decomposition temperatures of the individual ingredients may change—both when slowly heated as a pyrotechnic mixture in the TGA instrument and when heated at the greater rate experienced in a burning whistle—it is unlikely that the ingredients will decompose at precisely the same temperature. It has already been demonstrated that, within a burning whistle tube, the pressure level varies greatly with time; this would likely lead to concurrent temperature fluctuations between the active and quiescent cycles and slightly disparate ingredient decomposition times. The fuel would continue to decompose in a low pressure and low temperature environment, while the oxidiser

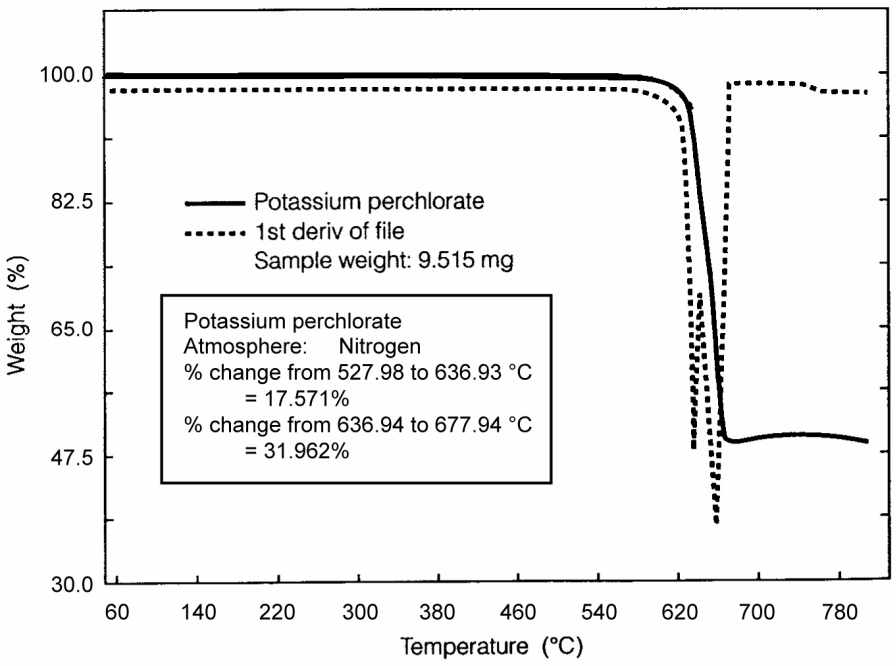

Figure 9. TGA analysis of potassium perchlorate showing onset decomposition temperature at approximately 600 °C.

component would not fully decompose until the incoming pressure pulse had sufficiently raised the temperature of the reaction front.

4.4 Decomposition Products

An experimental analysis of the thermal decomposition of selected whistle fuels in a reducing atmosphere has been performed by Wilson.[1] The dehydration reactions indicated the formation of highly energetic fuel species (confirmed by the explosion of several of the reaction vessels that had likely admitted air during the experiment). While this phenomenon has not been directly observed at the combustion front of a whistle device, it is thought to be a key factor resulting from the oscillating burning environment in whistle compositions. The observation that the whistle fuels exhibit a lower onset decomposition temperature than the ignition threshold temperatures of their pyrotechnic compositions suggests that the physico-chemical properties of the fuels might be altered within the reaction zone, immediately before ignition of the fuel–oxidant mixture occurs. This is not necessarily an uncommon phenomenon in pyrotechnics technology and can normally occur as an ongoing process just ahead of the combustion front as the reactants are preheated as a result of the permeability of the compact, particularly when combustion occurs under pressure.[5] Consolidated whistle compositions, however, have been demonstrated to exhibit very low permeability, probably due to the physical properties of the aromatic fuels.[1] This would restrict the mass of reactants involved to a thin layer on the surface of the consolidated compact.

Thermal decomposition analyses in reference 1 indicated the presence of the following combustible volatiles for potassium benzoate ($KC_7H_5O_2$): CH_4, C_2H_4, C_2H_6, C_3H_8, C_4H_{10}, C_6H_6, CO, and for sodium salicylate ($NaC_7H_5O_3$): CH_4, C_2H_4, C_2H_6, C_3H_8, C_4H_{10}, C_6H_6, CO, C_6H_5OH. The relative abundance of these species varied with decomposition temperature, and the reader is referred to reference 1 for complete details. It is important to note, however, that the presence of approximately 40% by mass of elemental carbon or carbon compounds was found in the condensed residue. The residue was examined under a Scanning Electron Microscope (SEM) and this revealed that in the condensed state, the residue is mostly carbon and takes the form of spheroids of approximately 1μm diameter (Figure 10).

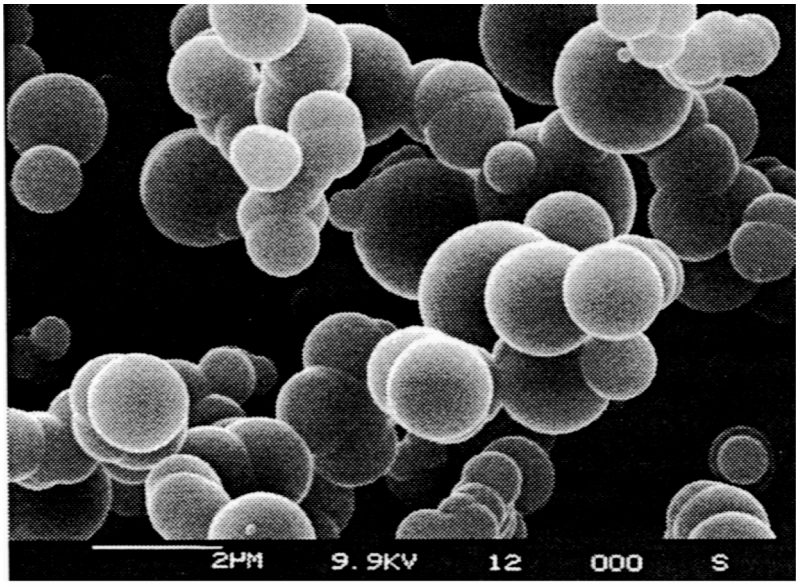

Figure 10. SEM of carbon spheres resulting from the thermal decomposition of whistle fuel in a reducing atmosphere. Crushing the spheres revealed that they were hollow.

Mechanical compression of the carbon spheres has provided strong evidence that at least some of them are hollow. This leads to speculation regarding the dynamics of the formation process and the nature of the gas species that may fill the spheres. The actual form that carbon takes at the moment of the destruction of the aromatic ring at the elevated temperature of the combustion front in a pyrotechnic whistle can only be guessed at, but it is probable that it is in a finely divided state. This hot and highly reactive carbon, together with any combustible gases, which form from the aromatic fuel, would represent a new and relatively energetic fuel mixture. This, when burning under pressure in the oxygen gas resulting from the thermal decomposition of the oxidiser, might account for the observed acoustic efficiency and explosive power of pyrotechnic whistles.

4.5 Explosive Behaviour

The proposed ability of whistle compositions to form a highly reactive fuel–oxygen mixture under certain conditions of temperature and pressure might also explain their tendency to occasionally explode violently, for example when accidentally ignited as a loose powder at the bottom of a filling funnel or as a result of the 'flash down the side' phenomenon in a functioning whistle device (see reference 1). In both these circumstances, the mass of reactants is uncontrolled by the normal constraints of a finite and consolidated reaction layer, and a limited combustion pressure environment. Under uncontrolled conditions, the production rate of the energetic fuel species and oxygen would likely become exponential—resulting in the observed explosions.

So far, experimental evidence and some theoretical considerations have lead to the conclusion that the participation of acoustic stimuli in the explosive failure of pyrotechnic whistles is unlikely. The acoustic waves tend to quench the linear combustion rate of whistle compositions and although more reactive fuel species may be created during the quiescent phase of the oscillating burn, they would normally be produced in small discrete quantities before being consumed in the active phase of the combustion cycle.

The role of higher harmonics as stimulants for runaway reactions is virtually ruled out. First, the upper harmonic components are usually weak, and second, only the odd harmonic components are able to physically participate in the reaction control in a quarter-wave resonator. In practical whistle devices, such components

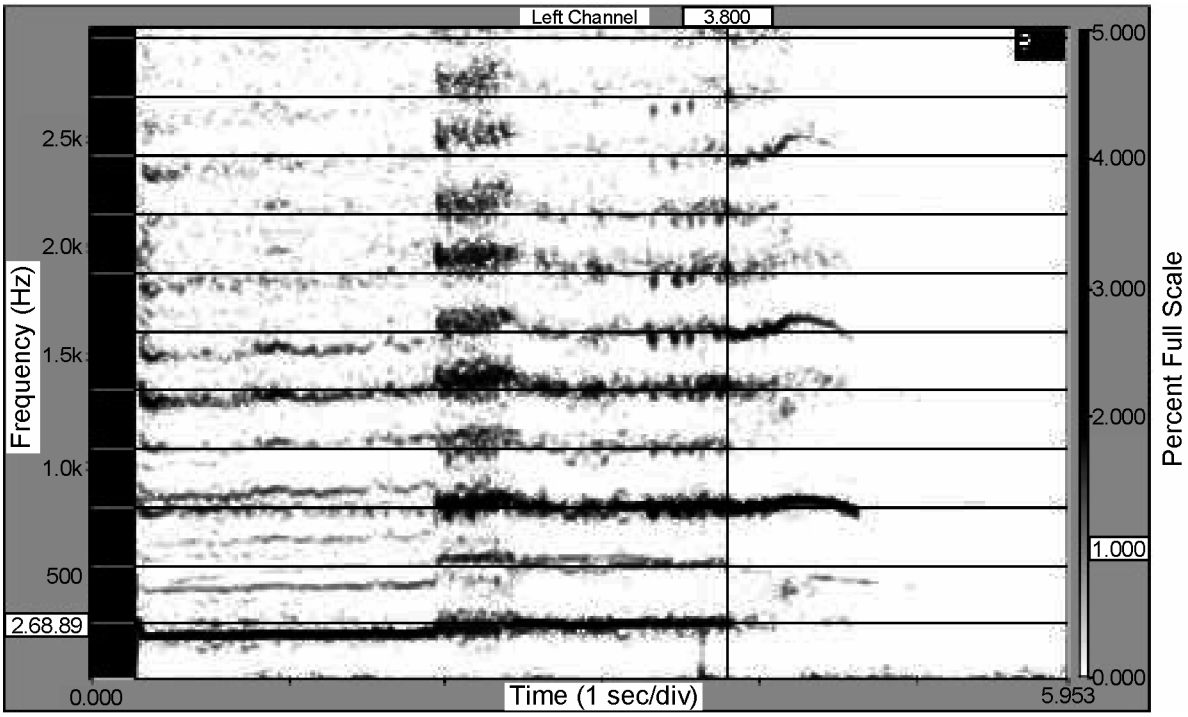

Figure 11. Spectrogram of whistle output for an experiment with a 450 mm chimney extension. It shows the peaks of the whistle spectrum as a function of time and a harmonic cursor has been laid over the temporal spectrum lines. The first harmonic frequency is at approximately 270 Hz. A strong switch to oscillation at the third harmonic frequency is evident at the 2 s marker, and at 3.8 s (position of cursor) the first harmonic is extinguished while the third harmonic component continues—together with its non-linearly generated overtones—until the composition has burnt out.

will be well above the critical cut-off frequency of the oscillatory burn and will therefore be excluded. However, in experiments with chimney extensions, where the fundamental burn frequency (approximately 270 Hz) was well below the cut-off frequency, switching of the burn oscillations to third harmonic frequency was evident (see Figure 11) and consistent with the model. The switch to a higher mode frequency did not result in runaway reaction, though, and the behaviour could probably be described as preferential mode competition.

Other experiments, in which strong tonal acoustic stimuli were externally applied to functioning whistles, demonstrated an effect on the reaction rate, but only by way of disrupting or altering the control cycle.[1,6] Similarly, experiments with externally applied acoustic shock stimuli have not had a detrimental effect on safe whistle performance, indicating that acoustic pressures are unlikely to induce fragmentation of the fuel–oxidiser compact.

5. Concluding Remarks

The acoustic model shows that acoustic pressure doubling at the reaction front may be critical to the coupling between acoustic waves trapped in the whistle chimney and the combustion process. Temperature and pressure switching is believed to control the decomposition rates of the whistle fuel and oxidant resulting in a two-stage combustion cycle. The first, quiescent stage, involves the decomposition of fuel to form highly reactive species in an oxygen poor atmosphere through acoustically lowered pressure and temperature. The second, active stage, involves the rapid combustion of the new fuel species in an oxygen rich atmosphere through acoustically elevated temperature and pressure. The energy released in the active cycle feeds positively into the acoustic wave trapped in the chimney, but its final amplitude will be governed by the balance of energy in-

jected by the combustion and the radiation and visco-thermal losses. Furthermore, the internal wave amplitude cannot exceed vacuum during the pressure doubling in the rarefaction phase, so this will be also a limiting factor in the acoustic output, particularly for long chimney lengths. However, further investigation (possibly assisted by sampling the combustion residues at the burning front from a whistle that has been 'switched off' by sudden exposure to vacuum) is required to validate the proposed combustion model before definite conclusions are drawn.

6. References

1) M. A. Wilson, *The Combustion and Explosion of Pyrotechnic Whistling Compositions*, Report DSTO-TR-0717, Aeronautical and Maritime Research Laboratory, Defence Science and Technology Organisation: Melbourne, Australia, 1998, 68 pp.

2) W. R. Maxwell, "Pyrotechnic Whistles," *4th Symposium on Combustion at MIT Cambridge*, Massachusetts, USA (1952). Reprinted in *Journal of Pyrotechnics*, Issue 4 (1996).

3) N. H. Fletcher and T. D. Rossing, *The Physics of Musical Instruments*, Springer Verlag: New York, 1991, 474 pp.

4) J. W. S. Lord Rayleigh, *The Theory of Sound*, Vol. 2, Dover: New York, 1945, 226 pp.

5) F. S. Scanes, "Thermal Analysis of Pyrotechnic Compositions Containing Potassium Chlorate and Lactose", *Combustion and Flame*, Vol. 23 (1974) pp 363–371.

6) J. A. Domanico, Technical Discussions. Edgewood Research, Development and Engineering Centre, Aberdeen proving Ground, Maryland, USA (1996).

Guide for Authors

Style Guide

The *Journal of Pyrotechnics* has adopted the *ACS Style Guide* [ISBN 0-8412-3462-0]. It is not necessary that authors have a copy; however, a copy can be ordered through a local bookstore.

Subject Areas

Fireworks, Pyrotechnic Special Effects, Propellants, Rocketry and Civilian Pyrotechnics

Manner of Submission

Submissions should be made directly to the publisher at the address at bottom of page. Upon receipt of an article, the author will be sent an acknowledgment and a tentative publication date. For specific requests regarding editors, etc. please include a note with that information. Preferably the text and graphics will be submitted electronically or on a 3-1/2" diskette or CD in IBM format with a print copy as backup. The Journal is currently using Microsoft Word 2002, which allows for the import of several text formats. Graphics can also be accepted in several formats. Please also inform us if any materials need to be returned to the author.

General Writing Style

- The first time a symbol is used, it is preferred to write it out in full to define it [e.g., heat of reaction (ΔH_r) or potassium nitrate (KNO_3)].
- Avoid slang, jargon, and contractions.
- Use the active voice whenever possible.
- The use of third person is preferred; however, first person is acceptable where it helps keep the meaning clear.

Format

In addition to the authors' names, please include an affiliation for each author and an address for at least the first author.

A short abstract is needed. (An abstract is a brief summary of the article, not a listing of areas to be addressed.)

Include 3 to 7 keywords to be used in a reference database: However, multi-word names and phrases constitute only one keyword (e.g., potassium nitrate and heat of reaction are each one word).

Use of SI units is preferred. If English units are used, please provide conversions to SI units.

Figures, Photos, and Tables are numbered consecutively. For submission, place them at the end of the text or as separate files. During page composition, they will be inserted into the text as appropriate. For graphs, please also submit "raw" X–Y data.

References cited in the text are referred to by number (i.e., "Smith[1] states"; or "the research[2,3] shows ..."). In the reference section, they will be ordered by usage and not alphabetically. It is preferred that a full citation, including author, title, book or journal, publisher for books, and volume and pages for journals, etc. be provided. Examples:

1) A. E. Smith, *Pyrotechnic Book of Chemistry*, XYZ Publishers (1993) [p nn–nn (optional)].
2) A. E. Smith, R. R. Jones, "An Important Pyrotechnic Article," *Pyrotechnic Periodical*, Vol. 22, No. 3 (1994) [p n–n, (optional)].

Editing

The *Journal of Pyrotechnics* is refereed. However, the editing style is friendly, and the author makes the final decision regarding what editing suggestions are accepted.

More Information

Contact Bonnie Kosanke, Publisher, the Journal of Pyrotechnics, Inc., 1775 Blair Road, Whitewater, CO 81527, USA.
or
email bonnie@jpyro.com

Reasons for Fuse Failure and Drift Distance of Spherical Fireworks Shells

Marc Speer

Speer Pyrotechnik, Hans-Böckler-Allee 51, 52074 Aachen, Germany / www.speerpyro.de

ABSTRACT

This work investigates the reasons for the ignition-failure of spherical (round) shells. It further statistically assesses the probability that the resulting blind (dud) shells will fall within a certain range from the launch point.

Keywords: fuse failure, shell drift, Magnus effect, interior ballistics, exterior ballistics, shell ballistics, blind shell, dud shell

Introduction

Prompted by an accident at a public fireworks display in 1997, German regulators have stepped up efforts to re-examine safety distances for viewers at public displays. The BAM (Federal Institute for Material Research and Testing) performed research to establish an overall model of interior- and flight-ballistics of spherical (round) firework shells.[1]

In support of this regulatory effort, representatives of the professional pyrotechnics association conducted their own research program on safety distances. The German Professional Pyrotechnic Association (VDBF)[2] allocated the necessary funds to perform statistical research on drift distances of 4-, 5- and 6-inch (100-, 125-, and 150-mm) fireworks shells.

The main intention of the VDBF was to provide statistical data on shell drift, using parameters that should match—as close as possible—the conditions of firework displays. Contrary to the existing safety distance table, which was formed with practical experience, this review provided scientific data to assess the risks of blind (dud) shells. The experimental drift distance data were used to establish a statistical model of probability of impact distance for three shell sizes. Nonlinear functions of probability were found to match the given conditions best. A new distance table was created—based on those data—using the shell diameter as the basic parameter.

The results of both the BAM research program and this work led to a fundamental change in the safety distance table for display shells in Germany. The safety distances now used are equivalent to the National Fire Protection Association *Code for Fireworks Displays* (NFPA 1123).[3a]

The other fundamental topic of research was to find out why when fireworks shells are fired that sometimes they do not ignite and subsequently fall to earth as blind shells. This study starts with interior ballistics of fireworks shells (within the mortar), investigating the reasons for time fuse failure and some countermeasures. The main part details the flight (exterior) ballistics and statistic evaluation of drift distance. Impact ballistics for blind shells in our tests are also given.

Interior Ballistics: Reasons for Fuse Failure

The first reason for fuse failure is fire transfer failure due to systematic material deficiencies (SMD) such as insufficient priming of the fuse. This may lead to a critical temperature drop as soon as the shell clears the hot exhaust plume from the mortar. Another example of SMD would be the incorporation of inert material into the fuse, which will cause instant cessation of the ignition sequence. A third important SMD is crumbling of the surface of the prime composition on the fuse during mortar passage.

The other potential cause for fuse failure in an otherwise perfect shell is the shearing off of the fuse from rotation of the shell inside the

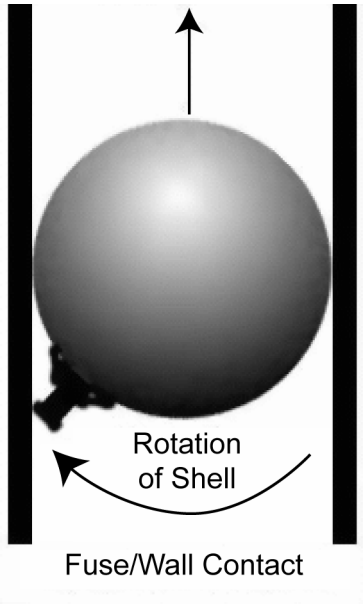

Figure 1. Sketch indicating fuse contact, rotation and direction of shell in mortar.

mortar and energetic fuse to mortar contact. (See Figure 1.)

Upon inspection, the outer part of the time fuse is usually found to be dislocated. The inner powder core inside the shell casing is still intact. When samples of this remaining powder core were ignited with an electric match, the fuse functioned normally from that point onward.

In our tests we used a plastic heat shield to cover the end of the time fuses that protrude from the shell. The exact preparation of the heat shield is described below under "Experimental Setup". The destructive effect was found to be dependent on the shell size, based on the damage the head shields sustained:

- None of the heat shields of the 4-inch (100-mm) shells were damaged; all shells came down as expected.
- None of the heat shields of the 5-inch (125-mm) shells were damaged sufficiently that the fuse ignited. Slight scratches (0.1–0.2-mm deep) were barely noticeable in only 10% of all recovered shells; the other 90% of the heat shields were completely intact.
- On the other hand, over 17% of the 6-inch (150-mm) shells used in the tests ignited in spite of a well prepared heat shield over the fuse. This value is consistent with earlier tests by Kosanke.[4] The heat shield was rubbed off during passage through the mortar, because the shell rotated in a way that the shield and fuse came in contact with the mortar wall. The fuses recovered from the exploded shells had the heat shield missing or destroyed.
- Approximately 20% of all recovered 6-inch (150-mm) shells were found to have parallel scratches in the outer plastic layer. Those scratches were up to 1-mm deep. It is assumed that the asymmetrically placed lift charge rotated the shell enough to bring the fuse into contact with the mortar wall.

Table 1. Energetic Wall Contacts.

Shell Diameter		Energetic Wall Contacts	Failure Rate for Single-Fused Shells[(a)]
(in.)	(mm)		
4	100	0/55 (0%)	0.1%
5	125	5/45 (≈11%)	
6	150	14/40 (≈35%)	

(a) Approximately, based on experience.

As a hypothesis, we propose that the increased torque of the larger shells is responsible for the damage to the heat shield. The scratches in the heat shields were on one side and parallel. Single sideward rotation seems the most likely explanation for the observed marks. Otherwise, irregularities in the marks or multiple marks would be inevitable. The orientation of the moving shell seems to be constant after the fuse hits the mortar wall.

Comparing the high rate of energetic fuse to mortar contact in the test shells (Table 1) with the good reliability of fireworks shells in general, shows that fuse to mortar interactions rarely cause fuse failure.

This choking-off mechanism explains the majority of fireworks shells fuse failures and is consistent with the physical appearance (ruptured and destroyed fuse) of recovered blind shells from fireworks displays.

Countermeasures, Multiple Fusing and Contact Stop

Multiple Fusing

To reduce the stress of impact between fuse and mortar wall, double fusing is recommended. This decreases the angle of rotation of the shell so that the fuse will contact the mortar wall at 20 to 30° rather than 40 to 50° as in the case of single fusing. See Figure 2. Due to the resulting shortened accelerating time, the imparted energy is lowered to 50–60% in all possible impacts. This reduces the impact force between the fuse and the mortar wall.

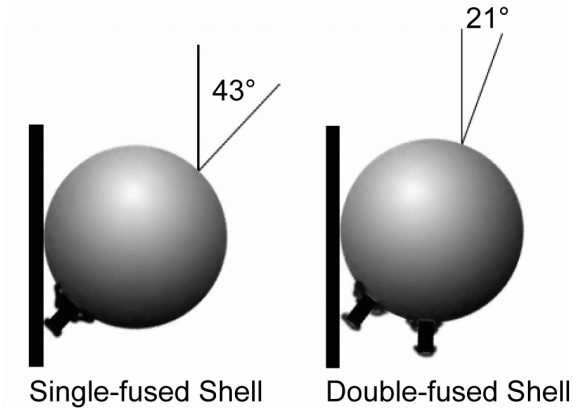

Figure 2. Angle of rotation for fuse contact with mortar wall for single-and double-fused shells.

If one fuse is approaching the mortar wall, the other fuse will be centered. Should the angle of rotation be vertical to the line between the two fuses, it may cause both fuses to contact the mortar wall at the same time. The angle of rotation is still somewhat smaller than that of single-fused shells, and the fuses each receive only half of the impact energy. Still, this might be enough to dislocate both fuses.

Contact Stop

An effective way of preventing fuse contact with the mortar wall is to attach a ring around the fuse, which keeps the fuse away from the mortar wall. The best way is a non-detaching lift charge with a downward facing pressure disc. See Figure 3. German shell maker ZINK® and other producers use such a system in combination with detaching quick match for optimum ballistics and spolette fusing.

Figure 3. Example of how a ring around the fuse prevents it from contacting the mortar wall.

Comets or other attachments on the top of the shell (see Figure 4) may effectively prevent rotation of the shell. Under no circumstances can the shell rotate into a position where a fuse would touch the mortar wall. Comets not only prevent physical contact, but they also center the shell's fuse. By entering the fast gas flow near the walls, the shell is subject to restoring forces just like in the example described under stabilizing interior ballistic factors below. Considering the flimsy comet configuration in some commercial oriental shells, the restoring forces may not be very great. Unfortunately, the muzzle ballistics of comet shells are more irregular than that of smooth ball shells, see below.

Stabilizing Interior Ballistic Factors

It has to be stated that the quick match seems to play a role in this process as well. The quick match tends to centre the shell as soon as a stable gas flow is established. The latter happens because the gas flow is much faster near the mortar wall and the quick match is moved out of the peripheral area. See Figure 5. The same

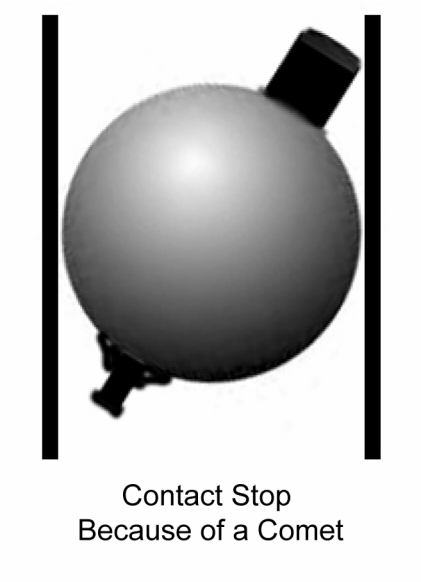

Figure 4. Example of a comet preventing the fuse from contacting the mortar wall.

scheme applies for other extensions placed on top of a round shell, like comets, etc. While these restoring forces are independent of the shell size, the angular momentum of a shell increases with radius. Therefore the quick match-stabilizing effect decreases with shell size. Since the heat shields of all shell sizes were made the same, this is another factor that explains the damage to the heat shield in the larger shells.

In conclusion, it has to be stated that the conditions for ignition are better with larger shells. The pressure in the mortar increases with shell size (e.g., by a factor of 1.5–2 when comparing 6-inch with 4-inch shell data), and the temperature during the lift process increases as well. This can be easily concluded from basic thermodynamics. Also, the shell remains in the mortar longer, which means better chances for ignition or even re-ignition—if the fuse has been quenched.

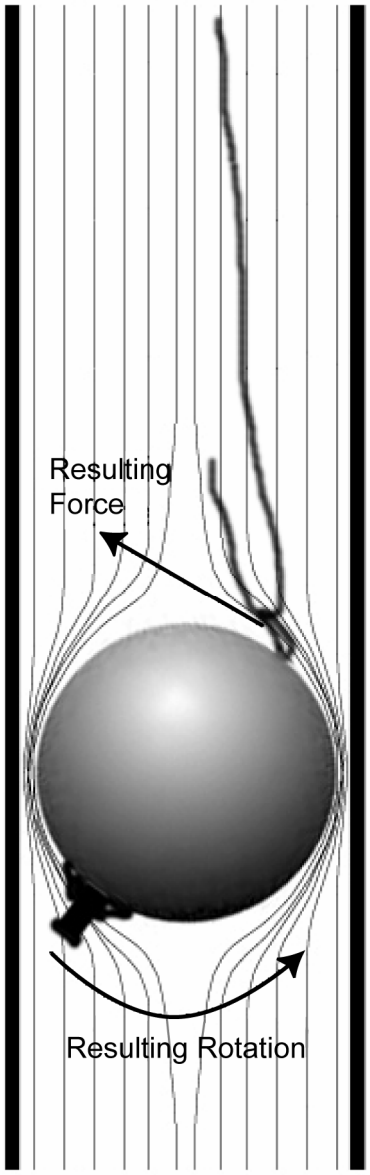

Figure 5. Influence of quick match.

Ballistics: The Deviation of the Ideal Trajectory and Statistical Investigation

Muzzle Ballistics

There are several forces affecting the shell when it exits the mortar that explain shell drift more appropriately than irregular mortar setup, wind drift and Magnus effect.

Irregular Mortar Clearance

When the shell leaves the mortar off-center, the gas flow on the side of major clearance pushes the exiting projectile sideways in the opposite direction. See Figure 6. This sideways push is more pronounced because of friction between the shell or its extensions (e.g., fuse, lift pocket, quick match) and the mortar wall in the upper regions of the mortar.

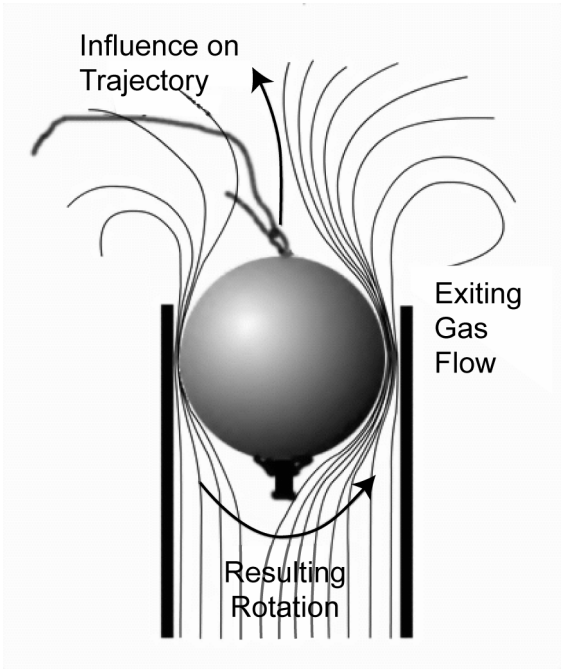

Figure 6. Demonstration of sideways push when the shell leaves the mortar off center.

Asymmetrical Frontal Air Flow

As soon as the shell leaves the mortar, the flow of the lift gases from the "rear" ceases within a small fraction of a second. The shell is now influenced by the frontal air flow. Since the shell is in an unbalanced aerodynamic position with regard to the new environment, asymmetrical extensions—like rising effects or remains of the quick match—cause forces that move the shell sideways and make it spin. The extension, which is pictured as a comet attachment in Figure 7, may also be the wadded remains of the quick match.

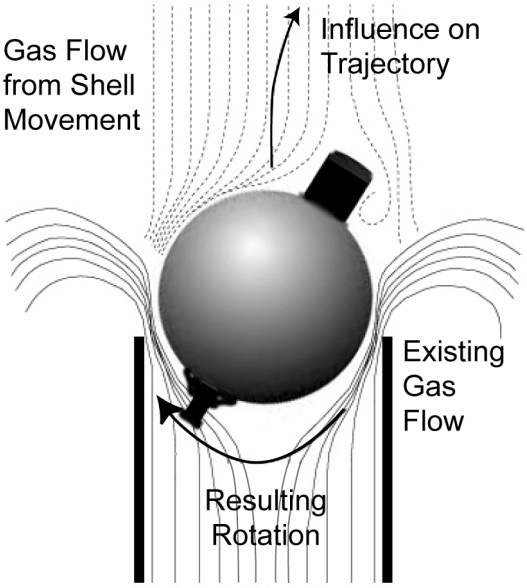

Figure 7. Asymmetrical frontal air flow.

Quick Match Effects

The quick match can cause two other important disturbances in muzzle ballistics, whether or not it is fastened to the mortar.

In the first case the mechanical sling-shot effect diverts the projectile from its course and induces a rotation. As the quick match is ripped away from the mortar rack that was holding it, the resulting rotation might cause a Magnus effect of sorts. This effect depends on how much of the quick match remains in the fuse loop. If a sufficient length remains, the rotation could pull the shell in the opposite direction of the sling-shot effect while the shell is ascending. See Figure 8.

Even an unfastened quick match may cause a slight slingshot effect if it is propelled sideways out of the mortar before the shell exits. In this case the force results from the mass momentum of the quick match and its aerodynamic drag. Letting the quick match hang loose out of the mortar will also risk dragging chained shells out of the next mortar. See Figure 9.

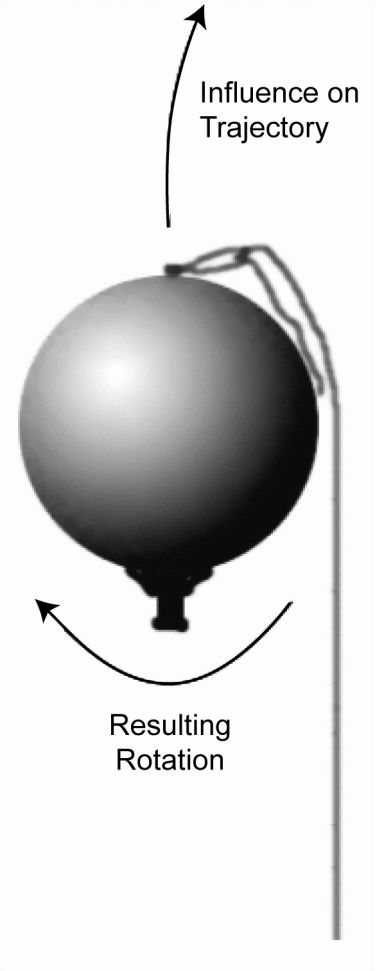

Figure 8. Slingshot effect with a fastened quick match shell leader.

The behavior of the quick match depends on its type, and the stability and size of the fuse loop. Because of the large number of different types of oriental shells, numerical simulations have only limited value. Further, the combination of the aerodynamic effects on the shell as described above is dependent on so many parameters and their correct logical combination that a "true" numerical model for "all" shells is nearly impossible. Nevertheless, numerical calculations are possible for certain types of shells when taking the statistical drag coefficient into account. But this factor can only arise from experimental testing.

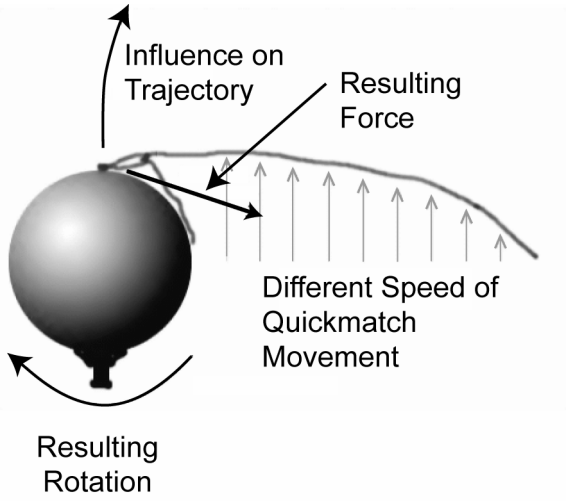

Figure 9. Slingshot effect with an unfastened quick match shell leader.

Flight Ballistics

General Ballistics of Round Shells

The density and muzzle speed of round shells are roughly independent of the shell size. The density is ~0.8 ± 0.1 g/cm^3 for most display shells, and the average muzzle speed is between 120 and 140 m/s. The shell apex height depends principally on its surface area to mass ratio. While the mass of a shell rises as the third order with its radius, the surface area rises only as the second order. The surface area to mass ratio rises linearly with shell size and so do the flight time and apex height. The approximate flight time is given in equation (1), which is valid for shells three-inch diameter and above and is a good fit to Shimizu's data[5] and our results:

$$\textit{Total ground to ground flight time}\ [\text{s}] \approx \textit{Shell diameter}\ [\text{in.}] + 6 \qquad (1)$$

Numerical modeling

A numeric model of a shell's flight was established before the tests. This model takes shell size, diameter, mass and muzzle velocity into account and calculates the trajectory depending on the mortar angle, side wind, air density and Magnus effects. The program is a step routine that solves the movement equations with a 0.1 ms time-step during the flight. It starts with a certain initial state, integrates all affecting forces for the period of the next tenth

millisecond and subtracts the result from the ground state, which gets the shell to a new state of time, place, velocity, direction and spin.

To calibrate this routine, shell apex heights were measured during a number of different long test series. The first method used shells with comets during ordinary firework displays, which were filmed from a greater distance. Rectangular landmarks (flares) on the ground were used as scale with the same parallax as the ascending shell. Shimizu's Tiger Tail comets were manufactured for these measurements, since the glowing charcoal particles were carried nearly uniformly by the wind. The long hang-time of the particles allows measuring the wind velocity depending on the height and the shell's behavior in the wind. This behavior was taken into account in the numerical model of the shell flight.

In the second approach a video camera was set up exactly vertical on the ground near the mortar setup. The film was digitized and the time difference of burst flash and burst report were recorded and used to calculate the burst height with an accuracy of 10 m in a series of several hundred shells per size. With regard to the firework shells the following were found:

a) They explode at or near the zenith of their flight.

b) The apex was found to be up to 25% lower than expected by the numerical model. The model used an average muzzle velocity of 130 m/s and the drag coefficient of a sphere depending on the speed (0.4–0.5).

c) The apex height varied up to ± 30% for shells of identical interior ballistics.

The tests revealed information about the appearance of a blind shell, especially that the quick match remains in the fuse loop after firing and that parts of the lift charge bag remain attached to the shell. [In over 80% of all shells portions of quick match (pieces at least 15 to 25 cm in length) remained in the fuse loop, see below]. This has an important influence on the drag coefficient. New numerical models now take this factor into account.

The variation of the apex height is caused by the quick match factor as well as by variation in the amount of lift powder. It seems that some Far East manufacturers measure the lift amount by volume and not by weight. Discrepancies up to 15% were found in general for the shells used in our tests. One four-inch shell was obviously double-charged with 72 g of lift powder compared to 40 ± 6 g for the other shells of that series. The quality of the lift powder, especially the moisture content, also varied. Apart from that, the results are consistent with the data of many Asian manufacturers.

There are three main influences on a shell's trajectory: (1) the angle of the launch caused by mortar setup and muzzle ballistics, (2) wind drift, and (3) Magnus effects. These are discussed in detail below.

1) *Launch Angle*: An intended launch angle adjusted by the mortar setup may be altered by the muzzle ballistics described above that adds an irregular angular momentum. Figure 10 shows the numeric simulations of trajectories of 4-inch (100-mm) round shells without any muzzle disturbances. The average shell weight is one pound (454 g), and the average muzzle velocity is 140 m/s. This is a rather heavy shell with a density of 0.9 g/cm^3 and a relatively high muzzle velocity. The angle of launch starts at 1° and increases in 5° increments up to 46°.

The horizontal distance at apex height (the normal burst point) increases effectively up to a launch angle of 25°. Angling the mortars further mainly lowers the burst height but does not substantially increase the horizontal distance. This is true for all sizes of round shells and important for the artistic design of fireworks shows.

The drift distance (horizontal displacement) for 1° angled shots increases from 25 m for 4-inch (100-mm) shells to 45 m for 12-inch (305-mm) shells at muzzle velocities of 130 m/s. One degree is considered the practical limit when using a water level to set up the mortars. It explains a large fraction of the average shell drift, especially if wooden mortar racks are used in chains. In this case the recoil of the first shot might influence the whole construction, especially in fast fired salvos when the battery tends to swing up.

2) *Wind Effect*: Wind is the most common influence on the trajectory and cannot be prevented. While being a small effect under normal circumstances, its influence can be severe

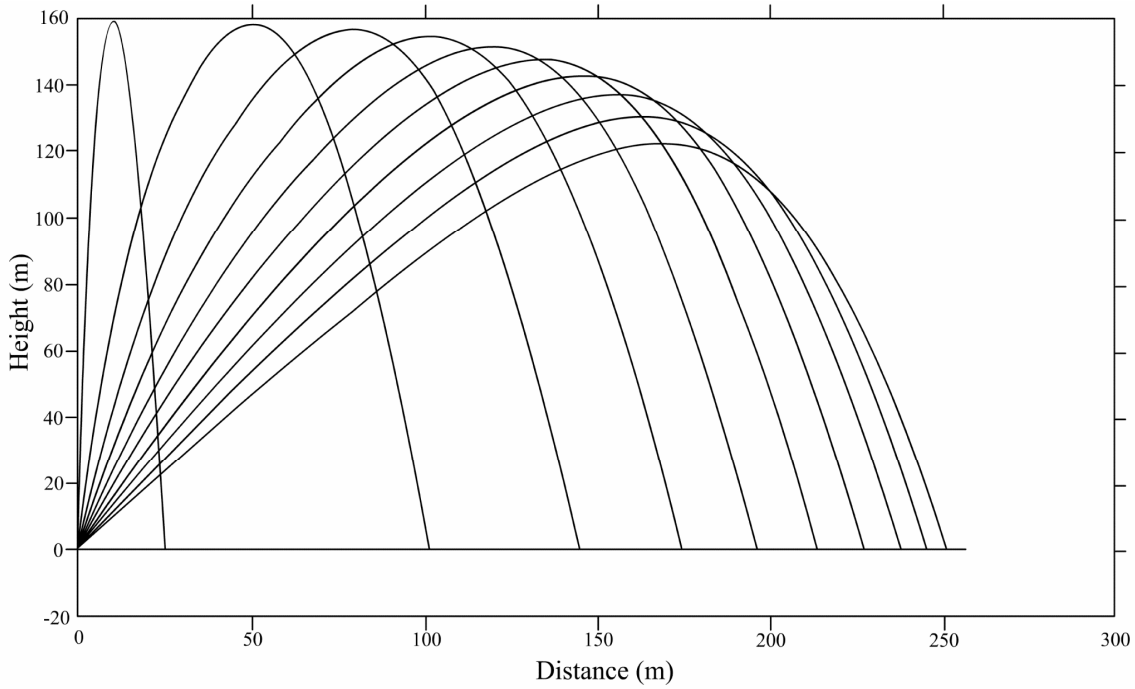

Figure 10. Effect on horizontal displacement distance for 4-inch (100-mm) round shells, as the mortar is angled from 1 to 46° in 5° increments.

in stormy conditions, making any display impossible. The reason for this is that the influence on the shell's drift rises as the second order with wind velocity. Wind drift of a shell is nearly independent of its diameter. Larger shells do not drift as much as smaller ones. This is caused by their greater surface-to-mass ratio, or in other words: larger shells remain in the air longer but are far less influenced by the wind. Stated another way—the same effect that makes a larger shell ascend higher explains its lower susceptibility to wind drift. The problem is to find a corresponding angle for each caliber to balance out the wind effect since smaller shells have to be more angled against the wind than larger ones. Figure 11 shows the numeric simulations of trajectories of 4-inch (100-mm) round shells, weighting 454 g, and shot at a muzzle velocity of 140 m/s. The wind velocity starts at 1 m/s and rises in 1 m/s increments up to 10 m/s. Based on the information in Figure 11, a wind drift of about 55 m occurs at 10 m/s wind velocity. To offset this amount of drift, one would need to angle the 4-inch (100-mm) mortars 3° against the wind as can be estimated from Figure 10.

A 12-inch (305-mm) shell of the same density and muzzle velocity would rise to 325 m and have a wind drift of about 40 m at a wind velocity of 10 m/s. That is equivalent to an angled shot of 1° for that size of mortar.

It should be kept in mind that measuring the wind velocity at ground level does not necessary give precise results for the average wind velocity during the flight. The difference between ground level wind and the wind at higher altitude increases with increasing wind velocity.

3) *Magnus Effects*: As a rotating shell moves through the air, the interaction of the side circling "against" the wind versus the side circling "with" the wind makes the shell move sideways toward the side circling "against" the wind. The Magnus effect only works for laminar (i.e., nonturbulent) flows. These are not the conditions for a shell immediately after leaving the muzzle, where mostly turbulent flows predominate. In broader understanding, the Magnus effect describes the transfer of rotational and vertical energy into linear movement in a horizontal direction, even under turbulent conditions and for non-round bodies. In the case of a round shell with extensions like fuse, quick match or

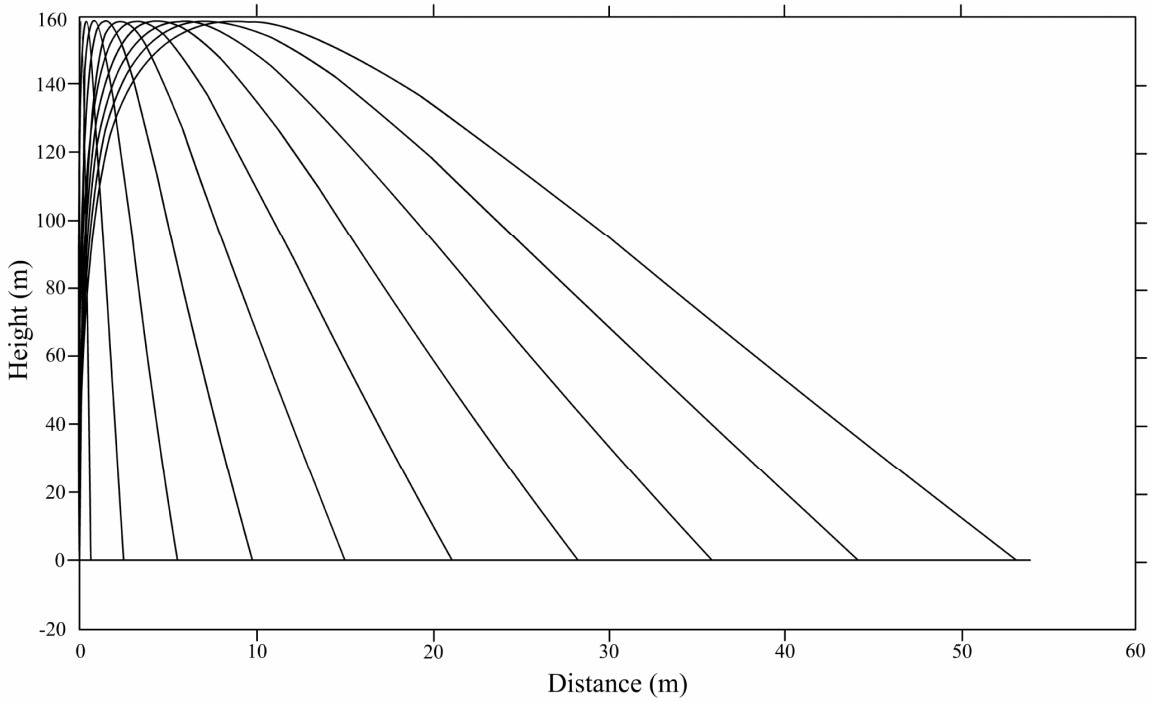

Figure 11. Effect of wind on 4-inch (100-mm) shells as the wind increases from 1 to 10 m/s in 1 m/s increments.

comets, these extensions can interact with the airflow like a paddle, causing turbulence. Additionally, the rotation of the shell decreases rapidly under these conditions. Exact modeling would be quite complicated under these circumstances. The Magnus effect and its turbulent analogies are responsible only for a fraction of the shell's deviation from its ideal trajectory as can be seen in Figure 12.

The time fuse of a normal fireworks shell prevents its free rotation in the mortar. Assuming the shell rotates 36° during the mortar passage of 10 ms duration at constant acceleration and the rotation is not stopped or slowed by the fuse contacting the mortar wall, we get a maximum rotating frequency of 10 Hz at a typical muzzle velocity of 130 m/s. The model used to calculate Figure 12 used the same parameters as for Figure 10 but with a slightly higher muzzle velocity.

The drift distance for a 1° angled shot with Magnus effect added to the direction of the angle is 42 m. Without the Magnus effect, it would have been only 25 m. (See Figure 10.) Earlier test series of 4-inch (100-mm) shells under windless conditions resulted in maximum drift distances of 64 m. So it can be seen that even slightly irregular angled mortars and Magnus effect together cannot fully explain the drift distances.

Research on 6-inch (150-mm) shells done by the BAM, showed rotations of up to 50 turns per second (50 Hz) for shells without extensions, rotating free in the mortar. In those tests the lift pressure was found to be significantly lower than in normal behavior, indicating that irregular gas flows may transfer a lot of energy (up to one third of the total energy) into rotation. That resulted in long drift distances by energy transformation from rotational and vertical energy to transversal energy by Magnus effects.[4]

The Magnus effect of a fast spinning spherical shell on the flight ballistics can be seen in Figure 13. The same parameters as in Figure 12 were used to calculate Figure 13, but the rotation was 80 turns/s (80 Hz). The drift distance for a 1° angled shot with this Magnus effect added to the direction of the shot would be approximately 120 m. Compared to a possible drift of 42 m for normal 4-inch fireworks shells (rotating at 10 Hz), this is quite enormous. Obviously, the prevention of free rotation of the shell in the mortar is one key to improving the

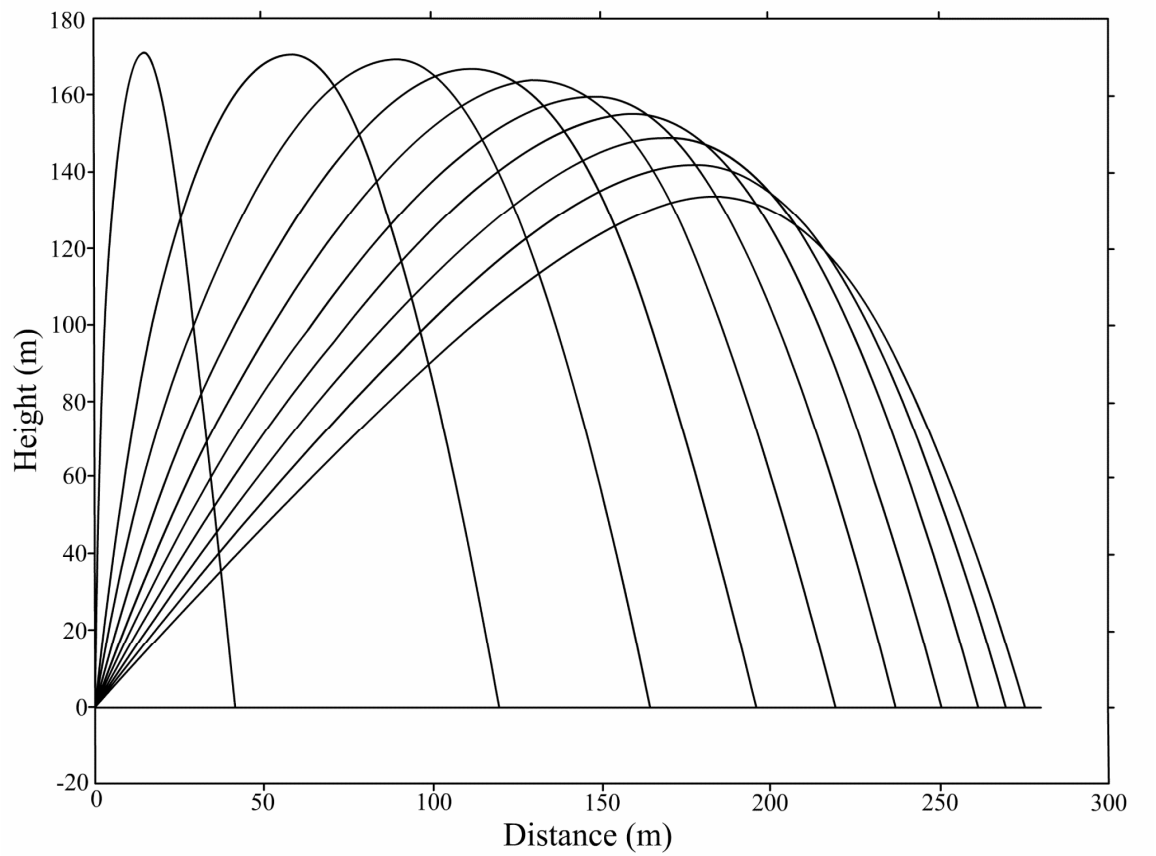

Figure 12. Magnus effect on the drift distance for 4-inch (100-mm) shells, assuming a 10 Hz Magnus influence on angled shots at 5° increments, from 1 to 46°.

safety at firework displays. This is possible by using a fit of 1/8-inch (3-mm) for the shell in the mortar as recommended in the National Fire Protection Association *Code for Fireworks Displays* (NFPA 1123).[3b]

When a shell fits loosely inside the mortar, the fuse is more likely to be damaged if the shell starts to rotate in the mortar during the launch process. This may result in multiple energetic fuse-to-mortar contacts. Additionally, the fast spinning shell will induce a strong Magnus effect on the trajectory. There seems to be a higher risk of creating blind shells in combination with long drift distances when using overly large inner mortar diameters.

Experimental Setup

Shells

The shells used in our tests were a representative range of display shells, mainly radially symmetric peony and chrysanthemum shells, as well as a few dozen asymmetrically charged Crisscross shells. The latter contained 25 to 30 small bombettes in an orderless mix with burst charge and were used to investigate the effects of charge symmetry on rotation and drift effects.

The shells were prepared as follows:

- The first step was to cut off the paper bag or cardboard cylinder containing the lift charge along the line where the container is attached to the shell. Then the primed end(s) of the time fuses were cut off and covered with a 1.5-mm thick layer of carbon-fiber reinforced epoxy-resin. This layer

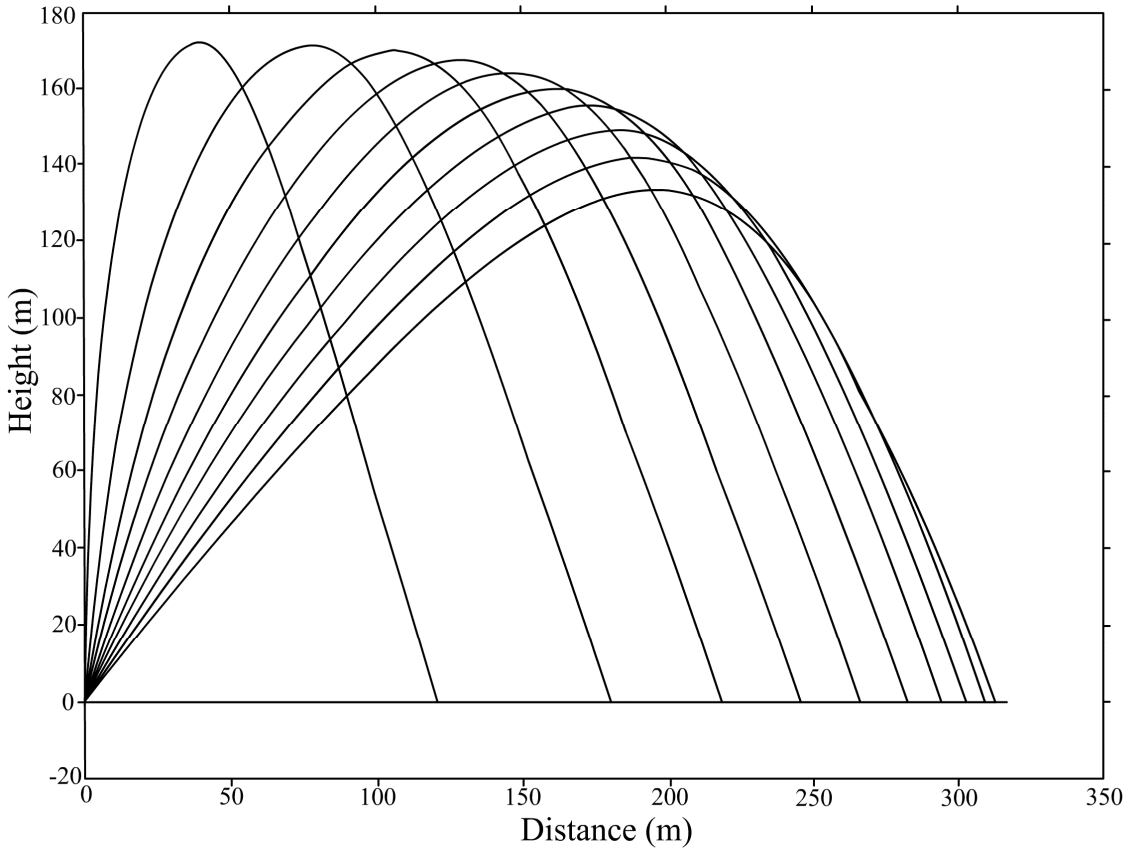

Figure 13. Magnus effect on the drift distance for 4-inch (100-mm) shells, assuming an 80 Hz Magnus influence on angled shots at 5° increments from 1 to 46°.

served as thermal insulation. To adjust the viscosity of the epoxy resin either 5 to 10 percent by weight of charcoal was added, or charcoal was used instead of the carbon fibers in the epoxy resin.

- After this layer cured, a second layer of 0.5-mm thickness was applied with a brush. This layer contained epoxy resin with a 5% load of flitter aluminum to reflect the IR-radiation of the lift charge and to protect the fuse against the hot dross of the charge.
- Before reattaching the lift charge with duct tape—to reestablish the original shell and lift charge configuration as close as possible—the shell was sprayed with yellow paint to improve visibility. In contrast to tests on 6-inch (150-mm) shells performed by the BAM[1] as described above, the test shells maintained their original inner and outer configuration, apart from the thin inert layers on their fuses.

We found the quality of the 6-inch (150-mm) shells to be superior to the smaller shells. The fuses were tightly wound with string, which provided more structural integrity to help prevent the fuses from being bent over during mortar passage.

Mortar Racks

The setup closely resembled the current practice. Standard Chinese fiberglass mortars were used. The fiberglass mortars were supported in wooden racks and secured with wedges. The mortar racks were set up vertically, checked with a water level, and connected with wooden boards nailed to the front sides of all racks.

The mortars were slightly deformed by the pressure of the wedges. This was tolerated because mortars become a bit irregular after some use.

Mortar Dimensions

The mortar dimensions are summarized in Table 2.

Table 2. Mortar Dimensions

Nominal Diameter (in.)	Nominal Diameter (mm)	Inner Diameter (mm)	Length (mm)
4	100	102	600
5	125	125	750
6	150	152	900

Experimental Procedure

The tests were performed under official supervision of the "Staatliches Amt für Arbeitsschutz" (roughly equivalent to the BATF) by the companies Ingmanns & Schmiedeknecht Pyrotechnik and Speer Pyrotechnik on a suitable ground in Loevenich near Aachen, Germany.

The shells were loaded into the mortar racks and chained with delay fuse by taping the bare ends of the quick match against the delay fuse with masking tape. The delay fuse was not fixed to the mortar racks to let the quick match fly freely with the shell. The delay fuse used was yellow WASAG® time fuse, which burns at approximately 23 s/m or 44 mm/s. After igniting the delay fuse, we watched the test from a distance of 150 m. After firing a salvo, the shells were located, and the distance from the blind shell to the launch point was determined using a Bushnell Laser meter (accuracy ± 1 m). The direction of drift was estimated in 5° increments by choosing "West" as the meridian and increasing clockwise.

Results

5-inch (125-mm) Shells

The shells for these tests were supplied by PyroArt, Berlin. Forty-five shells were fired; the average drift distance was found to be 45.8 m with a standard deviation of 23.6 m. The minimum drift was 4 m, and the maximum drift was 101 m. Four shells drifted further than the safety distance of 75 m, recommended by German law. This represents a probability of 8.7%. All impacts were within the 70 feet-per-shell-inch (22 m/25 mm) recommendation of NFPA 1123.

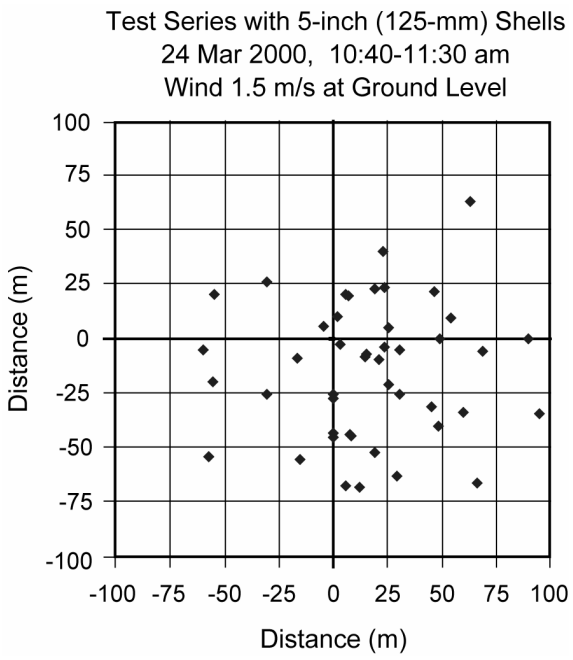

Figure 14. Impact diagram for 5-inch (120-mm) shells.

As one can see from Figure 14, the distribution of the shells' impact points were irregular, which could be caused by the wind or a very slight slope of the ground that falls in that direction. Perhaps the mortar angle was too small to be measured by the water level.

Impact Ballistics

Six shells landed on asphalt paving. All of them broke upon impact. None ignited on impact. The 39 remaining shells hit the ground; 4 broke upon impact. Similarly, there were no ignitions on impact. This turned out to be an important result of the tests, namely, there is not much chance for ignition upon impact with 5-inch (125-mm) star shells.

Approximately 20% of the shell casings were deformed severely by the impact and showed an axis ratio of 1.10–1.25 to 1. The rest of the shells were deformed only very slightly. Twenty-nine shells had at least 20 cm of quick match still attached.

It was found that the impact with the slightly muddy and unbroken ground caused them to penetrate to a depth of 5 to 7 cm.

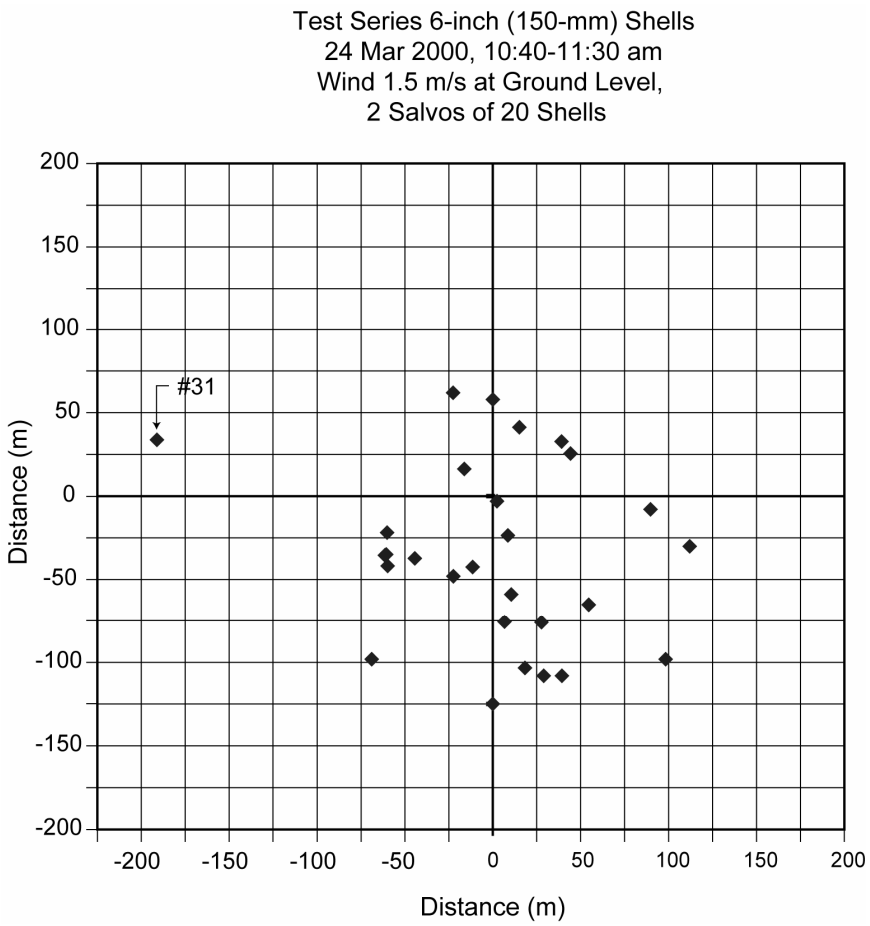

Figure 15. Impact distribution for 6-inch (150-mm) shells. The location of shell 31 is noted.

6-inch (150-mm) Shells

All shells for these tests were supplied by PyroArt, Berlin. Forty shells were shot in two salvos of 20 shells each. The minimum drift was 3 m, and the maximum drift was 160 m. The average drift distance was 78.5 m with a standard deviation of 33.3 m. Most of the larger drift distances were recorded in the second salvo. This appears to be an effect of the first salvo on the mortar setup. It is believed that the mortars were slightly angled out of their vertical position, because the mortar racks were not re-leveled after the first salvo. After the second salvo, the mortars were found to deviate up to 3° from the vertical. With the NFPA safety distance of 70 feet-per-inch of shell diameter, about 10% of all blind shells would leave the safety zone. Shell 31 shows another important result (see location of shell 31 in Figure 15). One mortar had not been secured in all directions because of a missing wedge. During the first salvo another wedge came off, which resulted in the mortar standing loose in the rack. The extreme drift distance of 194 m shows the importance of the stability to the mortar setup and should clearly indicate the need to secure the mortars tightly.

Impact Ballistics

Although the primed ends of the fuses were cut off and the ends of all fuses were completely covered with the same type of heat shield as the 5-inch shells [0.5 mm of flitter-aluminum-loaded (8 wt. %) epoxy cover over 1.5 mm carbon-fiber-reinforced epoxy resin], 7 shells exploded at the apex of their flight. This was explained above. This proves the reliability of ignition because under these circumstances no ignition was expected to occur. All shells were double fused.

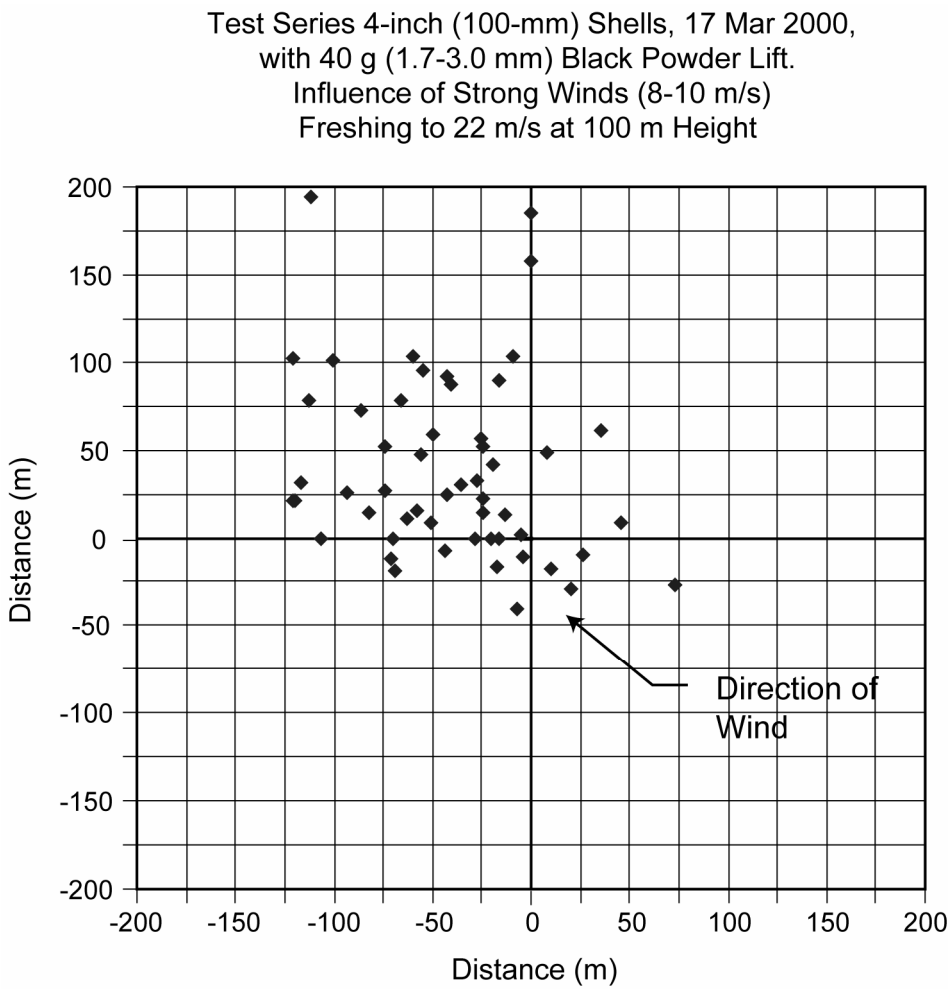

Figure 16. Impact distribution for 4-inch (100-mm) shells at wind velocities from 8 to 22 m/s.

The remaining 33 shells landed on the ground as expected. All were severely deformed from the impact, 21 shells cracked open and spilled part of their contents. This is explained by the smaller ratio between wall thickness and weight compared to smaller shells. The 6-inch (150-mm) shells in this investigation had a wall thickness of 8 mm as compared with 5-inch (125-mm) shells with a wall thickness of 7–7.5 mm and 4-inch (100-mm) shells with 6.5–7 mm wall thickness. The impact velocity rises with the shell size as well, adding some energy. With regard to the shell diameter, this influence is not as important as the mass, which is increasing as the cube of the diameter.

Four of the 6-inch (150-mm) shells ignited and burned upon impact. The result of the ignition was quite moderate and could by no means be compared with the normal burst. The burning debris was thrown less than 2 m from the point of impact. In no instance was a report produced, the sound was more a strong hiss from the burst charge and burning stars. Vegetation beyond 50 cm was not damaged. No crater was formed.

Reasons for Ignition of Larger Shells upon Impact

The remains of the shell cases were quite deformed near the fuse loop, the direction the shell was facing when it hit the ground. The cracks that spread radially from the point of the fuse loop were scorched more than the other edges of shell pieces. It was concluded that the cracks already existed at the time of ignition. It may be possible that glowing parts of the quick match might have ignited the contents of the shell. Parts of quick match were discovered in

the fuse loops in all cases. This is consistent with the content's moderate burning. The shells which "ignited" upon impact went 4 to 5 cm into the ground, non-"igniting" shells went 5 to 10 cm into the ground. With an estimated impact velocity of 70 m/s the ignition delay calculates to 1–2 ms before the case bursts. Even in the case of internal ignition, the pressure could not rise to critical values in this short time. So the danger of shock waves, burning stars and debris thrown over long distances is quite low. That risk should be considered primarily as a potential problem in the fallout area with regard to fire protection.

4-inch (100-mm) Shell Influence of Wind Drift (Shells in Storm)

All shells for this test were supplied by Weco. On a stormy day with wind velocities of 8 to 10 m/s at ground level and up to 22 m/s at 100 m height, 55 4-inch (100-mm) shells were shot. The average shell drift distance was 71.5 m; the minimum drift was 3 m, and the maximum drift was 224 m. The latter was reached by a shell with 72 g of lift powder of 0.8–1.25 mm grain size, which is quite unusual for that size of shell. Also the mortar was angled at 10° toward the "north" on the map. Other shells had approximately 40 g of lift charge of 1.68–3.2 mm grain size. Also, the whole length of the quick match remained within the fuse loop, which surely raised the drag-coefficient. The increased drag-coefficient lowers the apex height but does not decrease the flight time very much since the shell also falls slower. Thus, the drift distance caused by the wind is increased due to a higher drag coefficient.

Although any display would have been cancelled under these conditions (small unsecured items were literally blown away), we support the BAM proposal of a wind limit of 5 m/s for standard safety distances and accordingly greater distances for higher wind velocities.

It is known that the wind blows erratically even at high average velocities, making angling difficult since angled shots during periods with no wind would result in long drift distances.

Evaluation

Evaluation of Apex Height versus Drift Distance

As can be seen in Table 3, our results indicate that the apex height in meters, multiplied by a factor of 0.8, gives the maximum drift distance in meters.

The old German standard did not take shell size into account. This was changed after the BAM investigations and this report. Further it can be seen that multiplying the burst height by 0.8 results in the US 70 feet-per-shell-inch safety distance recommendation of NFPA 1123.

It has to be kept in mind that safety distances are only one possible way to prevent accidents and that equivalent technical means (redundant or spolette fusing) should always be taken into account when considering the safety distance.

Worst Case Statistical Evaluation

Despite performing a limited number of experiments, the results support the dependence of shell drift distance on shell diameter. The fact that no greater drift occurred during the limited number of test shots does not exclude the possibility that greater drifts may be possible. Therefore the drift distance results were put into a statistical model for closer investigation. It was found that the functions of impact probability versus drift distance shown in Figure 17 correlate best with the raw data without a preset upper range limit. The probability of impact above the maximum ballistic trajectory has to be zero. The upper, nonlinear part of the function, which is influenced by the few shells with high drift distances, comes close to the point to a good degree, with an error of 0.001% for the 5-inch (125-mm) shells (see bracketed value in Table 4) and 0.1% for the 6-inch (150-mm) shells (see bracketed value in Table 5). This worst case scenario considers that the shell may even be subject to a ballistic trajectory by a combination of muzzle- and flight-ballistic effects. In reality this is extremely unlikely but shall be the basis for further assumptions. From Figure 17 one can see that a 5-inch (125-mm) shell has an 88% chance to land within a radius of 75 m (old German standard) and a 96% chance to land within 105 m (new German standard). A 6-inch shell has a 57% chance to land within a

Table 3. Shell Data and Safety Distances According to Diameter.

Nom. Inner Mortar Diam. (in.)	2	2.5	3	4	5	6	8	10	12	16
Nom. Inner Mortar Diam. (mm)	50	65	75	100	125	150	205	255	305	405
Ave. Quick Match Length (cm)	50	60	75	90	110	122	140	170	170	220
Ave. Shell Diameter (in.)	2	2-1/3	2-5/6	3-3/4	4-2/3	6	7-1/2	9-5/6	11-3/5	15-5/9
Ave. Shell Diameter (mm)	52	59	72	95	119	150	190	250	295	395
Pieces per case	120	120	72	36	24	9	6	2	1	1
Mortar Length (mm)	300	405	500	600	770	950	1200	1300	1400	1810
Burst Height (m)	50	70	80	100	125	150	200	260	300	320
Burst time after firing (s)	2	2.2	2.4	3	3.4	3.5	4	4.3	5.4	6.6
Effect Duration (s)	3	3.6	4	4.5	5.2	6.5	8	8.5	9.5	13
Effect Diameter (m)	13	15	20	30	45	60	110	130	150	200
Safety Distance Standards:										
German Std. (old) (m)	70	75	75	75	75	75	125	125	125	125
German Std. (new) (m)	75	75	75	80	105	125	170	210	250	300
US-Std. (vertical) (m)	43	43	64	85	105	125	170	210	250	300
US-Std. (vertical) (ft)	140	175	210	280	350	420	560	700	840	1120
US-Std. (angled) (m)	29	29	43	58	70	85	113	140	171	200
US-Std. (angled) (ft)	95	95	140	190	230	280	370	460	560	—
Zenith × 0.8 (m)	40	56	64	80	100	120	160	208	240	256

radius of 75 m (old German standard) and an 85% chance to land within 125 m (new German standard), see Figure 18. For both calibers the risk for a blind shell to leave the safety distance was statistically reduced to one third of the old value by applying the new standard.

In any way, the asymptotic part of the functions shows the necessity to prevent blind shells, since a residual risk continues up to the maximum ballistic trajectory when using that model. Increasing the safety distance to that point would lower the risk of a blind shell to leave that area to zero, but it would be impractical for the shooter. Plus, many years of favorable experience with lower safety distances do not indicate the need for such drastic measures. The reason for that is the good reliability of today's shells. Given a blind shell rate of 0.01% and a safety distance allowing five percent of all blind shells to leave the safety radius, only one shell per 200,000 shots would fall back as a blind shell and outside the safety radius.

Even a blind shell leaving the safety radius does not mean an accident in most cases. Taking this into account, we would get a probability that is a fraction of a million for an accident per shot shell. This proportion has to be considered low enough to be comparable to other risks in life and serve as a basis for actuarial calculations.

Since the probability of coincidence of both a blind shell and long drift distance seems very small, the extrapolation of the linear part of up to 70% impact probability makes sense. One gets values of 75 m safety distance for 5-inch (125-mm) shells and 125 m for 6-inch (150-mm) shells. The first lies far below the NFPA recommendation of 105 m, and the latter matches the NFPA recommendation exactly. It is important to note that both 5- and 6-inch shells were used with a safety distance of 75 m in Germany from WWII until 1998 when the new safety distances were introduced. It is estimated that several million shells up to 6-inch diameter were shot during that period, using 75m safety distance, without any injury or casualty among the audience.

For shells larger than 6-inch, one single accident in 1997 resulted in two people being severely injured. This accident happened when a single-fused 8-inch (205-mm) shell came down 124 m away from the launch point. It could have been prevented if the shooter would have used the new distance table or angled the mortar slightly away from the spectators. From this,

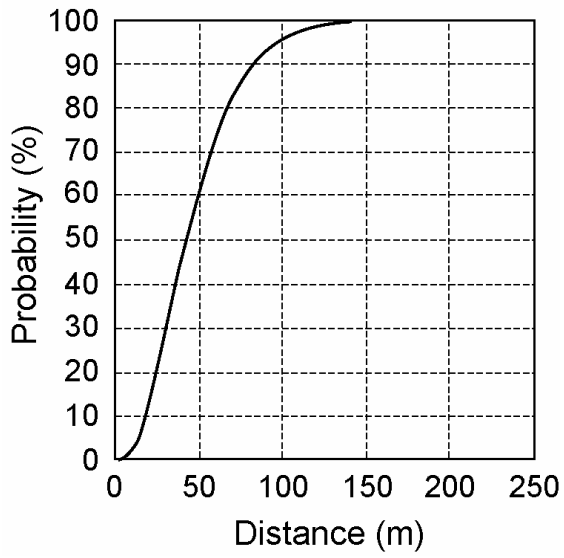

Figure 17. Impact probability for 5-inch (125-mm) shells.

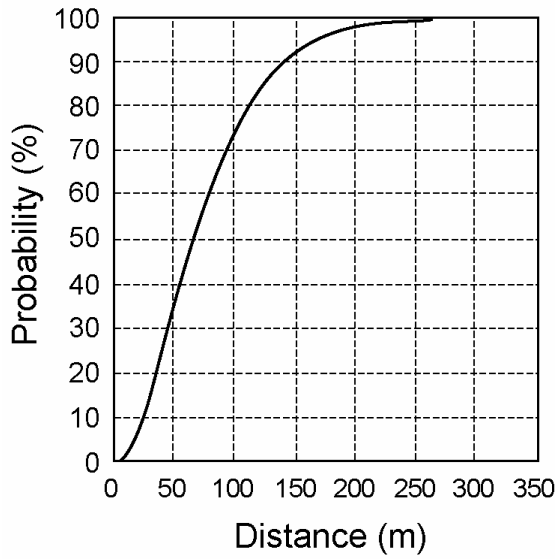

Figure 18. Impact probability for 6-inch (150-mm) shells.

Table 4. Drift Analysis for 5-inch (125-mm) Shells.

Probability (%)	Distance (m)
80	65
90	81
95	96
99	128
99.9	171
99.99	213
[99.999]	[253]

max flight distance (ballistic trajectory): 240 m
(Gamma distribution fit, scale: 15.26, shape: 3.00)

Table 5. Drift Analysis for 6-inch (150-mm) Shells.

Probability (%)	Distance (m)
80	111
90	141
95	169
99	232
[99.9]	[316]

max flight distance (ballistic trajectory): 280 m
(Gamma distribution fit, scale: 31.42, shape: 2.41)

one could deduce that the short car trip to view the fireworks display is statistically much more dangerous than watching a display at the current minimum safety distance.

Conclusions

Taking the shell diameter into account for the required safety distance proved to be correct over the last few years. Since the new safety distances have been used, no severe accidents have happened. Damages caused from fallout declined enormously. Bigger companies reported a decline of 40–50% for that kind of damage, saving some thousand €/$ per year for insurance expenses. Using the distance tables for angled shots and wind drift allows the shooter to ensure maximum safety. Correlation of the erratic drifts to mortar tilt angles allows the display operator to angle the mortars such that no blind shell will fall in the opposite direction of the angle. The necessity for increased safety distances for angled shots is based upon the shell size and angle of the mortar. Finally, the artistic value of display shows is better since the exact position of the effect can be predicted fairly precisely by the numerical model adapted by our tests.

Acknowledgements

The author acknowledges Mr. Zier for his help in mathematical matters and the German Professional Pyrotechnic Association for supporting the experimental part of this work. Thanks also to L. Weinman and M. Williams for their helpful comments.

References

1) D. Eckhardt and H. Andre, "Results and Conclusions from the Investigation of an Accident with a Display Shell", *Proceedings of the 5th International Symposium on Fireworks*, Naples, Italy, 2000.

2) Verband Deutscher Berufsfeuerwerker, VDBF e.V., Kirchhofstrasse 12, 44623 Herne, Germany; Phone: +49-2323-1919-0; Fax: +49-2323-1919-19; www.berufsfeuerwerker.de

3) National Fire Protection Association, *Code for Fireworks Displays* (NFPA 1123), Quincy, USA, 1995; [a] page 9, Table 3-1.3; [b] page 13, § A-2-1-2.

4) K. L. and B. J. Kosanke, "Drift Effect in Spherical Aerial Shells", *Pyrotechnics Guild International Bulletin*, No. 74 (1991); and "Aerial Shell Drift Effects", *Proceedings of the 1st International Symposium on Fireworks*, Montreal, Canada, 1992. Also appeared in *Selected Pyrotechnic Publications of K. L. and B. J. Kosanke. Part 2 (1990 through 1992)*. Journal of Pyrotechnics, 1996.

5) Takeo Shimizu, *Feuerwerk vom Pysikalischen Standpunkt aus*, Hower-Verlag, Hamburg, 1976, pp 188–189.

Some Properties of Explosion Generated Toroids

Fred Ryan and Joe Daugherty
PO Box 406, New Alexandria, PA 15670 USA

ABSTRACT

The mechanism of sound production from explosion-created toroids is discussed, as well as progress in rendering them more visible. The toroids, or "smoke rings", are easily formed by exploding a small charge at the bottom of a cylindrical barrel that is open at the top. The stability, self propulsion, velocities, visibility, and sound frequencies are discussed. The dependency of these properties on the toroid production parameters is experimentally compared with theoretical predictions.

Keywords: toroid, vortex, smoke ring, explosion generated, sound emission, velocity, stability, frequency, visibility

Introduction

One of the most amazing, yet easiest to produce fireworks effects, is the "howling smoke ring". A small charge is placed at the bottom of a cylindrical barrel that is open at the top. When the charge is exploded, a smoke ring (toroid) forms at the top of the barrel and rises upward for hundreds of feet into the air at high velocity, howling like a banshee all the way up. It can last for many seconds before it vanishes. The toroid is a type of vortex in which the two ends of the vortex are joined together, forming a doughnut shaped configuration. Many of its properties are shared with other types of vortex motion in that it can contain both large amounts of stored energy and possess near stability under the proper conditions. The large energy storage has led to attempts to develop the toroid as a device to shoot down airplanes and for use as an anti-personnel weapon.[1] The most familiar type of toroid is the "smoke ring". Other vortex types that are commonly known are the tornado, the "dust devil", and airplane wake turbulence.

The production of sound by a circular toroid, or by a linear vortex, is due to the turbulence produced by the circulating flow of the gases contained in it. While this flow can be supersonic, subsonic turbulence is also quite capable of producing sound. For example, turbulence is the source of the sound produced by brass instruments. The type of horizontal vortex produced in the wake of airplanes has long been known to emit sound, at frequencies typically of 1500 Hz or lower, and this sound has been proposed as a means of detecting wake turbulence vortices at airports.[2] Toroids have been seen to form in the firing of large cannons, but the noise produced by those toroids is masked by the larger noise of the cannon. In the type of toroid produced in fireworks, a rather small explosive charge is used to produce the toroid, so that the noise it produces can easily be heard, and under the proper conditions, the toroid can easily be seen. This paper discusses the physical properties of toroids, how they can be produced with explosives, and our work on making them more visible. The mathematics concerning toroid stability and the diameter/velocity relationships are fairly involved. The article concentrates less on formal mathematics and more on the use of descriptive terms, although some mathematics is necessary to quantify toroid properties.

This paper covers several fields; pyrotechnics, acoustics, optics, and aero/hydrodynamics. Going into detailed discussions in all of those fields might overwhelm some readers and cause a loss of interest in this fascinating phenomenon. The appendix contains additional information and references in the fields of optics, aerodynamics, and hydrodynamics, for those desiring more technical information. The authors are hobbyists and possess no sophisticated instrumentation for performing measurements. Consequently, our experimental measurements were often made using techniques yielding more qualitative than precise quantitative values. The most important missing instrumentation was a

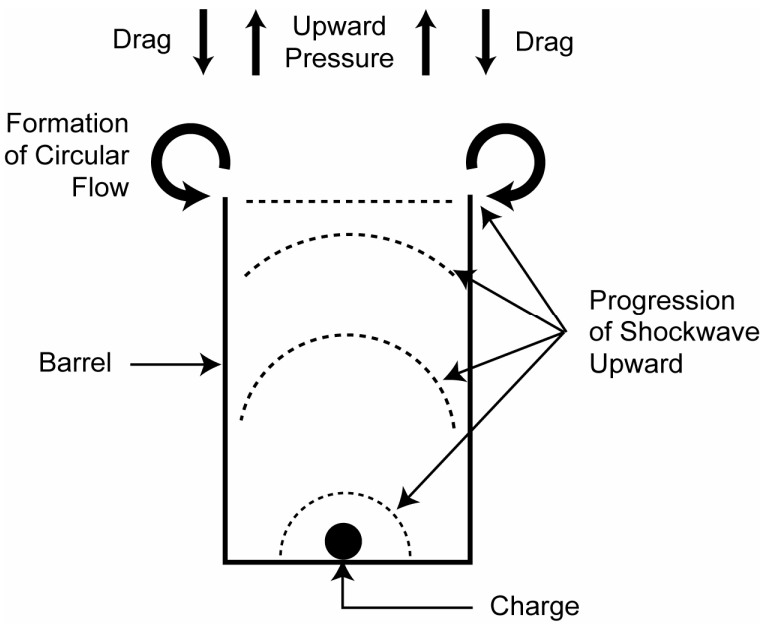

Figure 1. How the toroid is formed.

video camera, capable of directly measuring the upward velocities of the toroids and their physical dimensions versus time from formation. The experiments reported on here were performed during two time segments, separated by two years. In the first time segment, we had no video camera measurements, in the second some initial upward velocities could be measured by use of an inexpensive camcorder. Some limited correlation between those two measurements could be made. In spite of those deficiencies, we believe that our interpretations of the measurement results are reasonably consistent with the present state of understanding in the several fields.

Generation of the Toroid

If a small charge is exploded at the bottom of a cylindrical barrel that is open at the top, a shock (pressure) wave travels up the barrel as shown in Figure 1. As the shock wave travels upward, it changes from having a spherical wave front near the charge, to an almost flat wave front at the top of the barrel. When the shock wave reaches the top of the barrel, due to the high pressure inside the barrel and the low pressure outside, a circulating air current is formed at the lip of the barrel, as shown in Figure 1. This creates a toroidial smoke ring, as the effect occurs equally around the perimeter of the barrel. As the toroid rises, its shape remains relatively constant, as the centripetal forces attempting to enlarge the diameter of the circulating flow are balanced by the external aerodynamic forces acting on it.

The barrel used for most of our experiments was a "standard" American 55 gallon (200 L) steel drum. Its dimensions are approximately 23 inches (0.58 m) in diameter and 35 inches (0.89 m) in height. The explosive charge can be varied in weight and typically consists of 7 to 12 grams of a potassium perchlorate/aluminum "flash" powder, as used in fireworks salutes. The bottom of the barrel is protected by a ¼-inch (6-mm) thick steel plate.

With the dimensions of the barrel used, the ratio of height to diameter is approximately 1.5 to 1. A higher ratio would be desirable, but if the barrel diameter is kept at 23 inches (0.58 m), a longer cylinder would become difficult to handle. A diameter of much less than 23 inches would not be desirable, because the smaller diameter of the toroid produced would make it less visible. It is important to have the barrel sitting on a flat, rigid surface, or the impulse of the explosion on the bottom of the barrel could result in movement prior to the formation of the toroid at its top and interfere with the formation of the toroid.

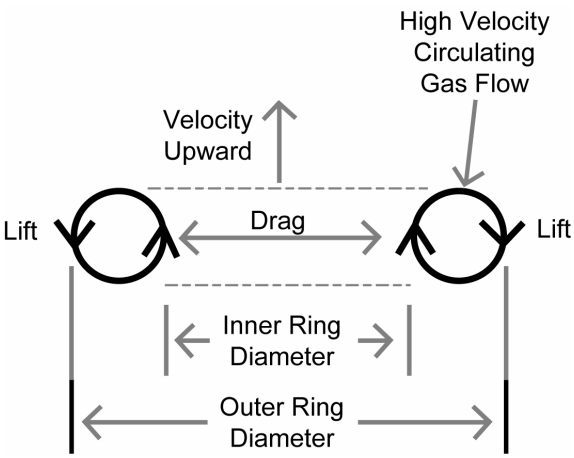

Figure 2. How the toroid propels itself upward.

Figure 2 shows the toroid rising. It propels itself upward because the downward movement of the gas at the toroid's outer diameter pushes down on the air around it, creating lift. There is a downward force produced by the upward movement at the inner diameter of the toroid, but due to the smaller circumference there, the lift contribution dominates. The sound emitted by the toroid has a principal frequency, which allows its velocity exiting the barrel to be measured using Doppler frequency shift measurements. The toroid exits the barrel at its maximum velocity, emitting a relatively low fundamental sound frequency, due to the Doppler shift. As it rises, its upward velocity continues to drop until it is practically stationary at its highest elevation, at which point it disappears. The frequency of the observed sound reaches a maximum when the smoke ring is standing still at its maximum altitude. We have measured the maximum velocity of the toroids as they exit the barrel by measuring the total Doppler frequency shift of the sound, from the frequency observed when it exits the barrel (maximum Doppler shift, minimum frequency), to the frequency emitted when it has become stationary at the top of its climb, (zero Doppler shift, maximum frequency). We assume that the intrinsic frequency of the toroid does not change during this time. The conditions necessary for this assumption to be correct are discussed in the following section.

Our Doppler measurement was done by recording the frequencies emitted and determining the frequencies exiting the barrel and at the top elevation reached, using a microphone and recorder located close to the barrel. The equation used was:

$$F_b = \frac{F_h (V_s - V_b)}{V_s} \qquad \text{Eq. 1}$$

where,

F_b = Observed frequency of toroid leaving barrel

F_h = Frequency of toroid at highest point

V_s = Velocity of sound, approx. 1100 ft/s (38 m/s)

V_b = Velocity of toroid leaving barrel

Depending on the size of the barrel and the strength of the explosive charge, velocities were measured of as low as 80 miles per hour (mph) (117 ft/s or 36 m/s), and as high as 200 mph (293 ft/s or 73 m/s). A smoke ring exiting at 200 mph is very difficult to see, as it moves so quickly that the eye has difficulty observing and tracking it, so that velocities below 100 mph (160 kph) are more desirable for fireworks purposes. The use of Doppler shift techniques to deduce the velocity of the toroid exiting the barrel was due to the simplicity of the measurement. A more desirable technique would be to measure the velocity directly, using a video camera capable of establishing a frame-by-frame time reference of the position of the toroid. We had no such equipment at the time of the Doppler shift measurements. A few video camera initial velocity measurements were made on toroids at a later date, during experiments to improve the visibility of the toroids. (See visibility of the toroids section). The flash charge used in the Doppler shift measurements was 12 grams in a two-foot (0.60 m) diameter barrel. Referring to the later video camera measurements on a reduced charge of 10 grams, also in a two foot diameter barrel, the velocity at the barrel for a 12 gram charge would be expected to be approximately 150 ft/s (102 mph or 164 kph). Our Doppler measurements for those conditions indicated an initial velocity of about 140 ft/s (43 m/s).

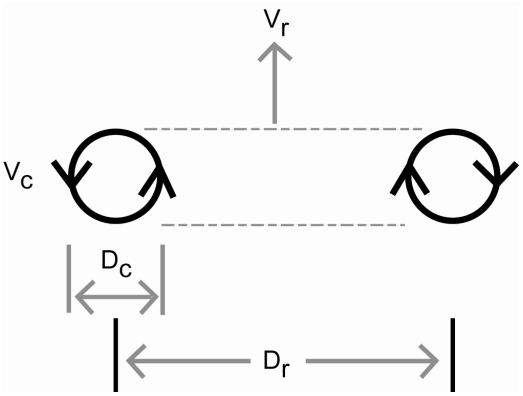

Figure 3. Drawing of toroid showing dimensions and velocities entering the stability equations.

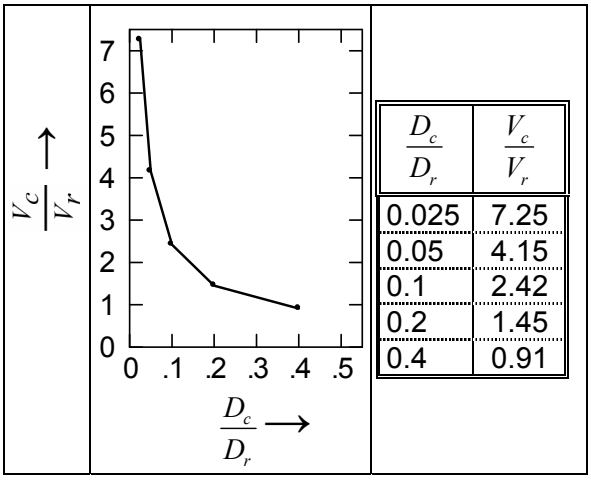

$\frac{D_c}{D_r}$	$\frac{V_c}{V_r}$
0.025	7.25
0.05	4.15
0.1	2.42
0.2	1.45
0.4	0.91

Figure 4. A plot of the relationship between V_c/V_r and D_c/D_r

Properties of the Toroid

A. Velocity Relationships

Another drawing of the toroid is shown in Figure 3, in which the major diameter is referred to as the "ring" diameter, and the small diameter of the circulating flow is termed the "core" diameter. V_r is the upward velocity of the ring, and V_c is the circulating velocity at the perimeter of the core. According to Prandtl,[3]

$$V_r = \frac{\Gamma}{\pi D_r}\left\{\ln\frac{8D_r}{D_c} - \frac{1}{4}\right\}$$

$$\text{where } \Gamma = \oint V_c \mathrm{d}r_c \cong \pi D_c V_c \qquad \text{Eq. 2}$$

$$\text{or } \frac{V_r}{V_c} \cong \frac{D_c}{D_r}\left\{\ln\frac{8D_r}{D_c} - \frac{1}{4}\right\}$$

This equation predicts a relationship between the core and ring velocities and their respective diameters. The relationship is plotted in Figure 4. While we could not measure D_c/D_r, under our test conditions the ratio does not appear to be less than 0.1. The core velocity was therefore no more than 2.4 times the ring velocity. Since the maximum ring velocity we measured was, at most, 200 mph (320 kph), our maximum core velocity was subsonic at only 480 mph (770 kph) or less, showing that supersonic turbulence is not required to produce the sound emitted by the toroids. This relationship is plotted in Figure 4. If one assumes that both the intrinsic frequency and D_r remain constant as the toroid rises, our Doppler measurements will yield correct initial velocities. The reasonableness of this assumption will now be treated.

B. Production of Sound

Toroids having low core and ring velocities produce no audible frequencies. Those toroids move silently through the air because no turbulence is produced at the interface between the moving toroid and the still air (laminar flow). The core velocities of explosion-generated toroids are sufficiently high that a great degree of turbulence is created at the interface. If the cross-section of the core remains perfectly circular, the noise created would consist of a broad spectrum of frequencies. While the toroids we produced possessed many frequency components, one primary frequency dominated the audible emissions observed. This primary frequency would vary with experimental parameters, such as the diameter of the barrel, and the size of explosive charge used, but there was always one primary audio frequency (or narrow frequency band) generated. It is of interest to consider how this can happen.

A large number of studies have been made on audible emissions from toroids. Most of those were studies in small water filled chambers, but some also in a compressible medium such as air. We refer here only to the measurements performed in air.

Toroids have been found to exhibit instabilities under turbulent conditions, leading to a distortion in the shape of the toroid. Consider the

core of a toroid in which no distortion exists (A) and a simple distortion (B). (See Figure 5.)

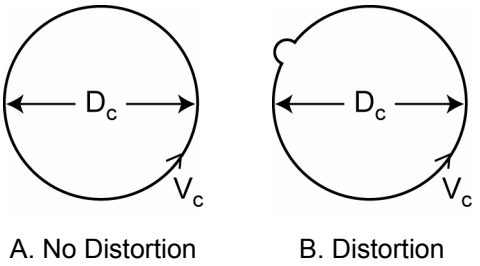

Figure 5. How sound can be generated by a distortion in the core.

A distortion, such as shown in (B), will obviously generate a primary frequency at:

$$f = \frac{V_c}{\pi D_c} \qquad \text{Eq. 3}$$

where the perimeter equals πD_c

From measurements performed in air, Zaitsev and Kop'ev[4] (also located in reference 5 on page 688) found that equation 3 is adequate to account for the dominant emitted frequency (or narrow frequency range), for a fast toroid in air.

Therefore, combining equations 2 and 3,

$$f = \frac{V_r}{\pi \frac{D_c^2}{D_r}\left\{\ln\frac{8D_r}{D_c} - \frac{1}{4}\right\}} \qquad \text{Eq. 4}$$

Since we have no present capability of measuring either V_r or D_c/D_r versus time, we make the following simplifying assumptions:

1) The intrinsic frequency does not change as the toroid rises. That is the assumption made in our Doppler measurements.
2) The ring diameter remains constant with time. That appears to be true from visual observations.

If both the frequency and the ring diameter remain constant with time, then as the ring velocity decreases as the toroid rises, the ratio of the core diameter to the ring diameter must also decrease or

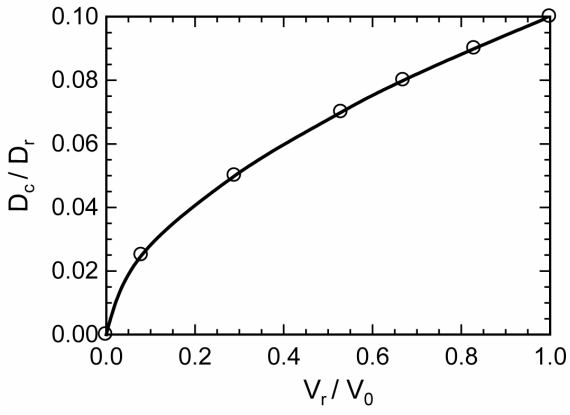

$\frac{D_c}{D_r}$	$\frac{V_r}{V_0}$
.1	1
.09	.83
.08	.67
.07	.53
.05	.29
.025	.08
0	0

Figure 6. Decrease in toroid core diameter with decrease in upward velocity of ring referred to initial velocity. Assumptions discussed in text.

$$V_r = \pi f \frac{D_c^2}{D_r}\left\{\ln\frac{8D_r}{D_c} - \frac{1}{4}\right\} = \pi f D_r \left(\frac{D_c}{D_r}\right)^2 \left\{\ln\frac{8D_r}{D_c} - \frac{1}{4}\right\} \qquad \text{Eq. 5}$$

This is plotted in Figure 6 for an initial ring velocity of V_0.

We now calculate the values of the parameters, using equation 5, for the following conditions:

1) The explosion of 12 grams of flash composition in a 2-foot diameter barrel.
2) The initial ratio of D_c/D_r at the barrel visually estimated to be about 0.1
3) An initial V_r at the barrel is V_0 and equals 150 ft/s (0.45 m/s) as estimated from a video camera measurement.

Table 1. Parameter Values for a Typical Rising Toroid.

$\frac{D_c}{D_r}$	D_c (ft)	$\frac{V_r}{V_0}$	$\frac{V_c}{V_0}$	V_c for V_0 = 150 ft/s (ft/s)	f for V_0 = 150 ft/s (Hz)
.1	.200	1	2.420	363.0	578
.09	.180	.83	2.178	326.7	578
.08	.160	.67	1.963	290.4	578
.07	.140	.53	1.694	254.1	578
.05	.100	.29	1.210	181.5	578
.025	.050	.08	0.605	90.7	578
0	0	0	—	0	—

Initial toroid velocity $V_r = V_0 = 150$ ft/s (45 m); $D_r = 2$ ft (0.6 m); $D_c/D_r = 0.1$; $D_c = 0.2$ ft (0.6 m).
To convert from ft/s to m/s multiply by 0.3048.

The calculated values of all parameters are listed in Table 1. The top line contains the values as the toroid leaves the barrel, while the bottom line contains the values at its highest point. The calculated frequencies in the last column are in reasonable agreement with the intrinsic measurement obtained by Doppler measurements. (550 Hz), and the initial velocity obtained by Doppler measurement (140 ft/s or 0.42 m/s).

A consistent picture emerges from Table 1 that can explain all of the phenomena observed. As the toroid rises:

1) D_c/D_r decreases, reducing lift, as the difference between the inner and outer toroid diameters becomes smaller. From Figure 3 $(D_r - D_c)$ and $(D_r + D_c)$
2) V_r decreases.
3) This process continues as the rotational energy stored in the core is drained, due to losses to turbulence, sound production, and gravitational potential energy.
4) The intrinsic frequency generated remains constant since, as the core's rotational velocity decreases, the transit time of a distortion around the perimeter of the ever-smaller core remains constant.
5) The toroid vanishes at its peak height, since the lift, D_c/D_r, and the stored energy, all go to zero.

Although this picture is logical and self-consistent, its validity should be tested by directly measuring D_c/D_r and V_r with time. That measurement is not within our capabilities at present.

Visibility of the Toroid

One problem with smoke rings is that they can be difficult to see. Not only are they rising at a great speed, but also they are normally pale white in color. They can be hard to see against the light blue color of the sky or the white color of clouds. Two approaches are useful in improving the visibility during daytime, increasing the scattering by incident sunlight and increasing the color difference between the toroid and the background by introducing color-absorbing material into the toroid.

A. Increasing the Light Scattering Power of the Toroid

The scattering power of the toroid depends on the index of refraction of the products of explosion contained within it and the size of the particles. Since we have no knowledge of the size of the particles trapped in the toroids, an exact analytical treatment of the scattering cannot be given. There are three distinct regions of light scattering, depending on the size of the particle relative to the wavelength of the light. These three regions are discussed in the appendix. In all of those cases, the effective index of refraction of the particles is important, as it distinguishes the particle from the surrounding air. For a given particulate weight trapped in the toroid however, the size is also very important in determining the total light scattering cross

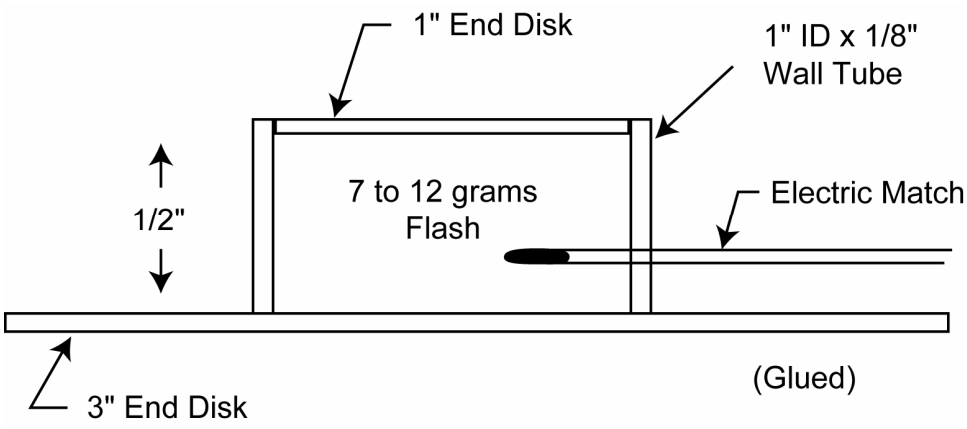

Figure 7. Assembled charge. [Note: to convert from inches to mm multiply by 25.4.]

section. Table 2 lists the indices of refraction of some typical flash powder by-products.

Table 2. The Index of Refraction of Some Flash By-Products.

Compound	Index of Refraction
KCl	1.49
Al_2O_3	1.7
MgO	1.74
TiO_2	2.5 to 2.9*

*varies with crystal structure

It is the difference between the index of refraction of the particles and the index of air (=1) that is important. From Table 2 it can be seen that the substitution of some or all of the aluminum with titanium should give the best visibility, and that was verified by our tests. Even increasing the relative amount of aluminum in the flash composition gives some improvement. Formulas that worked well are listed in Table 3.

Table 3. Flash Compositions for Increasing the Toroid Visibility.

Formula	$KClO_4$ Wt. Parts	Wt. Parts / Fuel
1	7	5 / Alcan-Toyo Al-105
2	6	3 / 'Very fine' Ti
3	50/50 mix of formulas 1 and 2	

The potassium perchlorate must be ground to an extremely fine dust for these formulas to work properly, as they are considerably off stoichiometry (the air in the barrel makes up for the missing oxygen). Alcan-Toyo Al-105 is a 6-micron, atomized aluminum; other very fine aluminum may be substituted. The "very fine" titanium was obtained from the Fire Art Corporation in Clearfield, PA. Similar particulate titanium from other sources could be substituted. The size distribution we measured for the Fire Art "very fine" titanium is listed in Table 4.

Table 4. Measured Size Distribution of the Fire Art Titanium.

Mesh Size	Pass/Stop	Wt. %	Size Micron
200	pass	100	<72
325	stop	15	>42.5
400	stop	45	>37.5
400	pass	40	<37.5

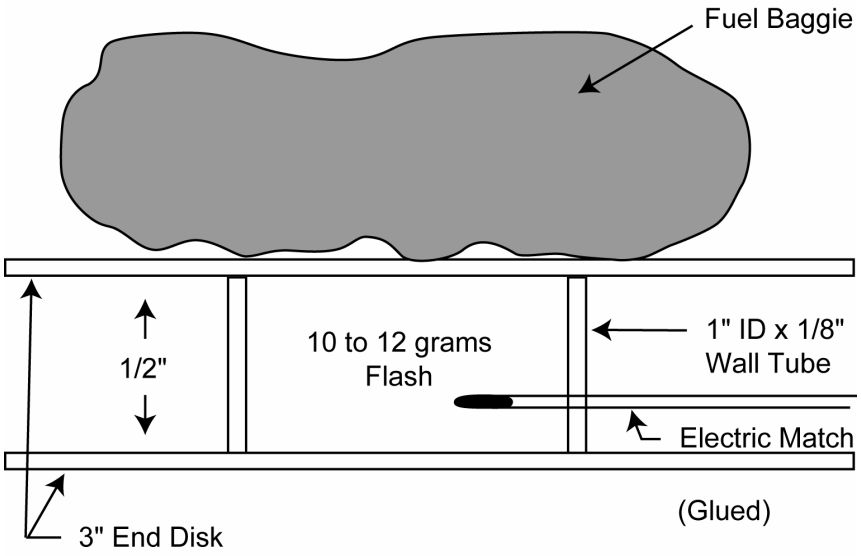

Figure 8. Plastic "baggie" full of fuel over flash configuration.
[Note: to convert from inches to mm multiply by 25.4.]

Of the three formulas given, formula 2 was the most visible, followed by formula 3, then 1. All could probably be changed to increase even further the fuel excess present, limited only by the ability of the composition to function properly. These mixtures were put into containers as shown in Figure. 7.

We also did optimization experiments in which an attempt was made to increase the visibility by incorporating material external to the charge. Two configurations were used as shown in Figures 8 and 9. In Figure 8, a plastic sandwich "baggie", which contained various fuels, was placed over the top of the charge. The hope was that some of the material in the baggie would be carried up with the shock wave, perhaps oxidizing on the way up, and become entrapped in the smoke ring to increase its visibility. The materials tried and the results are listed in Table 5.

Although some visibility improvement was seen with the "baggie" approach, we felt that much of the material was being scattered in directions that would not allow it to be trapped in the toroid, and that it was therefore being wasted. The configuration shown in Figure 9 was adopted to minimize the waste, as the material would be directed more in the direction of the toroid formation. That indeed proved to be the case, and visibility improvements equivalent to the "baggie" approach could be obtained with one third or less fuel. For example, as little as 20 grams of "very fine" titanium gave results comparable to 100 grams in the "baggie" approach. The flash compositions containing titanium worked as well as either of these approaches and used even less titanium. The configurations of Figures 8 and 9 are useful however, in evaluating the incorporation of new materials.

Table 5. Materials Used and Results of the "Baggie" Tests.

Material (100 g)	Test Results, Visual Observation
None	Standard for comparison
Lime dust	No improvement
Red Phosphorus	No improvement
#809 Dark Aluminum	No improvement
#401 Alcoa 12 micron Al.	Slight improvement in visibility
#813 Aluminum, bright flakes	Improved visibility
#105 Alcan-Toyo 6 micron Aluminum	Yet better improvement
Fire Art very fine Ti	Best improvement of all

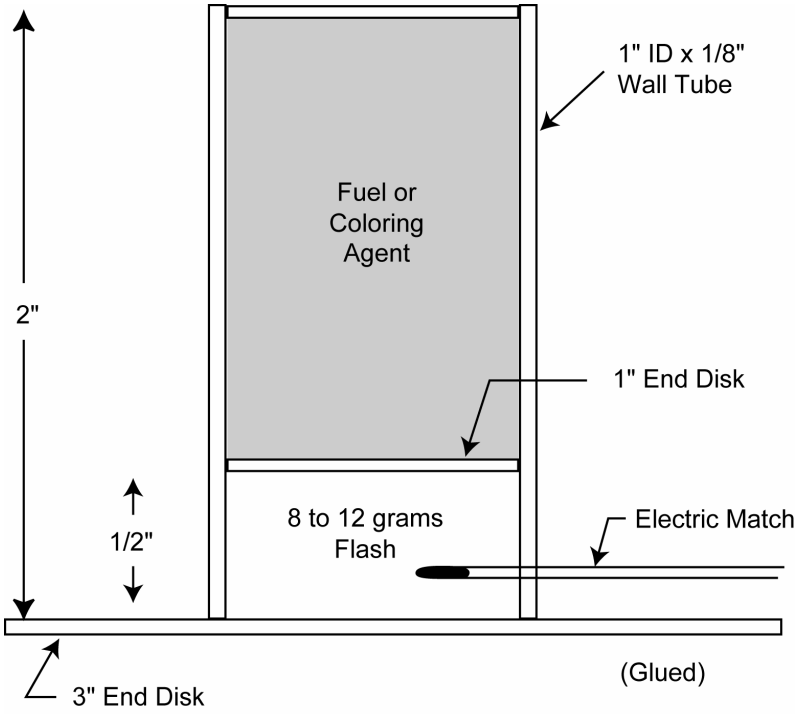

Figure 9. Coaxially stacked fuel or coloring agent over flash configuration. [Note: to convert from inches to mm multiply by 25.4.]

B. Increasing the Toroid Visibility by Introducing Light Absorbing Material into It

This method places colored absorbing material in the toroid, but it is not without problems. It not only adds coloration to the toroid but also reduces the visibility enhancement due to light scattering. Under the proper ambient conditions this trade-off is desirable. A series of experiments were run using both the "baggie" arrangement of Figure 8 and the arrangement of Figure 9. Materials used were carbon lamp black and three inorganic pigments: iron(III) oxide (red), chromium(III) (green), and an unspecified mixture of oxides of nickel, titanium, antimony (yellow). The inorganic pigments were obtained from suppliers of pigments for paints, and their particulate size distributions are unknown. The finest appeared to be the red iron(III) oxide. Observations were made both visually and recorded using a video camera. The two methods supplemented each other as some effects were most easily seen by eye and some by the camera. The camera witness also had the advantage that it could be played back, over and over, to establish the exact results. One very unexpected result was that two distinct toroids would often be formed, one traveling at high speed, and a second toroid traveling at a much slower velocity. Both toroids contained some of the color absorbing material. The results are listed in Table 6.

Only in test 7 were both "slow" and "fast" colored toroids seen. Sometimes only a "slow" colored toroid was seen, and sometimes only a "fast" colored toroid was seen. In a few tests apparently no "fast" toroid was formed, as evidenced by the lack of the sound normally produced. The "fast" colored toroids appeared to have the velocity typical of other toroids, while the "slow" toroids were moving much slower and emitted no sound. A moderate wind was blowing during the tests and the "slow" toroids would be quickly deflected away from the path of the "fast" toroid, and out of the range of the camera, so that they were best seen visually. We estimate that their velocities were about one tenth as fast as the velocities of the "fast" toroids and did not last nearly as long.

There are two plausible explanations for the formation of the "slow" colored toroids. One is that the pigments contained a large distribution

Table 6. Results of the Coloration Tests.

Test	Flash (g)	Color	(g)	Observation
1	10	Black	(20)	Fast black toroid seen with loud sound
2	10	Red	(20)	Fast faint red colored toroid with fair sound
3	10	Green	(20)	Slow green toroid, faint sound /fast toroid
4	7	Black	(20)	Fast toroid, no color, loud sound
5	7	Black	(10)	Slow black toroid, faint sound/fast toroid
6	7	Red	(10)	Slow red toroid only, no sound or fast toroid
7	7	Red	(20)	Slow red toroid, faint fast red toroid
8	7	Yellow	(10)	Fast yellow toroid only, fair sound
9	7	Green	(10)	Slow green toroid, faint sound/fast toroid
10	7	Red	(12.5)	Slow red toroid only, no fast toroid

Tests 1–9 used the arrangement of Figure 8. Test 10 used the arrangement of Figure 9.

of particle sizes and only the smaller ones could remain stably within the "fast" toroids. The larger ones would be thrown out, forming a somewhat larger, slower toroid. Another is that, since a great excess of pigment was present in the air following the explosion, with little actually becoming incorporated into the "fast" toroid, a pressure wave from the top of the barrel would be reflected to the bottom of the barrel and rise again, forming the "slow" toroid. Exactly how the "slow" toroids are formed still remains a mystery.

The coloration tests show that light-absorbing material can indeed be incorporated into the toroids. A more efficient approach to utilizing the material is needed, as very little of the material was actually incorporated. Finer pigment particle sizes would be desirable, and the explosive charges probably need to be increased in strength, as evidenced by the failure to produce "fast" toroids in some cases. More experiments should be done utilizing organic dyes, as their molecular structures are typically only about .01 microns long and would easily be stable within the toroids, assuming that they survive the combustion from the explosion.

Future Work

We intend to extend this work to utilizing organic dyes for daytime viewing. No work has yet been done on incorporating light emitting material for making the toroids visible at night. Two approaches that could have utility are the use of fluorescent organic dyes, excited by an external source of illumination, and chemiluminescent dyes. It is also possible that materials such as lampblack could leave a residual glowing effect if they are incorporated while burning. If greatly enhanced visibility of the toroids can be obtained, we may attempt to measure the toroid velocities directly and V_c/V_r as the toroids rise, using a higher quality video camera.

Acknowledgments

Some of this work was previously published in *American Fireworks News*, No. 222, March 2000, and No. 224, May 2000. We thank the publisher of AFN for permission to use that material. We also thank Robert C. Miller and Frederick Johnson for helpful suggestions that added to our understanding of toroids. The referees are also acknowledged for their very constructive comments.

References

1) D. Pasternak, "Wonder Weapons", *US News and World Report*, July 7, 1997, pp 41 and 45.

2) T. S. Perry, "Tracking Weather's Flight Path", *I. E. E. E. Spectrum*, Sept. 2000, p 42.

3) L. Prandtl, *Fundamentals of Hydro and Aeromechanics*, Dover Publications, 1957, p 212. [The equation referenced in the text appears much earlier in a translation of a paper by Helmholtz done by Sir W. Thomson that appeared in *Phil. Mag.*, Volume 33, No. 4 (1867) p 511.]

4) M. Yu Zaitsev and V. F. Kop'ev, *Akust. Zh*, Vol. 39, No. 6(1993) p 1068. [*Acoust. Phys.*, Vol. 39 (1993) p 562.]

5) V. F. Kop'ev and S. A. Chernyshev, "Vortex Ring Oscillations, the Development of Turbulence in Vortex Rings and the Generation of Sound", *Physics-Uspeckhi*, Vol. 43 No. 7, 2000, pp 663–690. English translation available from http://ufn.ioc.a.c.ru/abstracts/abst 2000 /abst.007.html

6) *American Institute of Physics Handbook*, D. E. Gray, Ed., McGraw Hill Inc., 1986, Sect. 6 p 7.

7) *Handbook of Optics*, W. G. Driscoll, Ed., McGraw Hill Inc., 1978, Sect. 14, p 11.

8) *Handbook of Laser Science and Technology*, *Vol. 4, Optical Materials*, Part 2, M. J. Weber, Ed., CRC Press, 1986, p 139.

Appendix

A. Aero- and Hydrodynamics

Kop'ev and Chernyshev[5] published a review paper on the generation of sound by toroids. Much of the experimental research reported there concerns toroids generated in an incompressible medium (water). Toroids can easily be made visible in water by launching them from a dyed region into a clear one. Studies on sound generation in a compressible medium (air) rely on sound detection more than visual detection. These studies are typically conducted in rather small measurement chambers, to facilitate measurements. By contrast, our measurements extend over hundreds of feet and involve toroids rising upwards. Since our measurement results were more difficult to obtain, we rely heavily on the "small chamber" work for analogy. The work of Zaitsev and Kop'ev[4] in an air chamber showed that the primary audio frequency range generated is due to the simple core rotational frequency of a core deformation. Much more complex core deformations have been observed in liquids, also capable of producing sound, such as those corresponding to the set of Bessel function modes (eigen values) of the toroids, due to their circular geometry. Drawings of some of these can be seen in reference 5 on pages 675 through 677. These modes involve distortions of the core such as a periodic bulging of the toroid at some sections, and a narrowing at others, or a periodic movement out of the plane of the toroid in some sections, and an opposite motion in others. The sound frequencies produced by the Bessel modes are much lower than the core rotational frequencies, but they could well have been observed by us. In every toroid we produced, a low frequency modulation of the primary frequency was present (a "wow"). Since we possessed no audio spectrum analyzer, an accurate measurement of the frequency(s) of these Bessel modes could not be measured, but they were below 10 Hz in frequency. Although the Bessel modes were observed in water chambers, analogous phenomena should appear in air also.

B. Optics.

The text treated the visibility of the toroids as a simple matter of light scattering and/or absorption, due to the index of refraction of the entrapped particles differing from the index of air. While that contains a good deal of truth, it is a simplification. The values of the index of refraction that we quoted were for well-defined, solid crystalline materials. Much of the scattering or absorbing material trapped in our toroids is anything but well defined. The products of explosion, such as TiO_2, have only microseconds to form as particles, and are certainly more amorphous than crystalline. While their effective index of refraction is certainly related to that of crystalline material, it surely differs. That is only one of many complicating issues. Another is that the index of refraction is a complex number in the case where the particle also absorbs some of the incident light.

The actual index is $N = n - ik$, where n is the index in the absence of absorption, and k is the so-called "extinction" coefficient, related to absorption, see reference 6. Three regions of scattering can be easily treated if the scattering particles are "well defined". For wavelengths much smaller than the dimensions of the particle, scattering can be treated as reflective or refractive scattering, where light is reflected or refracted from the particles. For a simple case of normal incidence on a well defined, geometrically shaped particle, the reflectance, P, is

$$P = \frac{(n_0 - n_1)^2 + k_1^2}{(n_0 + n_1)^2 + k_1^2} \qquad \text{Eq. 6}$$

For reflection from a particle of index $N = n - ik$, where in air, $n_0 = 1$. For light incident at angles off normal, the reflectance is higher, and refraction within the particle causes light to leave from its sides, reducing the transmitted intensity further. If one factors in the very irregular shapes that our trapped particles certainly possess, the calculation becomes intractable. Yet, the process is index of refraction dependent.

Light scattering from particles whose wavelength is comparable to the size of the particle is called "Mie" scattering.[7,8] Again, the Mie theory treats scattering from simple geometrical shapes, such as spheres. In spite of the complicated geometry of our trapped particles, Mie scattering still shows an increase with an increase in the index of refraction of the particles.

In the final limit, where the dimensions of the particles are much less than the wavelength of the light, the theory of Rayleigh applies,[7,8] in which the scattering power increases as

$$\frac{1}{\lambda^4}$$

where λ is the wavelength as the wavelength of the light approaches the dimensions of the particles. Here also, the scattering strength depends on the index of the particles.

The exact calculation for the scattering and absorbing power of our ill-defined particles is therefore not within reach. What remains, however, is that the index of refraction is an important parameter in all cases. Said another way, if the index of refraction of the particles was identical to that of the surrounding air, the light radiation would not know of the presence of the particles and no scattering would occur. The index values quoted in the text therefore have relative importance in the total removal of incident light, regardless of the theoretical treatment.

Feasibility Study on the Use of Nanoscale Thermites for Lead-Free Electric Matches

Darren L. Naud,* Michael A. Hiskey, Steven F. Son, James R. Busse, and Ken Kosanke†

* Los Alamos National Laboratory, High Explosives Science and Technology, DX-2, MS C920
Los Alamos, NM 87545, USA email: naud@lanl.gov, son@lanl.gov

†PyroLabs, 1775 Blair Road, Whitewater, CO 81527, USA email: ken@jpyro.com

ABSTRACT

Electric matches are used in the pyrotechnic industry to electrically initiate devices remotely and with precise timing. Unfortunately, most current commercial electric matches contain lead compounds, which when burned produce lead reaction products that may cause environmental pollution and contamination of firing areas. These lead compounds, namely lead thiocyanate, lead nitroresorcinate and lead tetroxide, are used in electric match pyrotechnic formulations because a small diameter resistive bridgewire can reliably initiate them. A possible alternative to lead-containing compounds is nanoscale thermite materials, otherwise known as Metastable Intermolecular Composite (MIC) materials. These super-thermite materials can be formulated to be sensitive to thermal stimuli, such as resistive heating. In the effort to produce a lead-free electric match, a feasibility study was performed using nanoscale aluminum and molybdenum trioxide mixtures in electric match formulations.

Keywords: nanoscale, thermite, lead-free, electric match, metastable intermolecular composite, performance test, sensitiveness test

Introduction

The pyrotechnic industry favors electrical ignition of fireworks and stage special effects over manual ignition when such displays are choreographed to music, when more precise timing is required for an artistic effect, or when ignition must be done remotely. In addition, very large firework shows are better and more safely managed with a central computerized firing station than by teams of personnel in the midst of the display area manually igniting devices. Unfortunately, electric matches are remarkably sensitive to electrical stimuli when compared to initiators sometimes used by other industries (e.g., aerospace, defense and petroleum), such as exploding bridgewires (EBW) or an exploding foil initiator (EFI or slapper). A current as small as 350 milliamps can reliably fire some electric matches, whereas an EBW requires a special capacitive discharge circuit to provide approximately 200 amperes of current and 2 joules of energy for proper functioning. The EFI has even higher power requirements. Although it is generally recognized by the pyrotechnic industry that electric matches are prone to accidental ignition, it is this same industry's demand for simple, relatively inexpensive initiators that has largely determined the performance characteristics of today's electric matches. This, along with the need for inexpensive firing sets and wiring, has played a predominant factor in their development. The need stems from the large number of individual ignitions that are required for a display. For example, a single pyrotechnic show may require hundreds, if not thousands, of electric matches and miles of wire.

For electric matches to fire at such low electrical energies, a thermally sensitive initiating composition is required. The typical means of initiation is a hot Nichrome wire having a diameter no greater than approximately 1 mil (25 microns). Of the compositions that are commonly used, many contain lead compounds in the form of lead thiocyanate, lead nitroresorcinate or lead tetroxide. These lead compounds—when formulated in appropriate ratios and with other constituents—produce the desirable thermally sensitive compositions. But, as expected, these match compositions produce lead reaction products that may cause environmental pollution

and contamination of firing areas, which is an undesirable feature. This paper reports on the performance and sensitivity test results of using nanoscale thermite, namely the aluminum and molybdenum trioxide pair, as a substitute for lead-based compositions in electric matches. Nanoscale reactants, which are also known as Metastable Intermolecular Composite—or MIC materials (pronounced "Mick"), were first developed by Los Alamos National Laboratory approximately 8 years ago.[1] Only in recent years, however, has research investigating the utility of MIC been expanded into the fields of explosives, thermobarics, lead-free primers, reactive projectiles, rocket propellants and electric matches.[2]

Match Head Design

While the construction and composition of commercially available electric matches are varied, a common form is diagrammed in Figure 1. The bridgewire, usually a fine filament of Nichrome, is strung and soldered across the edge of a copper-foil-clad substrate somewhat similar to circuit board material. The size of the substrate is approximately 0.4 inch long by 0.1 inch wide and 0.03 inch thick (10 by 2.5 by 1 mm). A bead of pyrotechnic material is formed over the bridgewire by dipping the end of the substrate into a slurry of a pyrotechnic composition. Although not shown in the diagram, a commercial match often contains two distinct layers of composition. The composition most sensitive to initiation by the bridgewire is applied first (generally referred to as the primary coating or layer). This is followed by a secondary coating of a different pyrotechnic mixture. The secondary composition, which is ignited by the primary, produces the desired thermal output (e.g., flame, sparks, molten slag or droplets) that initiates the pyrotechnic device, such as a Black Powder charge. To supply power to the bridgewire, electrical leads (approximately 24 gauge) are soldered at the base of the electric match substrate. The substrate containing the bridgewire and pyrotechnic bead is usually called the *match-head* (or *fuse-head* in other countries).

The outer lacquer coating (see Figure 1) protects the match head from physical damage during handling and, if the composition is water sensitive, seals the match head from moisture. In addition, a non-conductive coating such as

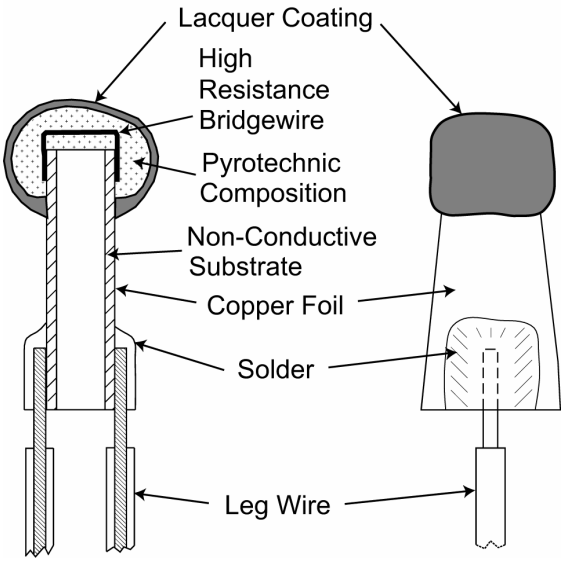

Figure 1. General diagram of an electric match.

lacquer can act as an electrical insulator to prevent accidental ignition by electrostatic discharge (ESD). In one possible accident scenario, the current induced by static electricity can travel from a point external to the electric match tip, through the outer match coating and pyrotechnic composition, then to the electrical leads via the bridgewire. In this process, if the ESD energy is sufficient, the electric match composition is ignited. In an earlier study, the outer coating of a number of commercially available matches was examined.[3] It was found that matches with imperfections or holes in the outer coating are much more susceptible to this type of accidental ESD ignition.

The typical bridgewire resistance in commercially available electric matches is between 1 and 2 ohms.[4] Matches with higher resistances function better but are more difficult to manufacture, while those with lower resistances (less than 1 ohm) require more current to fire and are therefore less desirable to the industry. To illustrate the importance of the bridgewire's resistance to overall performance of an electric match, Figure 2 shows an electric match in a typical firing configuration. The electric match, presumably imbedded within a pyrotechnic device, such as a fireworks aerial shell lift charge or star mine, is connected to a fire set by two annealed copper leads of 100 feet (30.5 m) length.

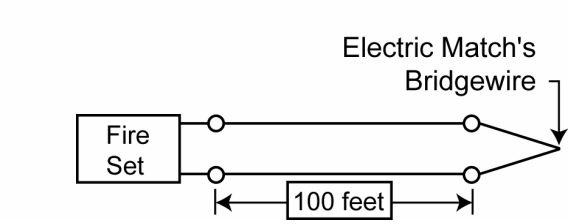

Figure 2. A typical setup for firing an electric match in a pyrotechnic display. A distance of 100 feet between the fire set and the electric match provides a safe operating distance between the fire set and the display site.

For the purpose of this example, the 100 feet distance was arbitrarily chosen as a safe distance between the operator of the fire set and the display site. As the fire set powers the electric match, not all of the energy provided by the fire set is deposited into the bridgewire. The wire leads have electrical resistance that dissipates part of the energy. This is especially problematic when the resistance is substantial in comparison with that of the igniter (i.e., when the leads are long or the wire is of small diameter).

To better illustrate how the wire leads can affect the proper functioning of an electric match, Table 1 lists the resistance and diameter of three example wire gauges that might be used by an operator. (One should note from the table that the resistance of a copper wire increases with decreasing wire thickness, since electrical conductivity is proportional to the cross-sectional area of the wire.) The percentage of electrical energy deposited by the fire set onto the bridgewire (denoted as $\%E_{bw}$) is expressed in the most simple terms by the following equation, where

Table 1. Measured Properties of Annealed Copper Wire of Three Gauges.

Gauge	Wire Thickness (mils)	Resistance for 100 ft wire at 20 °C (Ω)
18	40	0.64
20	32	1.02
24	20	2.57

Note 100 ft = 30.5 m, and 1 mil = 25 microns.

R_{bw} is the resistance of the bridgewire in ohms,

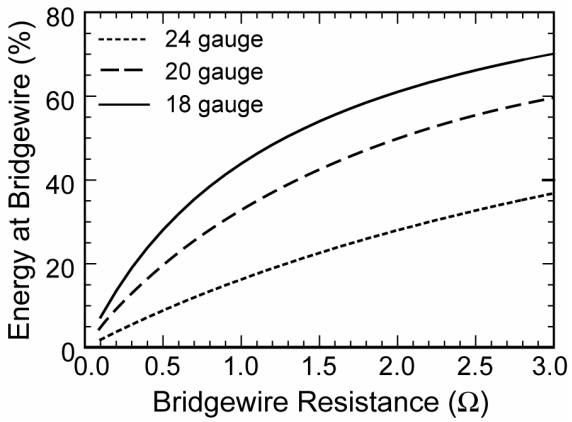

Figure 3. Percent energy at the bridgewire ($\%E_{bw}$) as a function of the bridgewire's resistance and the type of wire leads used. The upper curve represents two 100 feet wire leads with 18 gauge thickness; the middle curve represents that for 20 gauge; and the bottom curve is that for 24 gauge.

and R_w is the resistance of 200 feet of copper wire leads.

$$\%E_{bw} = \frac{R_{bw}}{R_{bw} + R_w} \times 100$$

Figure 3 shows the change of $\%E_{bw}$ as the resistance of the bridgewire, R_{bw}, is varied from 0.1 to 3 ohms for the three different wire gauges. It can be seen that the energy deposited at the bridgewire significantly decreases for a bridgewire resistance less than 1 ohm, especially when thin wires—with relatively high resistances—are used. For this reason, commercially available electric matches intended for pyrotechnic displays generally have a bridgewire resistance of 1 ohm or more. To approximate the industry standards, the electric match chosen for this study had a resistance of about 1 ohm.

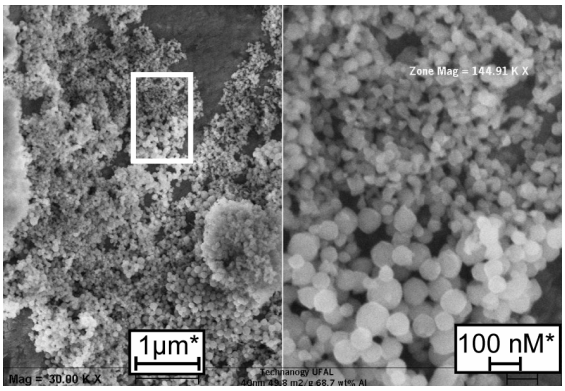

Figure 4. SEM of 40-nm Technanogy aluminum.

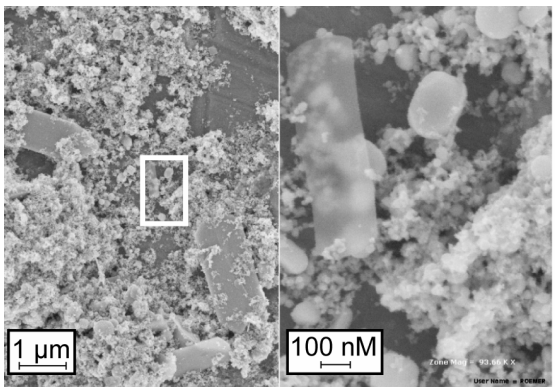

Figure 5. SEM of Climax molybdenum trioxide.

Materials Used

Nanoscale Thermite

Interest in nanostructures has grown since it has been demonstrated that the reactivity of MIC materials is much greater than those composed of micron-sized grains. For example, aluminum and molybdenum trioxide mixtures with an average particle size ranging from 20 to 50 nm react more than 1000 times faster than mixtures using conventional micron-sized or larger particles. The reason for such reactivity has been attributed to the large reduction in the diffusion barrier between reactants.[1] One process for manufacturing nanoaluminum involves vaporization of the metal from a resistively-heated ceramic boat followed by rapid condensation of the vapor in an inert atmosphere (argon or helium). Particle size and distribution can be controlled using various techniques.[5] Because pure aluminum of such small particle size is pyrophoric, the surface of the aluminum is passivated by controlled addition of oxygen (to form an oxide coating on the metal surface) soon after the aluminum has condensed. The oxidant of the thermite pair, molybdenum trioxide, is also produced in a similar fashion, except the addition of passivating oxygen is not needed.

Technanogy, Inc.[6] provided the three sizes of nanoaluminum that were used in this study, specifically 40, 121 and 132 nm powders (T40, T121 and T132, respectively). These sizes represent the approximate mean of their particle distributions. Only one type of nanoscale molybdenum trioxide was used as the oxidant with the above aluminums; this material was purchased from Climax Corporation.[7] Figures 4 and 5 are scanning electron micrographs (SEM) of the 40 nm aluminum and the Climax molybdenum trioxide powders, respectively. Unlike the nanoaluminums, the molybdenum trioxide has a more varied morphology and distribution of particle size, consisting of thin sheets and rounded particles. From small-angle scattering analysis, the sheet thickness was measured to be approximately 15 nm.[8]

The aluminum and molybdenum trioxide thermite mixtures used for the test matches were composed of approximately 40 to 45 percent aluminum (by weight) with the remainder being molybdenum trioxide. The exact amount of aluminum used in the thermite mixtures depended on the thickness of the oxide coating for a given aluminum sample. The procedure for quantifying free aluminum was by thermogravimetric analysis (TGA), where the aluminum sample mass was monitored with increasing temperature in the presence of oxygen. Oxidation of the aluminum causes the sample mass to increase until all of the aluminum has reacted. Knowing that the increase in mass is attributed to the conversion of free aluminum to aluminum oxide, the amount of free aluminum can therefore be calculated.

Simple mechanical mixing of the thermite mixture does not produce a homogeneous mixture of nanosized reactants; rather coarse agglomerates of each reactant are formed. To break up the agglomerates, hexane is added to the dry mixture and the resulting slurry was sonicated for about 30 seconds. The hexane was

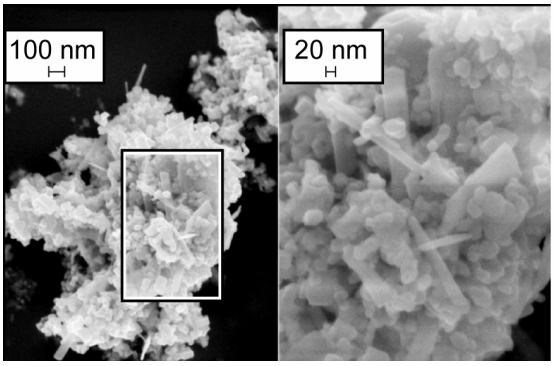

Figure 6. SEM of a 40 nm aluminum and molybdenum trioxide mixture.

then evaporated and the resulting granulated powder sieved through a 45 mesh screen to break up the mass of powder. Because the resulting powder is ESD sensitive, small amounts (about 0.5 gram) are mixed and handled to minimize the hazards of an accidental initiation. Scanning electron micrographs (see Figure 6 for one example) have verified that the sonication procedure produces a highly intimate mixture of fuel (aluminum) and oxidant (molybdenum trioxide).

Three different batches of electric match composition were prepared during the course of this study and are designated as Batch Nos. 1, 2, and 3. The differences between the batches are the types and amounts of MIC powders used in the primary formulations, which are given in greater detail below. (In general, the reactivity of the MIC powders increases with smaller particle size distribution.)

Blank electric matches (i.e., without pyrotechnic material dipped on the bridgewire) for this study were obtained from two sources. Batch No. 1 test matches used blank match heads purchased from Firefox Enterprises, Inc.[9] Unfortunately, these match heads had a bridgewire resistance of less than 0.1 ohms, and while they were deemed not suitable for firing current tests, they were suitable for most of the sensitiveness tests. To have match heads with a higher resistance and a narrower range of resistance values, other blank match heads were obtained from Martinez Specialties, Inc.[10] These blanks had a distribution of resistance values of approximately 0.9 ± 0.1 ohm. This resistance is somewhat low as compared to other commercially available matches[4] but is within the acceptable range. With these blanks, Batch Nos. 2 and 3 of electric matches were prepared for additional performance testing.

The first manufacturing step was to prepare the slurries for each layer in the match. The first layer, the primary, consisted of 91% MIC and 9% nitrocellulose (13.5% nitrogen content), which was dissolved with ethyl acetate containing 0.3% FC 430 surfactant from 3M, Inc. Depending on the viscosity of the slurry, the primary layer was built up on the bridgewire by dipping the match head three or four times. The secondary composition was composed of 56.1% potassium perchlorate (sieved through 120 mesh screen), 27.0% 12µ German black aluminum, 8.6% nitrocellulose, 8.1% sponge titanium (–80 to +100 mesh), 0.2% super-fine iron oxide[11] as a catalyst for decomposition of the potassium perchlorate, and enough ethyl acetate solvent to form a thin slurry. Approximately 6 to 8 dips into the secondary composition were needed to build up the match head to the desired size. The outer protective coating was produced by dipping the match head in a vinyl solution.[12] For Batch No. 1 test matches, only a single dip in the vinyl solution was performed; for Batch Nos. 2 and 3, four dips were performed. Between each of these 3 layers (primary, secondary and vinyl coating), the match heads were dipped once in 10% nitrocellulose lacquer to serve as a barrier between each layer.

As previously mentioned, the amount and type of MIC in the primary formulations were different for the three batches. For Batch No. 1, the aluminum portion of the thermite mixture was composed of 60% T121 and 40% T132. For Batch No. 2, only type T132 aluminum was used. Batch No. 3 matches were made somewhat differently from Batch No. 2, whereby the blank match head was dipped once in a thermite formulation composed with T40 aluminum only. Thereafter, the primary layer was built up with two to three successive dips into a thermite slurry composed with T132 aluminum. This was done to see if less electrical current would be required to fire a nanoscale thermite composed with 40-nm aluminum rather than that containing the 132-nm aluminum. Previously, matches were made using a primary composition that contained only the T40 aluminum.

However, when these matches were fired, it was found that their reactivity was too great. These matches exploded or ignited violently and had difficulty in fully igniting the secondary composition. Therefore, to reduce the quantity of the most reactive T40 aluminum in the primary layer, the T40 thermite was limited to a single dip on the bridgewire. Then the less reactive T132 thermite was used to complete the build up of the primary layer. Again, as stated previously, only one type of molybdenum trioxide, obtained from Climax, was used as the oxidant pair in all of the above thermite mixtures.

Results and Discussion

A reasonably thorough study of electric match sensitiveness has been published for ten different match types from four commercial suppliers in a series of short articles in *Fireworks Business* as well as in this journal.[3,13] Since testing of the prototype MIC matches was performed under similar conditions using the same equipment, some comparisons can be made between data of the MIC test matches and the data reported for the commercial matches. However, because of the voluminous amount of data that has been presented in these published works, the authors do not wish to reprint the data, but rather compare the results in qualitative terms. Furthermore, since these MIC matches are the first prototypes (i.e., not finalized designs for commercial production) and future iterations with improved performances are expected, strict interpretation of the test results may be considered superfluous. (Readers wishing for more information on the setup and conduct of the testing than is given below should consult reference 3.)

Impact Sensitiveness

The impact sensitiveness test apparatus is of a standard drop hammer design, except that a lighter than normal drop hammer (1 kg) was used. To better simulate the typical use environment of an electric match in a fireworks display (e.g., electric match inside the paper tube of a piece of quick match), the test match was inserted inside the fold of a 0.01-inch (0.25-mm) thick card stock, and the hammer was allowed to fall onto the assembly. For these tests, the match heads had their wire leads removed, as it was believed that the thickness of the solder connection and wire could absorb some of the impact energy. Earlier testing had shown that a protective shroud on electric matches provided a substantial decrease in their impact sensitiveness. However, at this time, the impact sensitiveness of these test matches covered with a shroud was not investigated. The impact result, typically reported in inches of hammer drop height, was determined for the test match heads following the standard stair-step (Bruceton) method for 20 samples from Batch No. 1.[14] A value of 56 cm (22 inches) was obtained for the test matches using the 1 kg drop hammer. This was significantly better than all of the commonly used commercial matches.[3] Only the low-sensitiveness matches had better performance (the Daveyfire *AN 26 F*, the Luna Tech *Flash* and the Martinez Specialties *Titan*).

The match head samples were also subjected to impact testing in the presence of Black Powder. In these tests, the inside surface of the card stock was heavily painted with a slurry of Black Powder (bound with 5% dextrin) and thoroughly dried. Using the previously obtained impact height of 56 cm, ten matches were consecutively struck at that height. A result of five ignitions out of ten suggests that the presence of Black Powder does not appear to increase their sensitivity to impact.

Friction Sensitiveness

Because a standard friction apparatus is more suitable for powdered samples, a modified test apparatus was used for friction testing the match heads. In these tests, the test match was used as the striker, held at a 45^{o} angle to a moving abrasive surface (#100 grit sand paper). Each test consisted of a set of three trials of three matches at the lowest force setting (a 1.5 N force holding the match head to the abrasive surface). If the matches failed to ignite, a greater force (3.0 N) was used for another set of three trials. Again, if there was no ignition, a still greater force of 6 N was applied on a final set of three matches. Test matches from Batch No. 1 demonstrated no ignition, even at the maximum force setting of 6 N. This is better than all of the commonly used commercial electric matches and

as good as any of the low sensitiveness matches that were tested.[3]

Thermal Sensitiveness

Two thermal test methods were employed for characterizing the match samples. In the first test, described as a *Ramp Ignition Temperature* test, electric match heads were placed inside individual small wells drilled into an aluminum block, which was heated at a rate of 5 °C per minute—beginning at room temperature. The test was concluded when all of the test matches ignited or a temperature of 300 °C was reached. With Batch No. 1 test matches, it was found that no matches ignited below 300 °C, which was as good as any of the electric matches tested previously, including the commercially produced low sensitiveness matches.[3]

Because some electric match compositions can slowly decompose without producing an ignition event while the temperature is ramped up, a second test method, described as a *Time to Ignition* test, was employed using the same heating block. However, the block was heated to a specific temperature and held constant. Then a single match was inserted into a well. If the match ignited within approximately 5 seconds, the temperature of the block was taken as an indication of its thermal sensitiveness. For those matches not igniting at this temperature, the block's temperature was increased by ten degrees and the test repeated. Similarly, if the match ignited in less than 5 seconds, the block's temperature was reduced 10 degrees and the test repeated. For the test matches, the time to ignition at the highest temperature attainable of 300 °C was 28 seconds. Again, this result was as good as any of the electric matches previously tested, including the commercially available low sensitiveness matches.[3]

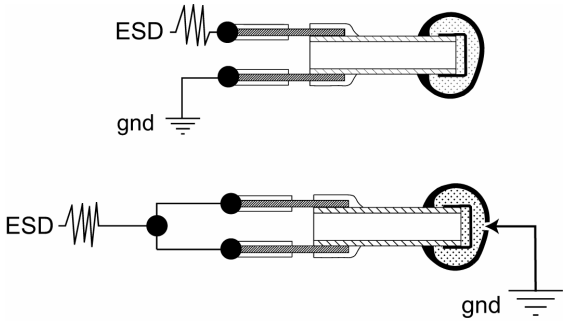

Figure 7. Illustration of the two basic ESD test configurations used in this study.

ESD Sensitiveness

Two tests were performed on the prototype matches to characterize their ESD sensitiveness. In the first test, sensitiveness to electrostatic discharge through the bridgewire was determined by passing discrete amounts of discharge energy through the bridgewire in much the same fashion as the intended firing current (see top configuration, Figure 7). Using an energy storing power supply, the electric match is subjected to electrical discharge energy at a low setting and a positive or negative ignition is noted. The discharge energy is increased incrementally until an ignition is achieved. Much like the impact testing, the discharge energies are raised or lowered following the standard stair-step (Bruceton) method for a series of approximately 20 match tests. The resulting stair-step value provides an ESD energy value that should initiate approximately half of the matches. This test was performed on Batch Nos. 2 and 3 test matches. For Batch No. 2 matches, the ESD energy value was measured at 230 mJ, which is significantly better than all of the commonly used commercially produced electric matches and on a par with the low sensitiveness matches. For Batch No. 3 matches, which contained the more reactive T40 aluminum, the ESD result dropped to 120 mJ, which is comparable to the least sensitive of the commonly used matches.[3]

In the second series of tests, the discharge current is typically passed from the bridgewire through the pyrotechnic composition to ground, as illustrated in Figure 7 (bottom configuration). However, the test results can at times be difficult to interpret because they are highly de-

pendent on the nature of the outer coating. All commercial matches have a protective coating that covers the pyrotechnic composition. This coating strengthens the match head, limits physical damage during normal handling, and, if the composition is water sensitive, offers protection of the match head from moisture. However, an important characteristic of a nonconductive coating is that it can act as an electrical insulator to prevent accidental ignition by an electrostatic discharge through the composition. Unfortunately, imperfections in the coating seem to occur frequently, whether such imperfections are created at the time of manufacture or as a result of abrasion or crushing during rough handling. The effect is that such imperfections can greatly increase the sensitiveness of the match to electrostatic discharge through the composition.[3] Thus, before the test matches were subjected to this electrostatic discharge test, the integrity of the coatings was inspected.

An instrument designed to make high resistance measurements was used to evaluate the resistance from the coating to the bridgewire. In this analysis, the leg wires of the electric match are tied to one terminal of the instrument and a test probe is connected to the other terminal. The test probe applies up to 200 volts (but with limited current) to help induce a dielectric breakdown at the match surface as the probe is moved over the match tip to find points of low resistance. A good protective coating with no defects was generally found to provide more than 500 megohms (MΩ) of resistance. Some matches, specifically those with surface defects, register much lower surface resistance values. For Batch No. 1 test matches, which were coated with only one dip in vinyl lacquer, the surface resistance values varied greatly, measuring from less than 1 MΩ to approximately 200 MΩ. The consequences of the poor coating was demonstrated by subjecting these same matches to 18 mJ of electrostatic discharge energy through the coating; out of 10 matches tested, 9 ignited. Compared to some of the commercially produced matches, the Batch No. 1 matches faired poorly.[3] Gaining insight from these test results, Batch Nos. 2 and 3 matches were coated with four dips of vinyl instead of one, with the hope of covering any imperfections, such as tiny bubbles or cracks. The surface resistance values of 10 test matches from Batch No. 2 yielded only one match with 400 MΩ resistance, with the remainder registering 500 MΩ. For Batch No. 3, all were greater than 500 MΩ, which was the limit of the testing device. Undoubtedly the additional coats improved the surface resistance values. Out of 10 Batch No. 2 matches that were subjected to 18 mJ of electrostatic energy, 3 ignited; for Batch No. 3, only 1 match out of 10 ignited. For Batch No. 3, an additional 10 matches were subjected to 180 mJ of electrical discharge energy, and again only one ignited. While these results are positive, they do demonstrate that the matches are not entirely free of surface defects. An inspection using light microscopy indeed revealed the occasional presence of tiny bubbles in the vinyl coating.

Because it cannot be assumed that the electric match coatings will be in sufficiently good condition to completely protect the matches from discharges through the composition, the second type of ESD test was performed on matches that had intentional coating damage inflicted upon them. In this way, the test would be a measure of the ESD sensitiveness of the electric match composition only and not the degree of protection afforded by the coating. In this test, a portion of the outer coating of the electric match was removed using emery paper before they were subjected to the electrostatic discharges. Similar to the first test described above, the matches are exposed to increasing increments of discharge energy until initiation is observed. Using the Bruceton method, the discharge energy is raised or lowered for a series of 20 matches. From these results, an approximate 50% ignition energy value is obtained (i.e., the energy that would initiate 50% of the matches tested). Only Batch No. 1 matches were tested, which yielded an ESD value of 0.7 mJ, which is very low, but not quite as bad as the worst of the commonly used matches.[3] This is not surprising to the authors, as the aluminum–molybdenum trioxide MIC thermite has been previously demonstrated to be ultrasensitive to spark initiation.[15] Attempts to reduce the spark sensitivity of MICs by using fluorocarbon coatings have produced positive results, but how such coatings may affect other performance and sensitivity parameters have yet to be investigated.

Table 2. Estimates of the Likely No-Fire, All-Fire and Recommended Firing Currents for Batch Nos. 2 and 3 Prototype Electric Matches.

Batch No.	Resistance (Ω)		Current (Ampere)		
	Average	Range	No-Fire	All-Fire	Recommended
2	0.9	0.8–1.0	0.45	0.90	1.4 / 1.8
3	0.9	0.8–1.0	0.35	0.70	1.1 / 1.4

Firing Current Tests

The preferred electric match is one where its sensitiveness to friction, impact and other stimuli are low, while leaving the match with a recommended firing current that is less than 1 ampere. This value is not arbitrary, but rather a performance criterion that has been shaped by the electrical firing equipment in use by the pyrotechnic industry. However, the recommended firing current of commercially available matches fall into two groups.[4] One group, which consists of the electric matches most sensitive to accidental ignition by all causes, has a range of recommended firing currents between 0.5 and 1.0 amperes. The second group, with recommended firing currents of 2.0 to 3.5 amperes, is much less sensitive to accidental ignition. That is to say, the least sensitive matches are also the most difficult to ignite intentionally. What would be ideal, and what was hoped for with the MIC electric matches, is that they would combine general low sensitiveness to accidental ignition and yet have a firing current below 1 ampere (i.e., similar to those in the most sensitive group). Table 2 lists the no-fire, all-fire and recommended firing currents for Batch Nos. 2 and 3. These values are only estimates, since the number of electric matches made and tested was not sufficient to develop very accurate firing current values. The two values listed as recommended firing current are for firing individual matches (1.5 times the approximate all-fire current) and matches in series (2 times the approximate all-fire current). Because the matches of Batch No. 1 had relatively heavy gauge (large diameter) bridgewire, with resistance values around 0.1 ohms, they were deemed not suitable for current testing. For the prototype MIC electric matches, it appears that the firing current needed for ignition lies somewhere between those recommended for the sensitive and insensitive groups of commercially produced electric matches. It appears that less current was needed for Batch No. 3 matches (all-fire current of 0.70 ampere), which contained the most reactive T40 nanoaluminum. Batch No. 2 matches, having a primary composition composed entirely of the lesser reactive 132-nm aluminum, required a slightly higher current (all-fire current of 0.90 ampere).

A potential problem was discovered during the performance of the current-firing tests. It appears that the matches occasionally become non-ignitable when moderate currents, somewhat less than the no-fire current, are first passed through the bridgewire.[16] Thereafter, increasing the current only causes the bridgewire to fuse without initiating the composition. This occurred most often with those matches containing the less reactive 132-nm aluminum. It is speculated that the hot bridgewire, while not sufficiently hot to initiate the composition, is hot enough to decompose some of the material around the bridgewire, which creates a gap around it, thus thermally decoupling the wire from the remaining composition. This problem could be attributed to the decomposition of the nitrocellulose binder in the primary formulation. Future work may investigate the effect of binders on the reactivities of MIC thermites. It should be noted that some of the most commonly used electric matches also have a similar *fuse but no fire* problem when they are subjected to gradually increasing firing current.

Additional Discussion

There is concern that matches that contain nanoaluminum may not have good long-term storage, since moisture and atmospheric oxygen can oxidize the aluminum and render the composition useless. Such aluminum has extremely high-surface area and special care must be afforded to its storage, especially in humid envi-

ronments. However, two simple and severe tests demonstrated that the vinyl coating used on the prototype matches appears to serve as an excellent barrier to moisture. In one test, five test matches were submerged in a container of water for 1 week before they were removed and test fired. All of the matches ignited properly. In the second test, two matches were exposed to steam by suspending them over boiling water for 14 hours. Again, the matches fired readily despite the vinyl coating taking on a cloudy and wrinkled appearance.

While a secondary formulation with good ignitability characteristics (aluminum and potassium perchlorate mixture) was employed for these prototype electric matches, more difficult-to-ignite (and generally less sensitive) secondary formulations could be used instead. In one example, matches were prepared with a T132 aluminum and molybdenum trioxide primary composition, followed by a secondary composition of aluminum powder alone. In both compositions about 10 percent of nitrocellulose was used as a binder. This aluminum had a broad particle distribution that centered at 200 nm but contained particles of up to 1 micron in diameter. Igniting this match produced an entirely unique effect; a half dozen sparks were thrown to a distance of 6 feet and burned white hot for approximately 2 seconds. It is thought that the aluminum burned slowly because it was dispersed as large fragments whose burn rate was limited by the availability of atmospheric oxygen. It would seem that such matches, with pure aluminum as the secondary component, would be less sensitive to accidental ignition from stimuli such as friction and impact.

Insofar as the aluminum–molybdenum trioxide MIC thermite appears to have functioned well in our feasibility study, there is no doubt that some improvements could be made. Only one thermite pair was investigated for this study, but scores of other thermites exist, as well as intermetallic reactions. It may very well be that an altogether different primary composition can be employed with better results. Fischer and Grubelich[17] produced an extensive compilation of these reactions along with their respective energy output. In addition to thermites and intermetallic reactions, simple oxidant–fuel combinations could be used. Recently, potassium perchlorate has been produced as nanoscale particles with the hope of having enhanced reactivity.[18] Such materials and their use in electric matches in primary compositions have yet to be investigated.

Conclusion

The utility of a nanoscale aluminum–molybdenum trioxide thermite as an initiating composition for electric matches was examined. These nanoscale reactants, otherwise known as Metastable Intermolecular Composite (MIC) materials, were demonstrated to be sufficiently sensitive for electric match use. The estimated recommended firing current for the MIC matches lies approximately between those of the least and most sensitive matches that are commercially available. Best results for minimum firing currents were achieved for matches with the most reactive aluminum (i.e., 40-nm particle distribution). In addition, the sensitiveness of these test matches was measured and compared to commercial electric matches. The prototype matches faired very well in impact, friction and thermal stability tests, equal or better than the most commonly used matches. The same matches were on a par with the most commonly used commercial matches in electrostatic discharge tests, both through the bridgewire and through the composition. Improvements in the manufacture of the protective outer coating should alleviate much of the electrostatic discharge sensitivity. In addition, a myriad of yet uninvestigated nanoscale thermites, reactants, or intermetallic pairs may prove more useful as electric match compositions.

References

1) C. E. Aumann, G. L. Skofronick, and J. A. Martin, *Journal of Vacuum Science & Technology* B 13(2) (1995) pp 1178–1183.

2) S. F. Son, M. A. Hiskey, D. L. Naud, J. R. Busse and B. W. Asay, "Lead-Free Electric Matches", *Proc. of the 29th Int'l Pyrotechnics Seminar*, Westminster, CO, July, 2002, p 871.

3) K. L. and B. J. Kosanke, "Studies of Electric Match Sensitiveness", *Journal of Pyrotechnics*, No. 15 (2002).

4) K. L. and B.J. Kosanke, "Electric Matches: Physical Parameters", *Fireworks Business*, No. 206 (2001).

5) J. A. Puszynski, "Formation, Characterization, and Reactivity of Nanoenergetic Powders", *Proc. 29th International Pyrotechnics Seminar*, Westminster, CO, July, 2002, p 191.

6) Technanogy, Irvine Corporate Park, 2146 Michelson Drive, Suite B, Irvine, CA 92612, USA; phone, +1-949-261-1420; web-site, www.technanogy.net.

7) Climax Molybdenum Marketing Corp., 1501 W. Fountainhead Parkway, PO Box 22015, Tempe, Arizona 85285-2015, USA.

8) P. D. Peterson, J. T. Mang, S. F. Son, B. W. Asay, M. F. Fletcher and E. L. Roemer, "Microstructural Characterization of Energetic Materials", *Proc. 29th International Pyrotechnics Seminar*, Westminster, CO, July, 2002, p 569.

9) Firefox Enterprises, Inc., PO Box 5366, Pocatello, ID 83202, USA.

10) Martinez Specialties Inc., 205 Bossard Road, Groton, NY 13073, USA.

11) Super-fine iron oxide, or nanocat, is available from Mach 1, Inc., 340 East Church Road, King of Prussia, PA 19406, USA, phone +1-610-279-2340.

12) Vinyl lacquer was obtained from Firefox Enterprises; the lacquer was thinned with a 50/50 mixture of toluene and methyl ethyl ketone before use.

13) K. L. and B. J. Kosanke, A series of articles on Electric Matches: "General Safety Considerations and Impact Sensitiveness", *Fireworks Business*, No. 198 (2000), "Sensitiveness to Electrostatic Discharges Through the Bridgewire", *Fireworks Business*, No. 199 (2000), "Sensitiveness to Electrostatic Discharges Through the Composition", *Fireworks Business*, No. 200 (2000), "Sensitiveness to Friction and Temperature", *Fireworks Business*, No. 201 (2000), "Black Powder's Effect on Sensitiveness", *Fireworks Business*, No. 202 (2000), "Effect of Shrouds on Sensitiveness", *Fireworks Business*, No. 203 (2000).

14) A measured impact height using the Bruceton method correlates to a height where there is a 50% probability of initiation.

15) ESD tests on nanoscale thermites were performed at Los Alamos National Laboratory, Los Alamos, NM, USA.

16) In this test, the current was applied for 5 seconds or until an ignition event occurred. However, no match that did fire took longer than about 150 ms to fire (i.e., no ignition occurred in the interval between 150 milliseconds and 5 seconds in any of the test matches).

17) S. H. Fischer and M. C. Grubelich, "Theoretical Energy Release of Thermites, Intermetallics, and Combustible Metals", *Proc. 24th International Pyrotechnics Seminar*, Monterey, CA, July, 1998, p 231.

18) Private communication with Anita Renlund, Sandia National Laboratories, Albuquerque, NM, USA.

Events Calendar

Pyrotechnics and Fireworks

Recent Advances in Pyrotechnics

June 8–12. 1 2003, Chestertown, MD, USA
Contact: John Conkling
PO Box 213
Chestertown, MD 21620, USA
Phone: +1-410-778-6825
FAX: +1-410-778-5013
email: John.Conkling@washcoll.edu
web: www.John.Conkling.washcoll.edu

2003 Le Mondial SAQ Montreal Fireworks Competiton

June 21 Arc en Ciel (France)
June 28 Hop Kee Pyrotechnics Ltd (China)
July 05 Parente Fireworks (Italy)
July 09 Cienfuegos (Argentina)
July 16 Pirotecnia Minhota, LDA (Portugal)
July 16 Explosive Entertain. Int'l (Australia)
July 19 Atlas Pyrovision Productions (USA)
July 23 Royal Pyrotechnie (Canada)
July 26 Kimbolton Fireworks LTD (England
July 30 Panzera S.A.S. & La Ronde (Closing)

For more information, visit the web site:
www.montreal-fireworks.com or
www.lemondialsaq.com

30th Int'l Pyrotechnics Seminar held in conjunction with **Euro Pyro 2003.**

June 23–27 2003, Saint-Malo, France

Contact: Claude Prisset, Seminar Chairman
AFP, PO Box 121
45240, La Ferte, Saint Aubin, France
e-mail: europyro.2003@club-internet.fr
web: http://perso.club-internet.fr/afpyro

7th World Fireworks Championship

June 30 La Tirrena di Ferraro (Italy)
July 02 {restatecj Artifices (France)
July 04 Privatex Pyro (Slovakia)
July 06 Fuochi srl (Italy)
July 08 Hanwha Corp. (South Korea)
July 10 Apogée Fireworks (Canada)
July 12 Parente Fireworks – Grande Finale

Contact: Antonio Parente
Parente Fireworks srl
107 via Oberdan
Melara (RO) 45037, Italy
Phone: +39-0425-89035
FAX: +39-0425-89640
email info@parente.it
web: www.fioridifuoco.it

2003 Les Grands Feux Loto Québec Fireworks Competition

July 26 Steefes-Ollig & Co. (Germany)
July 30 F.A.S. srl (Italy)
Aug. 2 Pyro Spectacular cc (South Africa)
Aug. 6 Foti Int'l. Fwks. (Australia)
Aug. 9 APOGÉE Fwks. – Grand Finale

Contact: Amy Spooner, Public Rel. Dir.,
Les Grands Feux du Casino du Lac-Leamy
81 rue Jean-Proulx, bureau 200
Hull, Quebec, J8Z 1W2, Canada
Phone: +1-819-771-3389
FAX: +1-819-771-3858
Email: feux@qc.aira.com
Web: www.feux.qc.com

Chemistry of Pyrotechnics & Explosives

July 27 – Aug. 1 2003, Chestertown, MD, USA
Contact: John Conkling
PO Box 213
Chestertown, MD 21620, USA
Phone: +1-410-778-6825
FAX: +1-410-778-5013
email: John.Conkling@washcoll.edu
web: www.John.Conkling.washcoll.edu

Celebration of Light – Fireworks Competition in Vancouver, Canada

July 30 Czech Republic
Aug. 02 Canada
Aug. 06 China
Aug. 09 Finale

For more information visit the web site:
http://www.celebration-of-light.com

Pyrotechnics Guild Int'l Convention

Aug. 9–15 2003, Gillette, WY, USA
Contact:, Ed Vanasek, Sec. Treas.
18021 Baseline Avenue
Jordan, MN 55352, USA
Phone: +1-952-492-2061
e-mail: edvanasek@aol.com
web: www.pgi.org

31st Int'l Pyrotechnics Seminar

July 11–14, 2004, Fort Collins, CO, USA

Contact: Linda Reese, Appl. Res. Assoc., Inc.
5941 S. Middlefield Rd., Suite 100
Littleton, CO 80123, USA
Phone: +1-303-795-8106
FAX: +1-303-795-0125
email: lreese@ara.com

7th Int'l. Symp. on Fireworks

October 6–10 2003, Valencia Spain

Contact: Fred Wade
Box 100
Grand Pré, NS, B0P 1M0, Canada
Phone: +1-902-542-2292
FAX: +1-902-542-1445
email: fireworks@fireworksfx.com
web: www.ISFireworks.com

1st Workshop on Pyrotechnic Combustion Mechanisms

July 10, 2004, Fort Collins, CO, USA

Contact: Dr. Steve Son
Los Alamos National Lab
PO Box 1663
Los Alamos, NM 87545, USA
email: son@lanl.gov
web: http://www.intlpyro.org/pyro-combustion-mechanisms.htm

Energetic Materials

Computational Mech. Assoc. Courses–2003

Contact: Computational Mechanics Associates
PO Box 11314,
Baltimore, MD 21239-0314, USA
Phone: +1-410-532-3260
FAX: +1-410-532-3261
email: 74047.530@compuserve.com
web: www.compmechanics.com

34rd Int'l Annual Conf. ICT – Energetic Materials – Reactions of Propellants, Explos. and Pyro.

June 24–27 2003, Karlsruhe, Germany

Contact: Manuella Wolff
Fraunhofer-Inst. für Chem. Technologie (ICT)
P. O. Box 1240
D-76318 Pfinztal (Berghausen), Germany
Phone: +49-(0)721-4640-121
FAX: +49-(0)721-4640-120
email: mw@ict.fhg.de
web: www.ict.fhg.de

Franklin Applied Physics Lectures

July 21–25, 2003, Oaks, PA, USA

Contact: James G. Stuart, Ph.D., Pres.
Franklin Applied Physics, Inc.
98 Highland Ave., PO Box 313
Oaks, PA 19456, USA
Phone: +1-610-666-6645
FAX: +1-610-666-0173
email: JStuartPhD@aol.com

4th Int'l. Symp. On Heat Flow Calorimetry of Energetic Materials

Sept. 8–10, 2003, Leeds, United Kingdom

Contact: Ms. Sarah Goodall
The Centre for Thermal Studies
The University of Huddersfield,
Huddersfield, HD1 3DH, UK
Phone: +44-1484-473179
FAX: +44-1484-472643
email: s.goodall@hud.ac.uk

EFEE 2nd World Conference on Explosives and Blasting

Sept. 10–12, 2003, Prague, Czech Republic

Contact: Dr. Jan Novosad
Czech Soc. Blasting Tech. and Pyrotechnics
Novotného lávka 5, 116 68
Praha 1, Czech Republic
Phone: +420-2-2108-2248
FAX: +420-2-2108-2366
email: org@explosives.cz
web: www.explosives.cz

2003 Int'l Autumn Seminar on Propellants, Explosives and Pyrotechnics

October 15–18, 2003, Guilin, China

Contact: Prof. Feng Changgen
Mech. & Engr., School of Mech.-electr. Engr.
Beijing Institute of Technology
PO Box 327
Beijing 100081, China
FAX: +86-10-6891-1849
FAX: +1-602-938-2053 [USA]
email: lsc@iaspep.com.cn or hmcspaddn@aol.com
web: www.iasepep.com.cn

PARARI 2003 – An International Explosive Ordnance Symposium

October 29–31, 2003, Canberra, Australia

Contact: Ordinance Safety Group
Dept. of Defence, CP4-3-160
Canberra, ACT, 2600
Australia
Phone: +61-2-6266-3058
FAX: +61-2-6266-4781
email: dmo-jlc-osg-parari@cbr.defence.gov.au
web: www.defence.gov.au/dmo/jlc/osg/osg.cfm

3rd Int'l. Disposal Conference

November 10–11, 2003, Karlskoga, Sweden

Contact: Prof. Dan Loyd
LiTH, SE-581 83
Lingoeping, Sweden
Phone: +46-13-281-112
FAX: +46-13-281-101
Email: danlo@ikp.liu.se

13th Int'l Symp. on Chemical Problems Connected with the Stability of Explosives

May 2004 (tentative) Sweden

Contact: Stig Johansson
Johan Skyttes väg 18, SE 55448
Jönköping, Sweden
Phone/FAX: +46-3616-3734
email: srj@telia.com

Franklin Applied Physics Lectures

July 26–30, 2004, Oaks, PA, USA

Contact: James G. Stuart, Ph.D., Pres.
Franklin Applied Physics, Inc.
98 Highland Ave., PO Box 313
Oaks, PA 19456, USA
Phone: +1-610-666-6645
FAX: +1-610-666-0173
email: JStuartPhD@aol.com

Propulsion

AIAA/ASME/SAE/ASEE Joint Propulsion Conference

July 20–23 2003, Huntsville, AL, USA

Contact:
Phone: +1-703-264-7500 / 800-639-2422
web: www.aiaa.org

High Power Rocketry

LDRS 2003

Contact: see web site
www.tripoli.org/calendar.htm

Model Rocketry

NARAM 2003

Contact: — see web site for details:
web: www.naram2003.org
For other launch information visit the NAR
Web site: www.nar.org

Future Events Information

If have information concerning future—explosives, pyrotechnics, or rocketry—meetings, training courses or other events that you would like to have published in the *Journal of Pyrotechnics*, please provide the following information:

Name of Event

Date and Place (City, State, Country) of Event

Contact information — including, if possible, name of contact person, postal address, telephone and fax numbers, email address and web site information.

This information will also be published on the Journal of Pyrotechnics Web Site:
http://www.jpyro.com

A Curious Observation during the Burning of Bulk Whistle Composition

L. Weinman
Schneier/Weinman Consultants, LLC
Huntsville, Alabama
Lawrence@Weinman.net

C. Dayton, and K. Lemon
Luna Tech, Inc.
Owens Cross Roads, Alabama
CDayton@Pyropak.com

As is common in pyrotechnic manufacturing operations, occasionally excess or sub-standard compositions need to be destroyed. This is usually, but not always, done by burning the composition.

Recently, in the course of burning several pounds of excess potassium perchlorate-potassium benzoate whistle mix, a curious noise was produced.

The fairly standard, 70%/30% (plus less than 1% carbon black), composition is prepared by dry mixing, then wet with water, granulated through a coarse sieve and dried. No additional binder is used.

The excess composition was laid directly on the ground in a trail approximately 8 to 10 ft (3 m) long × 2 inches (50 mm) wide × 1/4 inch (7 mm) thick. The trail was touching another trail of other pyrotechnic gerb composition. The gerb composition was ignited by means of an electric match.

Upon ignition, the gerb composition burned smoothly and relatively quietly. However, when the burning zone reached the whistle composition, a moderately loud and distinct sound was heard, which was much different from the normal burning bulk pyrotechnic "whoosh". The sound was a "screech", which seemed to mimic a very high-pitched pyrotechnic whistle.

It was not, however, as loud as a common 1/2-inch (12-mm) ID whistle would have produced.

The pitch and intensity of the sound remained fairly constant for the duration of the whistle composition burn, which was approximately 2 seconds.

While several people, who all commented on it, heard the sound, it was completely unexpected and no particular observation protocol had been established prior to the burn.

Since such a burn, at this facility, is a rare occurrence, and because in the past, as far as personnel can remember, there have usually been other items in the burn that may have produced noise, it is not known if this has ever happened before.

Another occasion for such a burn has not, as yet, been needed, but at such time as it is, more attention will be paid to establishing a better noise observation technique.

If, and the authors stress the "if", this sound was real, it might require a re-examination of the several proposed mechanisms by which pyrotechnic whistles are postulated to operate.

If any other similar events have been noted, the authors would be extremely interested in learning about them.

Review of:

Proximate Special Effects Familiarization & Safety

J. Larry Mattingly, David A. Opperman, MD, Francis "Pinky" Pinkerton

American Firework News
[ISBN 0-929931-20-3] 2002

Stephen Miller M.I.Exp.E., Live Action FX, Ltd, email Steve@LiveActionFX.com

---

After many years of drought, the rain is falling for those praying for a basic technical reference book on stage pyrotechnics. The stage and special effects industry as a whole has been lacking a good, well written, reference book that is actually of use to the technician (there are plenty of titles aimed at the general public, but too few aimed at the practising technician).

Although "Britain and America are two countries kept apart by a common language", I have to say that I am rather impressed. The book is well laid out with chapters devoted to 'Professionalism, Responsibility & Licensing', 'General Application Information' (including security, permits, local inspectors and of course safety). I rarely have a good thing to say about the state of UK explosives law, but having read these chapters, I now realise that the problems I face are nothing in comparison to those tackled regularly by US technicians.

Further chapters cover: Manufacturers, Igniters & Airbursts; Comets, Mines, Crossettes and Gerbs; Flame Projectors, Flash Pots and Sparkle Pots; Concussion Effects; Flash Trays, Indoor Lances and Lycopodium Powder; Line Rockets & Saxons; and Firing Systems, Techniques, Tools and Supplies. These chapters are very useful and describe the various effects and techniques, while continuing to hammer home the 'safety' message, which is never a bad thing (although a little repetitive at times).

The information concerning 'Flame Projectors' was at odds with my experience: When igniting Flame Projectors at the top, I have found that the height of the flame is only affected slightly by the length of the tube; the inside diameter of the tube—and hence the top (open) surface area of the column of propellant powder—is the main contributing factor. The greater the surface area, the more unburned powder is available to be lifted by convection effects, this powder then burns higher up the column of flame, thereby increasing its overall height.

The duration of the effect is controlled by the height of the column of propellant powder when ignited to burn from the top down—I have created Flame Projectors that burned for 5 seconds and longer in the past.

In the UK, I have only seen Flame Projectors of cardboard construction, not the metal pot variety shown in the book. I would recommend against using the bottom ignition method mentioned in the book for creating a 'fireball' effect when using cardboard tubes, as they are likely to explode, even seemingly without confinement. Just a few inches head height of propellant over an igniter can be enough for the powder to 'self confine' and cause the cardboard tube to explode. I still have such a shredded tube from some tests I did about 8 years ago, to remind me about the power of these effects.

I was also concerned to see, or rather, NOT see any reference to the prevention of the accidental initiation of igniters (and ready assembled pyrotechnic devices) by radio frequency (RF) radiation and induced currents (i.e., Do NOT use radios or mobile phone while handling, wiring or within 20 feet of firing circuits; Do NOT lay firing cables along or near mains power and other cables.

In the UK, this is taken very seriously and there is a British Standard (BS 6657) that specifically deals with the prevention of such accidents. The British Standard is a comprehensive document and including a similar level of detail in the book would have at least doubled the page count. I also appreciate that stage events tend to be alive with RF and that doing away with radio traffic is near impossible. However, I do feel that the book, and the technicians who read it, would have benefited from a short section and some simple advice on this subject. Such coverage would allow the technicians to take a few basic preventative measures that will help mitigate

the majority of the risks associated with radio frequency radiation and induced currents, even in the transmission rich environments found at stage productions.

Putting these criticisms aside, I have to say that "Proximate Special Effects – Familiarization & Safety" is an excellent book, and I will be recommending it for inclusion on the reading list for the "Special Effects" specialist paper of the Institute of Explosives Engineers. Successful completion of this examination is used as a mark of competence on the UK "Joint Industry Special Effects Grading Scheme" (the recognised structure that the UK Special Effects industry operates within).

Cost including shipping within the US, Canada, and Mexico is US $44.95; visit web site for cost, including shipping to other countries.

Order from:
American Fireworks News
HC67 Box 30
Dingmans Ferry, PA 18328
USA
Fax: +1-570-828-8695
or visit web site: www.fireworksnews.com

Editorial Policy

Articles accepted for publication in the *Journal of Pyrotechnics* can be on any technical subject in pyrotechnics. However, a strong preference will be given to articles reporting on research (conducted by professionals or serious individual experimenters) and to review articles (either at an advanced or tutorial level). Both long and short articles will be gladly accepted. Also, responsible letters commenting on past Journal articles will be published, along with responses by the authors.

Journal Sponsors

Journal of Pyrotechnics **wishes to thank the following Sponsors for their support.**

Individual Sponsors:

Ed Brown
P.O. Box 177
Rockvale, CO 81244, USA
email: edwinde@cs.com

John Giacalone, Criminalist III
5500 E. Tudor Rd.
Anchorage, AK 99507, USA
Phone: 907-269-5689

Gerald Laib
17611 Longview Lane
Olney, MD 20832, USA

Sam & Trudy Zarkoff
Sam & Trudy Zarkoff
1241 S. Hayworth Ave.
Los Angeles, CA 90035, USA
email: Trudybeadspirit@aol.com

Corporate Sponsors:

Industrial Solid Propulsion Inc.
Gary Rosenfield
2113 W 850 N St
Cedar City, UT 84720, USA
Phone: 435-867-9998
FAX: 435-867-9993
email: garyr@powernet.net
web: aerotech-rocketry.com

Allied Specialty Insurance
David H. Smith
10451 Gulf Blvd.
Treasure Island, FL 33706, USA
Phone: 800-237-3355
FAX: 727-367-1407
email: info@alliedspecialty.com
web: www.alliedspecialty.com

American Fireworks News
Jack Drewes
HC 67 Box 30
Dingmans Ferry, PA 18328, USA
Phone: 570-828-8417
FAX: 570-828-8695
email: afn@fireworksnews.com
web: www.fireworksnews.com

American Pyrotechnics Association
Julie Heckman
4808 Moorland Lane - Ste 109
Bethesda, MD 20814, USA
Phone: 301-907-8181
email: jheckman@americanpyro.com
web: www.americanpyro.com

Astro Pyrotechnics
Leo Autote
2298 W. Stonehurst
Rialto, CA 92377, USA
Phone: 909-822-6389
FAX: 909-854-4749
web: www.astropyro.com

Australian Soc. of Accredited Pyros.
Chris Larkin
PO Box 606
Mt. Ommaney, QLD 4074, Australia
Phone: +617-371-20804
FAX: +617-327-90614
email: nitrotech@smartchat.net.au

Brooke Mawhorr, PC
Douglas K Mawhorr
112 East Gilbert StPO Box 1071
Muncie, IN 47305, USA
Phone: 765-741-1375
FAX: 765-288-7763
email: dlmmawhorr@aol.com

Canadian Explosives Research Laboratory
Dr. Phil Lightfoot, Manager
CANMET - 555 Booth St.
Ottawa, ON K1A 0G1, Canada
Phone: 613-947-7534
FAX: 613-995-1230
email: plightfo@nrcan.gc.ca
web: www.nrcan.gc.ca/mms/cerl

Daveyfire, Inc.
Alan Broca
2121 N California Blvd. Ste. 290
Walnut Creek, CA 94596, USA
Phone: 925-926-6414
FAX: 925-926-6439
email: info@daveyfire.com

Delcor Industries Inc.
Sam Bases, President
19 Standish Ave.
Yonkers, NY 10710, USA
Phone: 914-779-6425
FAX: 914-779-6463
email: delcor@hotmail.com
web: www.delcorind.com

Dolliff, Inc. / Insurance
John and Alice Allen
6465 Wayzata Blvd. - Suite 850
St. Louis Park, MN 55426, USA
Phone: 800-338-3531/952-593-7418
FAX: 952-593-7444
email: JAllen@dolliff.com
web: www.dolliff.com

European Pyrotechnic Arts Newsletter
Rob Driessen
Grenadiersweg 55
Riemst, B 3770, Belgium
Phone: +32-12-210-630
FAX: +32-12-210-630
email: epan@pandora.be
web: http://users.pandora.be/epan

Fawkes Fireworks
Tony Cardell and David Watts
89 Lingfield Road
Edenbridge, Kent TN8 5DY, United Kingdom
Phone: 44-1732-862-862
FAX: 44-1342-317-818
email: Tony@fawkes.co.uk

Fire One
Dan Barker
863 Benner Pike
State College, PA 16801, USA
Phone: 814-238-5334
FAX: 814-231-0799
email: info@fireone.com
web: www.fireone.com

Firefox Enterprises Inc.
Gary Purrington
11612 N. Nelson
Pocatello, ID 83202, USA
Phone: 208-237-1976
FAX: 208-237-1976
email: custserv@firefox-fx.com
web: www.firefox-fx.com

Fireworks

PO Box 40
Bexhill, TN40 1GX, England
Phone: 44-1424-733-050
FAX: 44-1424-733-050
email: editor@fireworks-mag.org
web: www.fireworks-mag.org

Fireworks and Stage FX America
Kevin Brueckner
P.O. Box 488
Lakeside, CA 92040-0488, USA
Phone: 619-596-2800
FAX: 619-596-2900
email: go4pyro@aol.com
web: www.fireworksamerica.com

Fireworks Business
Jack Drewes
HC 67 Box 30
Dingmans Ferry, PA 18328, USA
Phone: 717-828-8417
FAX: 717-828-8695
email: afn@fireworksnews.com
web: www.fireworksnews.com

Fireworks Professionals
Anthony Lealand
PO Box 19-912
Christchurch, 8030, New Zealand
Phone: 64-3-982-3473
FAX: 64-3-982-3474
email: firework@firework.co.nz
web: www.firework.co.nz

Fullam's Fireworks, Inc.
Rick Fullam
P.O. Box 1808 CVSR
Moab, UT 84532, USA
Phone: 435-259-2666
email: Rfullam_3@yahoo.com

Goex, Inc.
Mick Fahringer
PO Box 659
Doyline, LA 71023-0659, USA
Phone: 318-382-9300
FAX: 318-382-9303
email: email@goexpowder.com
web: www.goexpowder.com

High Power Rocketry
Bruce Kelly
PO BOX 970009
Orem, UT 84097-0009, USA
Phone: 801-225-3250
FAX: 801-225-9307
email: 71161.2351@compuserve.com
web: www.tripoli.org

Iowa Pyro Supply
Mark Mead
1000 130th St.
Stanwood, IA 52337, USA
Phone: 563-945-6637
FAX: 563-945-0007
email: iowapyro@netins.net
web: www.iowapyrosupply.com

IPON srl
Pagano Benito
Via Trofa
Ottaviano, Napoli 80044, Italy
Phone: +39-81-827-0934
FAX: +39-81-827-0026
email: info@ipon.it
web: www.ipon.it

Island Fireworks Co. Inc.
Charles Gardas
N735 825th St.
Hager City, WI 54014, USA
Phone: 715-792-2283
FAX: 715-792-2640
email: islndfwk@pressenter.com
web: www.pyro-pages.com/island

Kastner Pyrotechnics & Fireworks Mfg. Co
Jeri Kastner
607 County O
Mineral Point, WI 53565, USA
Phone: 608-987-4750
FAX: 608-987-4750
email: kastner@mhtc.net
web: www.kastnerpyrotechnics.com

Lantis Fireworks & Lasers
Ken Lantis
PO Box 491
Draper, UT 84020, USA
Phone: 801-768-2255
FAX: 801-768-2433
email: info@fireworks-lasers.com
web: www.fireworks-lasers.com

LaRosa Fireworks
Lorenzo LaRosa
Via Mortillaro No. 57
Bagheria, Palermo 90011, Italy
Phone: +39(0)91-969-031
FAX: +39(0)91-967-580
email: info@larosa-firewoks.it
web: www.larosa-fireworks.it

MagicFire, Inc.
Paul McKinley
PO Box 896
Natick, MA 01760-0896, USA
Phone: 508-647-9645
FAX: 508-647-9646
email: pyrotech@magicfire.com
web: www.magicfire.com

Marutamaya Ogatsu Fireworks Co., Ltd.
1-35-35 Oshitate Fuchu
Tokyo, 183-0012, Japan
Phone: 81-42-363-6251
FAX: 81-42-363-6252
email: hanabi@mof.co.jp
web: www.mof.co.jp

Mighty Mite Marketing
Charlie Weeth
122 S. 17th St.
LaCrosse, WI 54601-4208, USA
Phone: 608-784-3212
FAX: 608-782-2822
email: chzweeth@pyro-pages.com
web: www.pyro-pages.com

MP Associates Inc.
P.O. Box 546
Ione, CA 94640, USA
Phone: 209-274-4715
FAX: 209-274-4843

Precocious Pyrotechnics, Inc.
Garry Hanson
4420 278th Ave. N.W.
Belgrade, MN 56312-9616, USA
Phone: 320-346-2201
FAX: 320-346-2403
email: ppinc@midstate.tds.net
web: www.pyro-pro.com

Pyro Shows, Inc.
Lansden Hill
P.O. Box 1406
LaFollette, TN 37766, USA
Phone: 800-662-1331
FAX: 423-562-9171
email: info@pyroshowsusa.com
web: www.pyroshowsusa.com

Pyrodigital Consultants
Ken Nixon
1074 Wranglers Trail
Pebble Beach, CA 93953, USA
Phone: 831-375-9489
FAX: 831-375-5225
email: pyrodig@aol.com
web: www.infinityvisions.com/pyrodigital

PyroLabs, Inc.
Ken Kosanke
1775 Blair Road
Whitewater, CO 81527, USA
Phone: 970-245-0692
FAX: 970-245-0692
email: ken@jpyro.com

Pyrotechnics Guild Int'l., Inc.
Ed Vanasek Treas.
18021 Baseline Avenue
Jordan, MN 55352, USA
Phone: 952-492-2061
FAX:
email: edvanasek@aol.com
web: www.pgi.com

RES Specialty Pyrotechnics
Steve Coman
21595 286th St.
Belle Plaine, MN 56011, USA
Phone: 952-873-3113
FAX: 952-873-2859
email: respyro@earthlink.net
web: your email address

Rozzi Famous Fireworks
Arthur Rozzi
PO Box 5
Loveland, OH 45140, USA
Phone: 513-683-0620
FAX: 513-683-2043
email: art@rozzifireworks.com
web: rozzifireworks.com

Service Chemical, Inc.
Ben Cutler
2651 Penn Avenue
Hatfield, PA 19440, USA
Phone: 215-362-0411
FAX: 215-362-2578
email: ben@servicechemical.com
web: www.servicechemical.com

Skylighter, Inc.
Harry Gilliam
PO Box 480
Round Hill, VA 20142, USA
Phone: 540-338-3877
FAX: 540-338-0968
email: custservice@skylighter.com
web: www.skylighter.com

Starburst Pyrotechnics & Fireworks Displays Ltd
Bonnie Pon
2nd Fl-Sui Hing Hong Bldg - 17 Commissioner St
Johannesburg, Gauteng 2000, South Africa
Phone: 27-11-838-7704
FAX: 27-11-836-6839
email: info@starburstpyro.co.za
web: www.starburstpyro.co.za

Sunset Fireworks Ltd.
Gerald Walker
10476 Sunset Drive
Dittmer, MO 63023, USA
Phone: 636-274-1500
FAX: 636-274-0883
email: lisab@sunsetfireworks.com
web: www.sunsetfireworks.com

Western Pyrotechnics, Inc.
Rudy Schaffner
2796 Casey Road
Holtville, CA 92250, USA
Phone: 760-356-5426
FAX: 760-356-2051
email: rudys@holtville.net
web:

Sponsorships

No advertising as such is printed in the *Journal of Pyrotechnics*. However, a limited number of sponsors have been sought so that the selling price of the Journal can be reduced from the listed cover price. The cost of helping sponsor an issue of the *Journal of Pyrotechnics* is $70 per issue for business and organizations [$35 for individuals]. In addition to a listing in the Sponsor section of the Journal, full sponsors receive two free copies of the sponsored Journal [one copy for individual sponsors] and a brief listing on a flyer inserted under the transparent cover of the Journal.

Additionally, if you so desire, we will provide a link from the Journal of Pyrotechnics Web Site to sponsors' web site, e-mail address or simply a company name, address and phone information listing. If you would like to be a sponsor contact the publisher.